ABSTRACT

Title of Document: ADVANCED METHODOLOGIES FOR RELIABILITY-BASED DESIGN OPTIMIZATION AND STRUCTURAL HEALTH PROGNOSTICS.

Pingfeng Wang, Doctor of Philosophy, 2010

Directed By: Dr. Byeng D. Youn,
Assistant Professor,
Department of Mechanical Engineering.

Failures of engineered systems can lead to significant economic and societal losses. To minimize the losses, reliability must be ensured throughout the system's lifecycle in the presence of manufacturing variability and uncertain operational conditions. Many reliability-based design optimization (RBDO) techniques have been developed to ensure high reliability of engineered system design under manufacturing variability. Schedule-based maintenance, although expensive, has been a popular method to maintain highly reliable engineered systems under uncertain operational conditions. However, so far there is no cost-effective and systematic approach to ensure high reliability of engineered systems throughout their lifecycles while accounting for both the manufacturing variability and uncertain operational conditions.

Inspired by an intrinsic ability of systems in ecology, economics, and other fields that is able to proactively adjust their functioning to avoid potential system failures, this dissertation attempts to adaptively manage engineered system reliability during its lifecycle by advancing two essential and co-related research areas: system RBDO and prognostics and health management (PHM). System RBDO ensures high reliability of an engineered system in the early design stage, whereas capitalizing on PHM technology enables the system to proactively avoid failures in its operation stage. Extensive literature reviews in these areas have identified four key research issues: (1) how system failure modes and their interactions can be analyzed in a statistical sense; (2) how limited data for input manufacturing variability can be used for RBDO; (3) how sensor networks can be designed to effectively monitor system health degradation under highly uncertain operational conditions; and (4) how accurate and timely remaining useful lives of systems can be predicted under highly uncertain operational conditions. To properly address these key research issues, this dissertation lays out four research thrusts in the following chapters: Chapter 3 – Complementary Intersection Method for System Reliability Analysis, Chapter 4 – Bayesian Approach to RBDO, Chapter 5 – Sensing Function Design for Structural Health Prognostics, and Chapter 6 – A Generic Framework for Structural Health Prognostics. Multiple engineering case studies are presented to demonstrate the feasibility and effectiveness of the proposed RBDO and PHM techniques for ensuring and improving the reliability of engineered systems within their lifecycles.

ADVANCED METHODOLOGIES FOR RELIABILITY-BASED DESIGN OPTIMIZATION AND STRUCTURAL HEALTH PROGNOSTICS

By

Pingfeng Wang

Dissertation submitted to the Faculty of the Graduate School of the
University of Maryland, College Park, in partial fulfillment
of the requirements for the degree of
Doctor of Philosophy
2010

Advisory Committee:
Assistant Professor Byeng D. Youn, Chair
Professor Ali Mosleh
Professor Shapour Azarm
Associate Professor Jeffrey Herrmann
Associate Professor Yunfeng Zhang

Acknowledgements

I would first and foremost like to express my sincere thanks to my advisor, Dr. Byeng D. Youn, with a deep sense of gratitude. He patiently guided me through the dissertation process, continuously challenging me to set my sights higher and never accepting less than my best efforts. His wisdom, knowledge and commitment to the highest standards inspired and motivated me.

I am also indebted to all my dissertation committee members, Dr. Ali Mosleh, Dr. Shapour Azarm, Dr. Jeffrey Herrmann, and Dr. Yunfeng Zhang. Their insightful guidance and valuable comments were indispensable to the accomplishment of this dissertation.

I would like to express my deep thanks to my lab-mates and friends, Mr. Zhimin Xi, Dr. Soobum Lee, Mr. Byung Chang Jung, Ms. Lulu Wang and Mr. Chao Hu, for sharing innumerous days and nights in the lab and for their encouragements and support whenever I was in need. I also would like to express my sincere gratitude to Dr. John Cafeo and Ms. Artemis Kloess in General Motors R&D center, for their help and support during my summer internship at GM.

Last but not the least, I wish to extend my special and sincere thanks to my parents for their love and unwavering support during my study.

Table of Contents

List of Tables

List of Figures

Chapter 1: Introduction

Failure of engineered systems may cause significant economic and societal losses. Although today U.S. industry spends more than $200 billion each year on reliability and maintenance [Mobley, 2002], catastrophic unexpected failures of engineered systems still take place. The I-35W bridge collapse in Minneapolis, MN in 2007 offers a good example, in which thirteen people lost their lives, more than 100 vehicles were damaged, emergency costs totaled $8 million, and societal costs totaled over $50 million. Growing costs incurred as a result of system failures and increasingly intense competition from global markets impose a great challenge for design engineers, who have to develop reliable engineered systems that can be cost-effectively operated throughout their lifecycles.

1.1 Background and Motivation

To ensure the reliability of engineered systems and avoid potential losses caused by failures, tremendous efforts have been made to design the systems with a desired reliability level in the presence of uncertainties such as manufacturing variability and uncertain operational conditions. As a result of these efforts, the probabilistic engineering design framework, called reliability-based design optimization (RBDO), has been developed to ensure high reliability of engineered system design under manufacturing variability. Most RBDO practices have accounted for uncertainties in manufacturing processes (e.g., material properties and geometric tolerance), but these practices very rarely account for operational conditions.

There are two fundamental deficiencies of RBDO when it is used as an engineered system design tool. First, in most engineering design practices, the amount of data for system uncertainties is lacking in order to precisely model them with statistical distributions. This lack of data is usually due to limited resources (e.g., time, budget, facilities). It is extremely difficult to account for uncertainties with the dearth of data in the existing RBDO framework. Second, the information about operational uncertainties could be completely unknown when the RBDO process is executed. Because of these deficiencies, it is almost impossible to maintain high reliability of engineered systems throughout their entire lifecycle. As a result, system owners have to pay significant maintenance expenses. It is thus crucial to develop adaptively reliable (or resilient) engineered systems to prevent potential failures throughout their lifecycles.

The concept of resilience comes from research in ecology, economics, organizational science, psychology and other fields. Resilient systems possess an intrinsic ability to sense and adjust their functioning prior to or following changes and disturbances, so that they can continue to function during and after a disruption or major mishap, and in the presence of continuous stresses. The human body offers a good example for its capability to sense environmental temperature changes and make appropriate decisions to avoid potential risks due to those changes. Resilience is a proactive concept and looks for ways to create processes that are robust yet flexible, to monitor health conditions, and to use resources proactively in the face of disruptions or ongoing changes. Compared with engineered systems, natural systems have attractive resilience features such as the ability to deal with potential threats with

optimally designed functionalities, and natural, inherent neural systems for sensing and reasoning.

To develop an engineered system with resilience features, a new system design framework must be established. This design framework should enable the design of reliable systems amidst the uncertainties brought about by manufacturing processes, and it should enable the design of intelligent sensing and health reasoning capabilities to proactively account for potential failures induced by uncertain operational conditions. Given the deficiencies of the existing RBDO methodology, there is a strong need for further technological advancement that enables the development of resilient engineered systems. On the other hand, significant technological advances in sensing have promoted the use of large sensor networks (SNs) to monitor structural system health conditions and have helped the development of prognostics and health management (PHM) technologies to predict system remaining useful lives (RULs). These advances make it possible for design engineers to develop engineered systems with embedded health prognostics capabilities, which enable the systems to be proactive against potential failures in the operational stage. Despite the tremendous advances in sensing and structural health prognostics, technical approaches have been application-specific. This necessitates the development of a generic PHM for resilient engineered system design, which is the objective of this dissertation.

Technical developments in both system RBDO and PHM will facilitate the establishment of a new resilient engineered system design framework. This framework will produce adaptively reliable (or resilient) engineered systems in the presence of uncertain operational conditions. It is expected that a system designed

under this framework will be in the presence of manufacturing variability and uncertain operational conditions.

1.2 Research Scope and Objectives

The main objective of this research is to advance two essential and co-related research areas for a resilient engineered system design: system RBDO and PHM. System RBDO will ensure high reliability of engineered systems early in their lifecycles, whereas capitalizing on PHM technology at their early design stage can transform passively reliable (or vulnerable) systems into adaptively reliable (or resilient) systems while considerably reducing their lifecycle cost. This design framework will therefore shift the design paradigm from reliability- to resilience-driven system design.

To achieve this objective, four key research challenges must be carefully addressed: (1) how system failure modes and their interactions can be analyzed in a statistical sense; (2) how limited data for input manufacturing variability can be used for RBDO; (3) how sensor networks can be designed to effectively monitor system health degradation under highly uncertain operational conditions; and (4) how accurate and timely remaining useful lives of systems can be predicted under highly uncertain operational conditions. To make an engineered system resilient, system reliability first needs to be ensured during the design and manufacturing stage. Thus, technical developments in the system RBDO area focus on producing a reliable engineered system considering multiple system failure modes and interactions, manufacturing variability, and uncertain operational conditions. Research questions (1) and (2) are thus addressed through system RBDO. As an engineered system enters

its operational stage from the design and manufacturing stage, it could be vulnerable due to uncertain operational conditions as well as the system performance degradation. Thus, technical developments in the system PHM area focus on designing an engineered system to be adaptively reliable and proactive to system failures during the operational stage through monitoring of the system performance degradation and predicting the system's remaining useful life. The third and fourth research questions in this dissertation are thus addressed through system PHM.

The scope of the work in this dissertation is therefore to develop the following research solutions to address the challenges discussed above:

Research Solution 1: Complementary intersection method (CIM) for system reliability analysis:

The CIM presented in Chapter 3 enables system reliability prediction regardless of system structures (series, parallel, and mixed systems). The CIM expresses the system reliability in terms of the probabilities of the innovatively defined CI-events based on the proposed probability decomposition theory. This theory allows the use of advanced reliability analysis methods for evaluating the probabilities of the CI-events. The CIM has a generalized system reliability analysis framework, which employs a new System Structure matrix (SS-matrix) and the Binary Decision Diagram (BDD) technique. The SS-matrix is used to present any system structure in a comprehensive matrix form. Then the BDD technique, together with the SS-matrix, automates the process to identify the system's mutually exclusive path sets, of which each path set is a series system.

Research Solution 2: Bayesian approach to RBDO:

To address one of the deficiencies of the RBDO, Bayesian inference is integrated with RBDO, referred to as Bayesian RBDO. Given the dearth of uncertainty data, reliability is modeled with a beta distribution based on Bayesian binomial inference, and a Bayesian reliability measure is defined based on a user-defined confidence level. With the defined Bayesian reliability measure, Bayesian RBDO can be generally used for engineering system design in the presence of both aleatory[1] and epistemic[2] uncertainties.

Research Solution 3: Sensing Function Design for Structural Health Prognostics:

To optimally allocate sensing units on the structural systems for monitoring system degradation and making the systems resilient against potential failures, a generic SN design framework is developed using a novel detectability measure. The detectability measure is defined in a probabilistic manner to quantify the performance of a given SN as evaluated by the detectability analysis. The generic SN design framework is formulated as a mixed-integer nonlinear programming problem using the detectability measure. Heuristic algorithms, such as the genetic algorithm (GA), are employed to solve the SN design optimization problem. This design framework can be used for designing a cost-effective SN for structural health monitoring and prognostics while achieving a desired high detectability level.

Research Solution 4: A Generic Probabilistic Health Prognostics Framework:

[1] Aleatory uncertainty, also referred to as irreducible, objective, or stochastic uncertainty, describes the inherent variability associated with a physical system or environment.
[2] Epistemic uncertainty can be classified as subjective and reducible uncertainty due to the lack of data or knowledge about a quantity [Helton et al. 2008].

The generic framework presented in this dissertation enables structural health prognostics with input sensory signals for any type of structural system. This generic framework is composed of four core elements: (i) a generic health index system with a physics health index (PHI) and a virtual health index (VHI), (ii) a generic offline learning scheme using the sparse Bayesian learning (SBL) technique, (iii) a generic online prediction scheme using similarity-based interpolation (SBI), and (iv) an uncertainty propagation map for prognostic uncertainty management. The VHI enables the use of heterogeneous sensory signals; the sparseness feature, employing only a few neighboring kernel functions, enables the real-time prediction of remaining useful lives (RULs) regardless of data size; the SBI predicts the RULs with background health knowledge obtained under uncertain manufacturing and operational conditions; and the uncertainty propagation map enables the predicted RULs to be loaded with their statistical characteristics.

1.3 Dissertation Overview

The dissertation is organized as follows. Chapter 2 reviews the current state of knowledge on RBDO and PHM. Chapter 3 presents the definition of a complementary intersection (CI) event, the probability decomposition theorem, and the complementary intersection method based on this theorem for system reliability analysis. The unified framework for system reliability analysis is also discussed. Chapter 4 proposes a Bayesian reliability measure when data for uncertainties are lacking. Subsequently, this Bayesian approach is integrated with RBDO, referred to as Bayesian RBDO. In Chapter 5, a new sensor network design framework for PHM

is discussed to maximize the degree of structural health detectability. Chapter 6 presents a generic framework for structural health prognostics. The framework has four essential elements: a generic health index system, a generic offline training scheme, an online prediction scheme, and generic prognostic uncertainty management. Finally, Chapter 7 summarizes the dissertation and its contributions to the field and recommends future work.

Chapter 2: Literature Review

This chapter provides the related state of knowledge of the research topics within the scope of this dissertation. The review is presented in the following four sections: Section 2.1 presents advanced methods for reliability analysis, Section 2.2 presents advanced methods for system reliability-based design optimization, Section 2.3 presents the sensor network design literatures and finally Section 2.4 presents the literature regarding health prognostics.

2.1 Reliability Analysis

An engineered system generally consists of numerous failure modes. Before the system is analyzed, all individual failure modes and their coupled effects must be carefully analyzed. All engineering (say, mechanical) parts in a system are designed to fulfill multiple missions. A failure is thus defined as a non-fulfillment of one of the missions. Each failure mode has a corresponding limit state, which separates the design space into failure and safe regions. The probability of failure, P_f, is denoted as

$$P_f = P(G(\mathbf{X}) > 0) \tag{2.1}$$

where $G(\mathbf{X})$ is the performance function and $\mathbf{X}$ is the random vector. The limit-state is denoted by the equation $G(\mathbf{X}) = 0$. An exact solution of P_f can be obtained by the multi-dimensional integration of the joint Probability Density Function (PDF), $f_{\mathbf{X}}(\mathbf{x})$, over the failure domain, $G(\mathbf{X}) > 0$, which is denoted as

$$P_f = \int_{G(X)>0} \cdots \int f_{\mathbf{X}}(\mathbf{x}) d\mathbf{x} \tag{2.2}$$

When multiple failure modes are considered for one system, the probability of the system failure can be similarly written as a multi-dimensional integration of the joint PDF over the system failure domain, Ω, as

$$P_{fs} = \int_{\Omega} \cdots \int f_{\mathbf{X}}(\mathbf{x}) d\mathbf{x} \tag{2.3}$$

It is very difficult to conduct a multi-dimensional integration over the implicit failure domain in Eqs.(2.2) and (2.3). Therefore, different numerical approaches have been developed to evaluate the probability of the failure and carry out the reliability analysis. This section reviews the state of the art techniques for component reliability analysis and system reliability analysis.

2.1.1 Component Reliability Analysis

This subsection provides a review of existing reliability analysis methods. A common challenge in probability analysis is a multidimensional integration to quantify probabilistic nature of system responses (e.g., fatigue life, corrosion, and injury metrics) in various engineering applications (e.g., vehicle, airplane, and electronics). Neither analytical multi-dimensional integration nor direct numerical integration is possible for large-scale engineering applications. Other than those approaches, existing approximate methods for probability analysis can be categorized into five groups: 1) sampling method; 2) expansion method; 3) the most probable point (MPP)-based method; 4) response surface approximate method; and 5) approximate integration method.

Sampling method: The sampling method is the most comprehensive but expensive method to use for estimating statistical moments, reliability, and quality of system responses. Monte Carlo Simulation (MCS) [Varghese et al. 1996; Lin et al. 1997] is

the most widely used sampling method, but demands thousands of computational analyses (e.g., finite element analysis (FEA), crash analysis, etc.). For reliability analysis, MCS provides a reliability estimation of p with a deviation of $\sigma_p = \sqrt{p(1-p)/N}$ where N is the total number of MCS samples and the reliability estimated by MCS can be reported with a confidence interval of [p-3σ_p, p+3σ_p]. To relieve the computational burden, other sampling methods have been developed, such as quasi-MCS [Niederreiter and Spanier 2000; Sobol 1998), adaptive importance sampling [Engelund and Rackwitz 1993; Melchers 1989; Bucher 1988; Wu 1994], directional sampling [Bjerager 1988], etc. Nevertheless, sampling methods are considerably expensive. Thus, it is often used for verification of probability analysis when alternative methods are used.

Expansion method: The idea of the expansion method is to estimate statistical moments of system responses with a small perturbation to simulate input uncertainty. This expansion method includes Taylor expansion [Jung and Lee 2002], perturbation method [Kleiber and Hien 1992; Rahman and Rao 2001], Neumann expansion method [Yamazaki and Shinozuka 1988], and polynomial chaos expansion [Kim, et al. 2006; Wei et al. 2008] etc. Taylor expansion and perturbation methods require high-order partial sensitivities to maintain good accuracy. The Neumann expansion method employs Neumann series expansion of the inverse of random matrices, which requires an enormous amount of computational effort. Lee and Chen provided a comparative study of uncertainty propagation methods based on their performances for black-box-type problems [Lee and Chen 2008]. In summary, all expansion methods could become computationally inefficient or inaccurate when the number or

the degree of input uncertainty is high. Moreover, as it requires high-order partial sensitivities of system responses, it may not be practical for large-scale engineering applications.

MPP-based method: The MPP-based method has been widely used to perform reliability analysis. Rotationally invariant reliability index is introduced through a nonhomogeneous transformation [Hasofer and Lind 1974]. Probability analysis can be conducted in two different ways: performance level (G-level) [Hasofer and Lind 1974] and probability level (P-level) [Wu 1990; Youn et al. 2004; Du and Chen 2002; Du 2008] methods. It has been found that the P-level method is more efficient and stable than the G-level method [Youn et al. 2004]. However, the MPP-based method requires the first-order sensitivities of system responses. Moreover, it could generate relatively large error caused by some nonlinearity of system response and is not suitable for multiple MPP problems as the MPP-based method estimates the reliability value based on the MPP found during the MPP search and all other MPPs will be ignored.

Response surface method: The response surface method (Myers and Montgomery 1995) is often used with MCS to perform reliability analysis. A true system response is approximated based on limited design of experiment (DOE) samples and a response surface approximation method. Once the response surface is constructed, the MCS can be used for reliability analysis without extra expense except for the DOE samples. In the literature, different approaches [Isukapalli and Roy 1998; Zhao and Ono 2001; Youn and Choi 2004; Lee and Kwak 2006; Gavin and Yau 2008] have been developed to approximate stochastic response surfaces. However, the accuracy

of this method greatly depends on the accuracy of response surface. Besides, the response surface method is not suitable for high-dimensional problems because of a curse of dimensionality.

The approximate integration method: The approximate integration method is a direct approach to estimate the PDF (or statistical moments) through numerical integration. Numerical integration can be done in the input uncertainty domain [Rahman and Xu 2004; Seo and Kwak 2003] or the output uncertainty domain [Youn et al. 2005a]. Recently, the dimension reduction (DR) method [Rahman and Xu 2004; Xu and Rahman 2004] and the Eigenvector Dimension Reduction (EDR) [Youn et al. 2008b] method has been proposed and is known to be a sensitivity free method.

The EDR method calculates the statistical moments (or PDF) of performance responses using an additive decomposition scheme [Rahman and Xu 2004] that converts a multi-dimensional integration into multiple one-dimensional integrations and then uncertainty of performance responses can be evaluated through these one-dimensional numerical integrations. To effectively calculate one dimensional integrations, the EDR method incorporates three technical components: (1) eigenvector sampling, (2) one-dimensional response approximations for efficient and accurate numerical integration and (3) a stabilized Pearson system for PDF generation [Johnson et al. 1995]. The EDR method has been proved to be quite efficient and accurate for engineering application with high dimensionality and nonlinearity compared with other methods [Youn et al. 2008b; Youn and Wang 2008].

A fairly amount of numerical methods have been developed to investigate the uncertainty propagation and reliability analysis for the engineering

components/systems subject to various engineering uncertainties. However, all of these methods are based on an assumption that the statistical information regarding the input uncertainties are completely known and given as their PDFs or CDFs. This is most likely not true for practical engineering applications. Typically these uncertainties are represented as limited amount of data coming from fielding testing, laboratory experiments, and maintenance records and so on. These data may evolve over the time through several system lifecycles. How to quantify the system input uncertainties based on the limited and incomplete data sets and how to update them with these evolving data sets are the primary challenges before the above discussed methods can actually be used for the practical engineering design and analysis problems.

2.1.2 System Reliability Analysis

Compared with tremendous advances in component reliability analysis, the research in system reliability analysis has been stagnant, mainly due to the technical difficulties in formulating system reliability explicitly for multiple system failure modes and their complicated coupling effects, as well as the computational efficiency and accuracy. Consequently, system reliability analysis has been dominated by reliability bounds methods. This subsection provides a review of existing system reliability bounds methods: first order bound method, second order bound method and the linear programming bound method.

First-order bound method: The first-order bound (FOB) method for serial system reliability and parallel system reliability were proposed in 1960's and 1980's by Ang and other researchers [Haldar and Mahadevan 2000; Ramachandran 2004], as shown

below. In basic, these methods give an upper system reliability bound by assuming that all system failure events are perfectly dependent; similarly a lower system reliability bound is obtained by assuming that all system failure events are mutually exclusive. The application of this first-order bound method is limited since they usually give quite wide bounds.

Second-order bound method: Ditlevsen et al. proposed the most widely used second-order bound (SOB) method for system reliability, which gives much tighter bounds than the first-order bounds [Ditlevsen and Bjerager 1984]. Other equivalent forms of Ditlevsen's bounds are given by other researchers. [Thoft-Christensen and Murotsu 1986; Karamchandani 1987; Xiao and Mahadevan 1998; Ramachandran 2004]. Second-order system reliability bounds or equivalent forms have been used for the system reliability analysis and system reliability based design optimization for many engineering system applications [Mahadevan and Raghothamachar 2000; Royset and Kiureghian 2001; Liang et al. 2007; McDonald and Mahadevan 2008].

Linear programming bound method: Song et al. formulated system reliability analysis as a linear programming (LP) problem, referred to as the LP bound method [Song and Der Kiureghian 2003; Der Kiureghian and Song 2008]. The LP bounds method treats the system reliability as the objective function and obtains the lower and upper bound through minimizing and maximizing the objective function accordingly. The LP bounds method is able to calculate optimal bounds for system reliability with the component reliabilities and/or probabilities of joint failure events as provided input information. However, it is known that the LP bounds method can suffer when an approximate LP algorithm is used for over-constrained problems. Besides, it is

extremely sensitive to accuracy of the given input information, which is the probabilities for the first-, second-, or high-order joint safety events. To assure high accuracy of the LP bounds method, the input probabilities must be given very accurately and the problem must not be over-constrained.

Besides the system reliability bound methods, one of the popular approaches is the multimodal adaptive importance sampling (AIS) method, which is found to be satisfactory for the system reliability analysis of large structures [Mahadevan and Raghothamachar 2000; Zou and Mahadevan 2006a, 2006b]. The integration of surrogate model techniques with MCS–based methods can be an alternative approach to system reliability prediction as well [Zhou et al. 2000]. In this approach, the surrogate model can be constructed for multiple limit state functions to represent the joint failure region. This approach is quite practical and highly valued, but accuracy of the method depends on the fidelity of the surrogate model and the number of random input variables.

Although SOB method and LP bound method can give fairly narrow system reliability bounds generally assuming that the system input uncertainty information are given precisely, evaluation of these bounds will suffer from numerical errors, since most of numerical methods cannot evaluate probabilities of second or higher order joint events effectively considering implicit coupling effects between different system failure modes. Besides, these bounds methods cannot provide continuous system reliability with respect to system input variables. In order to carry out system RBDO using these bounds methods, response surfaces have to be created for reliability bounds. How to explicitly formulate system reliability and how to

efficiently evaluate system reliability are two big challenges for system reliability analysis.

2.2 Reliability-based Design Optimization

Compared with deterministic design optimization, the RBDO model which employs the probabilistic approaches in design optimization enables the incorporation of available uncertainty information into the design process and produces reliable designs of engineered systems. Although the RBDO model based on the probabilistic approaches enables designers to achieve a reliable design, however, it is computationally significantly more expensive compared to deterministic approaches.

Reliability is of critical importance in product and process design [Hazelrigg 1998]. Hence in the literature, various methods [Youn et al. 2005b; Chen et al. 1997; Du and Chen 2004, Mcdonald and Mahadevan 2008] have been developed to systematically treat uncertainties in engineering analysis and carry out RBDO. In RBDO, a design optimization strategy has been advanced to improve computational efficiency and stability [Wu et al. 2001; Wang and Kodiyalam 2002; Youn et al. 2005c]. Additionally, new methods for reliability assessment have been proposed to enhance numerical efficiency and stability [Du et al. 2004; Rahman and Xu 2004a; Youn et al. 2006; Du 2008; Lee et al. 2008, 2009; Kim and Choi 2008; Youn and Xi 2009; Noh et al. 2009].

Although advanced methods have been developed to improve the numerical efficiency and stability, for the conventional RBDO framework itself all uncertainties regarding the system are required to be characterized as random variables with certain statistical distributions. There is still a big gap between the practical engineering

design applications and the theoretical RBDO framework, since most of engineering design problems are face the situation of lack of data, especially when new products are to be designed, new technologies are to be used. When available data is insufficient, the classical probability theory may be improper to model uncertainties because it may lead to a result with a relatively low confidence. To deal with insufficient data sets, different methods have been developed for reliability analysis and design optimization. Methods are based on various non-deterministic theories: the possibility theory [Utkin and Gurov 1996; Bai and Asgarpoor 2004; Du et al. 2006; Zhou and Mourelatos 2008; Youn et al. 2008a; Herrmann 2009], the evidence theory [Sentz and Ferson 2002; Bae et al. 2003; Helton et al. 2006], and the Bayes' theory [Coolen and Newby 1994; Huang et al. 2006; Youn and Wang 2008a]. Although different methods have been developed to deal with subjective and insufficient data sets, evolving data sets have little been considered in these methods.

Besides the RBDO model, to ensure the reliability of the product system, diverse design methodologies have been developed, such as possibility-based design optimization (PBDO) [Choi et al. 2006; De and Choi 2008], and evidence-based design optimization (EBDO) [Mourelatos and Zhou 2006]. Some recent publications [Allen and Choi 2009; Huang and Zhang 2009] delivered rigorous studies to deal with all kinds of uncertainty (e.g., aleatory/epistemic, discrete/continuous, statistical /fuzzy) for system analysis and design. Such research activities have focused on how to assess reliability effectively by simply assuming non-deterministic models of random system inputs without engaging raw data [Youn et al. 2003; Du and Chen 2004; Youn et al. 2008b]. Among these design methodologies, Bayesian approaches

have been widely used in many engineering and science fields where data is progressively accumulated. For example, Bayesian reliability analysis has been applied to series systems of Binomial (safe or fail) subsystems and components [Fickas et al. 1988], to reliability assessment of power systems [Yu et al. 1999], to the effectiveness of reliability growth testing [Quigley and Walls 1999], to robust tolerance control and parameter design in the manufacturing process [Rajagopal 2004], and to input uncertainty modeling [Chung et al. 2004]. Two advanced Bayesian (maximum likelihood and parsimony) methods have been compared for molecular biology applications [Merl et al. 2005]. Bayesian updating has been implemented using Markov Chain Monte Carlo simulation for structural models and reliability assessment [Beck and Au 2002]. Dynamic object oriented Bayesian networks have been proposed for complex system reliability modeling [Weber and Jouffe 2006]. Bayesian approach has also been investigated for the reliability modeling [Zhang and Mahadevan 2000], and for reliability based design with incomplete information to achieve Pareto trade-off designs [Gunawan and Papalambros, 2006].

As stated in subsection 2.1.1, current numerical methods for probability analysis are based on an assumption that the statistical information regarding the input uncertainties are precisely known and given by their PDFs or CDFs. Consequently, RBDO requires full statistic information of system uncertainty inputs since it relies on those numerical methods for probability analysis at each RBDO design iteration. However, most of practical engineering design problems face a common situation of lack of data for system uncertainty inputs. Moreover, the limited data may evolve

over the time through several system lifecycles and might be subjective such as data obtained from expert opinions or customer surveys. The challenge is how to systematically perform RBDO for an engineered system design with insufficient, subjective and evolving data set.

2.3 Sensor Network Design

Significant technological advances in sensing and communication promote the use of large sensor networks (SNs) to monitor structural systems, identify damages, and quantify damage levels. Prognostics techniques take full advantage of these advances and strive to enhance the safety and prolong the service lives of structural systems through the means of in situ data acquisition, data feature extraction and health diagnostics/prognostics to appropriately assess their health conditions and predict remaining useful lives (RULs). Through years of research efforts, structural health monitoring systems based on different types of sensors such as fiber optics, piezoelectric elements, and MEMS sensors have been developed for a wide variety of potential applications ranging from the civil, mechanical, and aerospace industries to automotive industry [Li et al. 2004; Zhao et al. 2007; Tanner et al. 2003; Ling et al., 2009; Bocca et al. 2009]. Despite the worldwide attention and significant advances in maturing the technologies for practical implementation, primary challenges still remain in sensing technologies to enhance sensitivity, repeatability, robustness and reduce limited power consumptions of sensors [Chang and Markmiller 2006]. It is clear that successful accomplishment of a structural health prognostic mission relies extremely on an effectively designed SN.

Most of the research activities for SN design in the past decade targeted on maximizing the coverage and minimizing the power consumption of SNs [Buczak et al. 2001; Chakrabarty and Chiu 2002] for various applications that require the data acquisition. Several methods have been developed to enhance the detection efficiency and minimize the uncertainty in decision-making based on data acquired from the SNs [Field and Grogoriu 2006]. The optimum SN was introduced as the sensor configuration that can achieve the target probability of detection. Guratzsch and Mahadevan also defined the optimum SN for structural health monitoring under uncertainties as the sensor configuration that can maximize the probability of damage detection [Guratzsch and Mahadevan 2006]. Furthermore, Li *et al.* obtained a vector of sensor placement indices based on the weighted components of the mode shape matrix corresponding to the sensor position [Li et al, 2006]. Ntotsios *et al.* presented another approach that addresses the stochastic nature of the sensor measurements [Ntotsios et al. 2006]. Azarbayejani *et al* employed an artificial neural network approach to identify the optimum sensor placement for a bridge case study [Azarbayejani et al. 2008]. The sensor allocation problem is handled within the context of uncertainty and information entropy. A Bayesian method is used to quantify damage in the structure based on the change in modal information. The information entropy is used to compute a scalar measure of uncertainty in the structural damage features. A heuristic sequential sensor placement algorithm is then used to predict the optimal sensor configuration. Flynn and Todd also employed a Bayesian method for optimal sensor placement with active sensing [Flynn and Todd 2010]. Research work [Ntotsios et al. 2006; Udwadia 1994; Heredia-Zavoni and

Esteva 1998] showed the importance of addressing the issue of uncertainty in handling the optimal sensor configuration. Other researchers [Papadimitriou et al. 2000; Kirkgaard and Brincker 1999] also reported the use of the information entropy and information functions such as the Fisher information to formulate the objective function for optimal sensor allocations. All of the aforementioned approaches showed the significance of considering the uncertainties introduced by sensor units, structure systems as well as the operation conditions in the SN design problem and presented unique methods to deal with uncertainties in the damage detection. Most of these methods were developed for the problem of distributing a finite set of sensors to detect a specific type of structural damage and their applications are tied to and restricted by the type of failure mechanisms under consideration.

Given the significance of a SN for system health monitoring and prognostics, and years of research efforts, the design of SNs nonetheless becomes tied to the structural damage features and the development of a generic design methodology is still a hurdle to overcome. The challenge problem is how sensor networks can be designed to effectively monitor system health degradation under highly uncertain operational conditions.

2.4 Prognostics and Health Management

Awareness of the health condition of engineered systems in real time is of great importance to critical decision-making processes such as maintenance and logistics. Research on health prognosis which interprets data acquired by distributed sensor networks, and utilizes these data streams in making critical decisions provides significant advancements across a wide range of applications. In the literature, health

prognostics has been implemented using approaches that are either model-based or data-driven [Pecht 2008; Pecht and Jaai 2010]. The model-based approaches takes into account the physical processes and interactions between components in the system, whereas the data-driven approaches use statistical pattern recognition and machine-learning techniques to detect changes in parameter data, thereby enabling diagnostic and prognostic measures to be calculated.

Model-based prognostic approaches attempt to incorporate physical understanding of the system degradation into the estimation of remaining useful life (RUL). Different stochastic degradation models have been investigated in the literature, to model various degradation phenomena of systems or components [Doksum and Hoyland 1992; Lu and Meeker 1993; Boulanger and Escobar 1994; Lu 1995; Tseng et al. 1995; Hamada 1995, Chiao and Hamada 1996; Meeker et al. 1998; Whitmore et al. 1998; Bagdonavicius and Nikulin 2000]. Dowling, Meeker and Escobar used convex and concave degradation models to study the growth of fatigue cracks and the degradation of printed circuit boards [Dowling 1993; Meeker and Escobar 1998]. Carey and Koenig used similar models to describe degradation of electronic components [Carey and Koenig 1991]. Lu and Meeker developed an exponential pattern model to study a the life distribution over a population of components [Lu and Meeker 1993], and similar exponential pattern degradation has been applied with stochastic process of modeling random error term to study the residual life of single operating device of ball bearings [Gebraeel et al. 2005]. Model-based approach to prognostics was demonstrated for lithium ion batteries [Saha et al. 2009] where a lumped parameter model was used along with extended Kalman filter

and particle filter algorithms to estimate RUL. Model-based prognostics methods have also been developed and applied for power semiconductors [Goodman 2001; Patil et al. 2009], digital electronics components and systems [Kalgren et al. 2007], switched-mode power supplies [Kulkami et al. 2009].

Although various system degradation models have been developed and used for the prognostics purpose, generally developing an accurate model is prohibitively expensive when the understanding of first principles of system operation is not comprehensive or when the system is sufficiently complex. In these circumstances, the data driven prognostics approaches are appropriate. Data-driven techniques are used to learn the system state of health and the trends or patterns of system degradation from data, and intelligently carry out life predictions. In these approaches, in situ monitoring of environmental and operational loads and system parameters through distributed sensor networks or inspections is needed. The data collected is analyzed using a variety of machine learning techniques depending on the type of data available. Many of the existing approaches to data-driven prognosis have used artificial neural networks to model the systems [Chinnam 1999; Brotherton et al. 2000; Wang and Vachtsevanos 2001; Gebraeel et al. 2004]. Besides, the Bayesian Belief Network has also been used as an approach for diagnosis and prognosis of aircraft avionics [Byington et al. 2003]. Symbolic time series analysis and Mahalanobis distance measure were used for feature extraction for health prognostics of notebook computers [Kumar and Pecht 2007; Kumar 2009]. Pattern recognition algorithms and statistical reasoning techniques for early fault detection have been applied for computer servers [Lopez 2007; Urmanov 2007]. Applications of data

driven prognostics approaches can also be found in the literatures [Keller et al. 2006; Saha et al. 2009; Gebraeel and Hernandez 2009]; Compared with model-based prognostics approaches, the data-driven approaches require less understanding of the system but more training data and eventually are computationally more expensive.

Despite the tremendous advances on health diagnostics and prognostics for engineered systems, techniques approaches and methodologies become application-specific. Difficulties in developing an application-generic methodology mostly result from heterogeneity of sensory data, a wide range of data acquisition frequency and size, and different characteristics in uncertain manufacturing and operation conditions. Developing a general probabilistic framework of structural health prognostics and uncertainty management for resilient engineered system design requires the development of four core elements: (i) a generic health measure for system health condition quantification; (ii) a generic offline learning scheme to extract system health characteristics from sensory signals and built up a background health knowledge; (iii) a generic online prediction scheme for remaining useful life prediction; and (iv) an uncertainty quantification and management scheme to manage uncertainties involved in the health prognostic process and improve the prediction confidence.

For a generally applicable prognostics framework, extracting health relevant information from heterogeneous sensory signals to build a generic health measure is the first essential step. Different signal processing methods have been studied and employed to find out a set of the most important physical signals and construct system health indexes. The methods include regression and classification based

methods [Harrell et al. 2006; Yan and Lee 2005], principle component analysis [Sharmin et al. 2008; Mina and Verde 2005], time domain analysis, frequency domain analysis, wavelet analysis [Wang and Vachtsevanos 2001; Liu et al. 2008], and autoregressive moving average methods [Pandit and Wu 1993]. The health index can use dominant physical signals as a direct health metric is referred as the physics health index, for example, impedance and open circuit voltage for battery health management. With the growing complexity of engineered systems and embedded sensor networks, the mapping of a multitude of heterogeneous sensory signals to a dominant health index is getting more and more difficult.

After extracting health relevant information from sensory signal and constructing system health indexes, system degradation characterization is another crucial task for structural health prognostics. Different machine learning techniques have been used for this purposes, such as support vector machine [Sotiris and Pecht, 2007], artificial neural networks [Huang et al. 2007; Heimes 2008; Byington et al. 2004; Shao and Nezu 2000], Bayesian modeling [Gebraeel et al. 2005], Gaussian process regression [Rasmussen and Williams 2006; Srivastava and Das 2009]. For the prognostic technique to be real-time applicable, the efficiency is one of the key factors to be considered. Besides the efficiency, the capability of handling uncertainties is another concern due to the uncertain nature of sensory signals in most engineering problems. The sparse Bayes learning scheme, for example the relevance vector machine (RVM) [Tipping 2001], is not only statistically loaded, but also has a great sparseness feature to employ only a few neighboring kernel functions. This sparseness feature of the background health knowledge will eventually speed up online data processing and

make possible a real-time RUL prediction, especially when sensory data are massive and heterogeneous for a set of physical components.

After the offline learning of the system degradation behavior, the RUL can then be predicted by comparing the real-time sensory signals with the background health knowledge, with the help of appropriate life prediction techniques, such as artificial neural networks, neuro-fuzzy approach [Chinnam and Baruah 2004], Bayesian updating approaches [Youn and Wang 2008b], filtering techniques [Qiu et al. 2008; Orchard et al. 2008; Saha et al. 2007], and the approach based on the similarities [Wang et al. 2008]. One of the grand challenges in structural health prediction is managing various uncertainties in RUL prediction. The uncertainties mainly come from manufacturing variability over a population of physical artifacts, uncertain nature in operational conditions, and sensor noise. To properly manage the uncertainty, it is important to build statistically rich background health knowledge (or curves) and use an optimal combination of the health curves for accurate RUL prediction.

In summary, current health prognostics methodologies using model-based or data-driven prognostics approaches are case-sensitive with strictly limited applications. Developing a generic structural health prognostics framework and corresponding technical solutions that can be generally applicable for the general purpose of resilient engineered system development remains to be a big challenge.

Chapter 3: Complementary Intersection Method for System Reliability Analysis

System reliability prediction is significantly important in aerospace, mechanical, and civil engineering fields, its technical development will have an immediate and major impact on complex engineered system designs. Despite tremendous advances in component reliability analysis, the research in system reliability analysis has been stagnant and dominated by system reliability bound methods as discussed in Chapter 2. This chapter presents the research solution to the first challenging question which is how multiple system failure modes and their interactions can be effectively analyzed in a statistical sense for system reliability analysis.

The work presented in this chapter aims at developing a pioneering method for system reliability analysis by which system reliability can be analyzed within a generic framework regardless the system structures (series, parallel and mixed systems). Section 3.1 proposes the first-ever defined event, referred to as the complementary intersection (CI) event, which facilitates the decomposition of the probability of the joint safety event. Section 3.2 presents the general formula for the decomposition of the probability of joint safety events. As a numerical showcase, the probability of the second-order joint safety event will be introduced and decomposed into the probabilities of the CI events. In order to deal with large-scale problems such as a system with a large number of components and system failure modes, Section 3.3 introduces the CI-matrix that is composed of the component reliabilities and the probabilities of CI events. Section 3.4 presents the system reliability analysis using

complementary intersection method (CIM) for series, parallel and mixed systems. As a series system or a parallel system can be viewed as a special case of a mixed system, Section 3.5 introduces a generalized CIM framework for system reliability analysis regardless of the system configurations. Section 3.6 provides four engineering case studies to demonstrate the developed CIM methodology and Section 3.7 summarizes the work presented in this chapter.

3.1 Definition of CI Event

Let an Nth-order CI event denote $E_{12\ldots N} \equiv \{\mathbf{X} \mid G_1 \cdot G_2 \cdot \ldots \cdot G_N \leq 0\}$, where the component safety (or 1st-order CI) event is defined as $E_i = \{ X \mid G_i \leq 0, i = 1, 2, \ldots, N\}$. The defined Nth-order CI event is composed of distinct intersections of component events E_i and their complements $\bar{E}_i$ where $i = 1,\ldots, N$. For example, for the second order CI event E_{ij}, it is composed of two distinct intersection events, $\bar{E}_1 E_2$ and $E_1 \bar{E}_2$. These two events are the intersections of E_1 (or E_2) and the complementary event of E_2 (or E_1). Thus, we refer to the defined event as the Complementary Intersection (CI) Event.

Based on the definition of the CI event, the second-order CI event can be denoted as $E_{ij} \equiv \{X \mid G_i \cdot G_j \leq 0\}$. The CI event can be further expressed as $E_{ij} = \bar{E}_i\, E_j \cup E_i\, \bar{E}_j$ where the component failure events are defined as $\bar{E}_i = \{X \mid G_i > 0\}$, $\bar{E}_j = \{X \mid G_j > 0\}$. The event E_{ij} is composed of two events: $E_i \bar{E}_j = \{X \mid G_i \leq 0 \cap G_j > 0\}$ and $\bar{E}_i E_j = \{X \mid G_i > 0 \cap G_j \leq 0\}$. Since the events, $\bar{E}_i E_j$ and $E_i \bar{E}_j$, are disjoint, the probability of the CI event E_{ij} can be expressed as

$$
\begin{aligned}
P(E_{ij}) &\equiv P(X \mid G_i \cdot G_j \le 0) \\
&= P(X \mid G_i > 0 \cap G_j \le 0) + P(X \mid G_i \le 0 \cap G_j > 0) \\
&= P(\bar{E}_i E_j) + P(E_i \bar{E}_j)
\end{aligned} \tag{3.1}
$$

Figure 3-1 illustrates the CI event E_{12} in the two shaded domains, $E_{12} = \{(X_1, X_2) \mid G_1 \cdot G_2 \le 0\}$. Two component safety events are defined as $E_1 = \{(X_1, X_2) \mid G_1 \le 0\}$ and $E_2 = \{(X_1, X_2) \mid G_2 \le 0\}$, where X_1 and X_2 are random variables (e.g., random manufacturing tolerances and operational conditions).

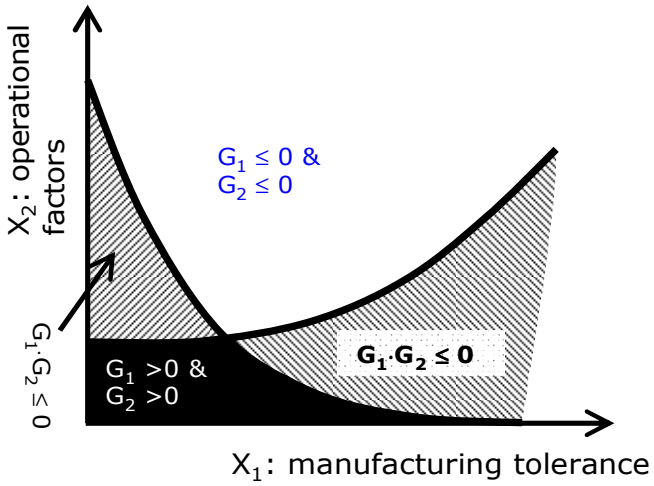

Figure 3-1: Definition of the second order CI event

3.2 Probability Decomposition Theorem

Theorem: Decomposition of the Probability of an Nth-Order Joint Safety Event

With the above definition of the CI event, the probability of an Nth-order joint safety event can be decomposed into the probabilities of the CI events as

$$P\left(\bigcap_{i=1}^{N} E_i\right) =$$

$$\frac{1}{2^{N-1}}\left[\sum_{i=1}^{N} P(E_i) - \sum_{\substack{i=1;\\ j=2;\\ i<j}}^{N} P(E_{ij}) + \cdots + (-1)^{m-1} \sum_{\substack{i=1;\\ j=2;\\ \vdots\\ l=m\\ i<j<\cdots<l}}^{N} P\left(E_{\underbrace{ij\cdots l}_{m}}\right) + \cdots + (-1)^{N-1} P(E_{12\cdots N})\right] \quad (3.2)$$

The detail derivation of Eq. (3.2) can be found in Appendix A as well as in [Youn and Wang, 2009]. It is noted that each CI event has its own limit state function, which enables the use of any reliability analysis methods. In general, higher-order CI events are expected to be highly nonlinear. Considering the tradeoff between computational efficiency and accuracy, the study in this dissertation uses the probabilities of the first and second-order CI events in Eq. (3.2) for system reliability analysis. However, more terms in Eq. (3.2) can be employed as advanced reliability analysis methods are developed.

Based on the probability theory, the probability of the second-order joint safety event $E_{\mathrm{i}} \cap E_{\mathrm{j}}$ can be expressed as

$$\begin{aligned} P(E_i E_j) &= P(E_i) - P(E_i \overline{E}_j) \\ &= P(E_j) - P(\overline{E}_i E_j) \end{aligned} \quad (3.3)$$

From Eq. (3.1) and Eq. (3.3), the probabilities of the second-order joint safety and failure events can be decomposed as

$$P(E_i E_j) = \frac{1}{2}\left[P(E_i) + P(E_j) - P(E_{ij})\right] \quad (3.4)$$

$$P(\overline{E}_i \overline{E}_j) = 1 - \frac{1}{2}\left[P(E_i) + P(E_j) + P\ (E_{ij})\right] \quad (3.5)$$

3.3 CI- Matrix

For large-scale systems, the probabilities of CI events can be conveniently written into a multidimensional matrix, referred to as the CI-matrix. In this matrix, the item CI(i, j, k,….,m) represents the probability of CI-event $E_{i,j,\ldots,m}$ where $i \le j \le k \le \ldots \le m$. As an example, CI(1, 2) in the second order CI-matrix represents the probability of CI event E_{12}, $P(E_{12})$. In the CI matrix, if two or more indices are equal to each other, it means that probability of a lower order CI event is presented. For example in a third-order CI matrix, element CI(1, 3, 3) represents the probability of a second order CI event E_{13}, as $P(E_{13})$. So if $i = j = k = \ldots = m$, then the element presents the probability of the first order CI event E_i.

As an example, for up to the second order CI-Events and the system includes m components in total, the CI-matrix is written as

$$\mathrm{CI} = \begin{bmatrix} P(E_1) & P(E_{12}) & P(E_{13}) & \cdots & P(E_{1m}) \\ - & P(E_2) & P(E_{23}) & \cdots & P(E_{2m}) \\ - & - & P(E_3) & \cdots & P(E_{3m}) \\ - & - & - & \ddots & \vdots \\ - & - & - & - & P(E_m) \end{bmatrix} \tag{3.6}$$

In the upper triangular CI-matrix, the diagonal elements correspond to the component reliabilities (or probabilities of the first-order CI events) and the element on i^{th} row and j^{th} column corresponds to the probability of the second-order CI event E_{ij} if $j < i$. The probabilities of the second-order joint safety and failure events in Eqs. (3.4) and (3.5) can be evaluated with the probabilities of all CI events that are found from the CI-matrix.

3.4 System reliability analysis using CIM

3.4.1 CIM for series systems

This section introduces an explicit formula for system reliability assessment for series systems using CIM, developed based a mathematical inequality equation. Considering a structural serial system with m components, the probability of system failure can be expressed as

$$P_{fs} = P\left(\bigcup_{i=1}^{m} \overline{E}_i \right) \tag{3.7}$$

where P_{fs} represents the probability of system failure and $\bar{E}_i$ denotes the failure event of the i^{th} component. Based on the well known Boolean bounds in Eq.(3.8), the first-order system reliability bound is then given in Eq. (3.9).

$$\max_i (P(\overline{E_i})) \le P(\bigcup_{i=1}^{m} \overline{E}_i) \le \sum_{i=1}^{m} P(\overline{E_i}) \tag{3.8}$$

$$\max\left[P\left(\overline{E_i}\right) \right] \le P_{fs} \le \min\left[\sum_{i=1}^{m} P\left(\overline{E_i}\right),\ 1 \right] \tag{3.9}$$

However, these methods provide wide bounds of system reliability. Thus, the second-order bounds method proposed by Ditlevsen in Eq. (3.10) is widely used because it gives quite narrow bounds of system reliability.

$$\begin{aligned} & P\left(\overline{E_1}\right) + \sum_{i=2}^{m} \max\left\{ \left[P\left(\overline{E_i}\right) - \sum_{j=1}^{i-1} P\left(\overline{E_i}\,\overline{E_j}\right) \right],\ 0 \right\} \le P_{fs} \\ & \le \min\left\{ \left[\sum_{i=1}^{m} P\left(\overline{E_i}\right) - \sum_{i=2}^{m} \max_{j<i} P\left(\overline{E_i}\,\overline{E_j}\right) \right],\ 1 \right\} \end{aligned} \tag{3.10}$$

where E_1 is the event having the largest probability of failure.

Since the probabilities of all events are non-negative, the following inequalities must be satisfied as

$$\max_i(P(\overline{E_i})) \le \sqrt{\sum_{i=1}^{m}\left[P(\overline{E_i})\right]^2} \le \sum_{i=1}^{m} P(\overline{E_i}) \tag{3.11}$$

First, the left-hand side inequality in Eq. (3.10) can be redeveloped as

$$\begin{aligned} P_{fs} &\ge P\left(\overline{E_1}\right) + \sum_{i=2}^{m} \max\left\{\left[P\left(\overline{E_i}\right) - \sum_{j=1}^{i-1} P\left(\overline{E_i}\,\overline{E_j}\right)\right],\ 0\right\} \\ &\ge P\left(\overline{E_1}\right) + \sum_{i=2}^{m}\left[P\left(\overline{E_i}\right) - \sum_{j=1}^{i-1} P\left(\overline{E_i}\,\overline{E_j}\right)\right] \end{aligned} \tag{3.12}$$

Then, applying the right-hand side inequality in Eq. (3.11) to Eq. (3.10) gives the following the inequality as

$$P\left(\overline{E_1}\right) + \sum_{i=2}^{m}\left[P\left(\overline{E_i}\right) - \sum_{j=1}^{i-1} P\left(\overline{E_i}\,\overline{E_j}\right)\right] \le P\left(\overline{E_1}\right) + \sum_{i=2}^{m}\left\langle P\left(\overline{E_i}\right) - \sqrt{\sum_{j=1}^{i-1}\left[P\left(\overline{E_i}\,\overline{E_j}\right)\right]^2}\right\rangle, \tag{3.13}$$

where $\langle A\rangle \equiv \begin{cases} A, & \text{if } A > 0 \\ 0, & \text{if } A \le 0 \end{cases}$

A similar logic can be applied to the right-hand side inequality in Eq. (3.10)and it gives

$$P_{fs} \le \min\left\{\left[\sum_{i=1}^{m} P\left(\overline{E_i}\right) - \sum_{i=2}^{m} \max_{j<i} P\left(\overline{E_i}\,\overline{E_j}\right)\right],\ 1\right\} \le \sum_{i=1}^{m} P\left(\overline{E_i}\right) - \sum_{i=2}^{m} \max_{j<i} P\left(\overline{E_i}\,\overline{E_j}\right) \tag{3.14}$$

Then, using Eq. (3.10) and Eq. (3.14) gives

$$\sum_{i=1}^{m} P\left(\overline{E_i}\right) - \sum_{i=2}^{m} \max_{j<i} P\left(\overline{E_i}\,\overline{E_j}\right) \ge P\left(\overline{E_1}\right) + \sum_{i=2}^{m}\left\langle P\left(\overline{E_i}\right) - \sqrt{\sum_{j=1}^{i-1}\left[P\left(\overline{E_i}\,\overline{E_j}\right)\right]^2}\right\rangle \tag{3.15}$$

The combination of Eq. (3.13) and Eq. (3.15) provides the following inequalities as

$$P\left(\overline{E_1}\right) + \sum_{i=2}^{m}\left[P\left(\overline{E_i}\right) - \sum_{j=1}^{i-1} P\left(\overline{E_i}\,\overline{E_j}\right)\right] \le P\left(\overline{E_1}\right) + \sum_{i=2}^{m} P\left(\overline{E_i}\right) - \sum_{i=2}^{m} \max_{j<i} P\left(\overline{E_i}\,\overline{E_j}\right) \tag{3.16}$$

Finally, Eq. (3.16) approximates the probability of a serial system failure as

$$P_{fs} \simeq P\left(\overline{E_1}\right) + \sum_{i=2}^{m} \left\langle P\left(\overline{E_i}\right) - \sqrt{\sum_{j=1}^{i-1} \left[P\left(\overline{E_i}\,\overline{E_j}\right) \right]^2} \right\rangle \tag{3.17}$$

It can be proven that this approximate probability lies in the second-order bounds in Eq.(3.10) [Youn and Wang 2009].

From Eq.(3.17), the system reliability for a serial system can be assessed as one minors the probability of system failure and formulated as

$$R_{s\_series} = P(E_s) \cong P\left(E_1\right) - \sum_{i=2}^{m} \left\langle P\left(\overline{E_i}\right) - \sqrt{\sum_{j=1}^{i-1} \left[P\left(\overline{E_i}\,\overline{E_j}\right) \right]^2} \right\rangle, \quad \langle A \rangle \equiv \begin{cases} A, & \text{if } A > 0 \\ 0, & \text{if } A \le 0 \end{cases} \tag{3.18}$$

Note that the terms inside the bracket, $\langle\ \rangle$, should be ignored if it is less than zero and Rs should be set to zero if the approximated one given by Eq. (3.18) is less than zero. Equation (3.18) provides an explicit and unique formula for system reliability assessment based on the second-order reliability bounds shown in Eq.(3.10) and an inequality equation Eq. (3.11).

3.4.2 CIM for parallel systems

System reliability formula for a parallel system can be obtained based on the formula of series system reliability by using the De Morgan's law. According to the De Morgan's law, the probability of parallel system failure can be expressed as

$$P\left(\bigcap_{i=1}^{m} \overline{E}_i\right) = 1 - P\left(\overline{\bigcap_{i=1}^{m} \overline{E}_i}\right) = 1 - P\left(\bigcup_{i=1}^{m} E_i\right) \tag{3.19}$$

where $\bar{E}_i$ is the i^{th} component failure event.

Equation (3.19) relates the probability of parallel system failure with the probability of series system safety (reliability). If we treat E_i as the i^{th} component failure event in a series system, the right side of Eq. (3.19) is then the series system reliability. Based on this relationship, the probability of parallel system failure can be

obtained from Eq. (3.18) by treating the safe events in the series system as the failure events in the parallel system as

$$P_{f\_parallel} \cong P(\overline{E_1}) - \sum_{i=2}^{m} \left\langle P(E_i) - \sqrt{\sum_{j=1}^{i-1} \left[P\left(E_i E_j\right) \right]^2} \right\rangle, \quad \langle A \rangle \equiv \begin{cases} A, & \text{if } A > 0 \\ 0, & \text{if } A \le 0 \end{cases} \tag{3.20}$$

Finally, parallel system reliability can be obtained from Eq. (3.20) by one minus the probability of system failure as

$$R_{s\_parallel} \cong P(E_1) + \sum_{i=2}^{m} \left\langle P(E_i) - \sqrt{\sum_{j=1}^{i-1} \left[P\left(E_i E_j\right) \right]^2} \right\rangle, \quad \langle A \rangle \equiv \begin{cases} A, & \text{if } A > 0 \\ 0, & \text{if } A \le 0 \end{cases} \tag{3.21}$$

3.4.3 CIM for mixed systems

A mixed system may have various system structures. There is no unique system reliability formula available for a mixed system. This study develops a generic procedure for mixed system reliability analysis. The developed procedure is introduced below with an arbitrary mixed system structure. Considering a mixed system with *N* components, the following procedure can be proceeded to carry out system reliability analysis.

Step I: Constructing a system structure matrix (SS-matrix)

SS-matrix, a 3-by-*M* matrix, is proposed in this study to characterize any arbitrary configuration of a given engineered system in a unified manner. With the SS-matrix, the components and their connections in a system are described with the component number and corresponding nodes numbers in a compact matrix form. This matrix form standardizes the representation of mixed system structures and facilitates the system reliability analysis in a unified way. The first row of the matrix contains component numbers, while the second and third rows correspond to the starting and end nodes of the components. Generally, the total number of columns of a SS-matrix,

M, is equal to the total number of system components, *N*. In the case of complicated system structures, one component may repeatedly appear in between different sets of nodes and, consequently, *M* could be larger than *N*, for example a 2-out-of-3 system.

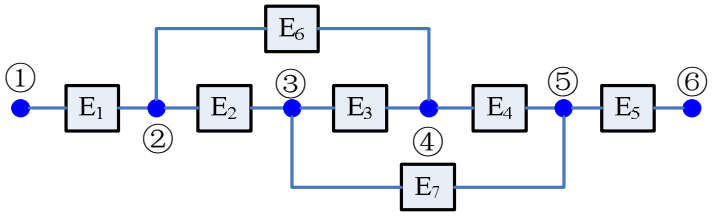

Figure 3-2: A mixed-system reliability block diagram

Let us consider a mixed system with 7 components, as shown in Fig. 3-2. The system structure matrix is a 3×7 matrix. The first column of the system structure matrix, $[1, 1, 2]^T$, indicates that the 1st component connects nodes 1 and 2. The SS-matrix for the system in Fig. 3-2 can be constructed as

$$\text{SS-matrix} = \begin{bmatrix} 1 & 2 & 3 & 4 & 5 & 6 & 7 \\ 1 & 2 & 3 & 4 & 5 & 2 & 3 \\ 2 & 3 & 4 & 5 & 6 & 4 & 5 \end{bmatrix}$$

Step II: Finding system path sets based on the SS-matrix

Based on the SS-matrix, the Binary Decision Diagram (BDD) technique can be employed to find the mutually exclusive system path sets, of which each path set is a series system. With the system structure characterized in a uniform way with a compact SS-matrix, the BDD technique can automatically identify the mutually exclusive path sets. Thus, the SS-matrix standardizes the representation of the structures of any given mixed system and facilitates the automatic system reliability analysis in a uniform way. More information on the BDD can be found in references [Lee 1959; Akers 1978]. For the mixed system shown in Fig. 3-2, the mutually exclusive path sets can be found using the BDD as

$$\text{Pathset} = \left\{ E_1E_2E_3E_4E_5,\ E_1\overline{E}_2E_6E_4E_5,\ E_1E_2\overline{E}_3E_7E_5,\ E_1\overline{E}_2E_6\overline{E}_4E_3E_7E_5 \right\}$$

Step III: Evaluating all mutually exclusive path sets and system reliability

Due to the mutual exclusiveness, the mixed system reliability, R_{s_mixed}, is the sum of the probabilities of all paths as

$$R_{s\_mixed} = \Pr\left(\bigcup_{i=1}^{N_p} \text{Path}_i \right) = \sum_{i=1}^{N_p} \Pr\left(\text{Path}_i\right) \tag{3.22}$$

where Path_i is the i^{th} mutually exclusive path set obtained by the BDD and N_p is the total number of mutually exclusive path sets. For the system in Fig. 3-2, the system reliability can be calculated as

$$\begin{aligned} R_{s\_mixed} &= \Pr\left(\bigcup_{i=1}^{4} \text{Path}_i \right) = \sum_{i=1}^{4} \Pr\left(\text{Path}_i\right) \\ &= \Pr(E_1E_2E_3E_4E_5) + \Pr(E_1\overline{E}_2E_6E_4E_5) + \Pr(E_1E_2\overline{E}_3E_7E_5) + \Pr(E_1\overline{E}_2E_6\overline{E}_4E_3E_7E_5) \end{aligned} \tag{3.23}$$

where the probability of each individual path set can be calculated using the series system reliability formula in Eq.(3.18).

3.5 Generalized CIM framework for system reliability analysis

As a series system or a parallel system can be viewed as a special case of a mixed system, the proposed generalized CIM framework with the SS-matrix and BDD can perform system reliability analysis with any system structures (e.g., series, parallel, and mixed). Figure 3-3 shows a generalized CIM framework for system reliability. As shown in the figure, the first step of the system reliability analysis using the CIM framework is to prepare the input system information which includes the limit state functions for system components, the system structure of all system components, and the statistical information for system random input variables. With system

information as input, the CIM will go through a four-step process for the system reliability analysis, (1) constructing SS-matrix, (2) evaluating CI-matrix using one of probability analysis methods as introduced in chapter 2, (3) identify mutually exclusive path sets using BDD with the SS-matrix, and (4) evaluation the probability of each path set using CIM system reliability formula of series systems. After finishing the process of system reliability analysis, CIM will provide the output of reliability of each component, probability of each joint failure event, and the system reliability.

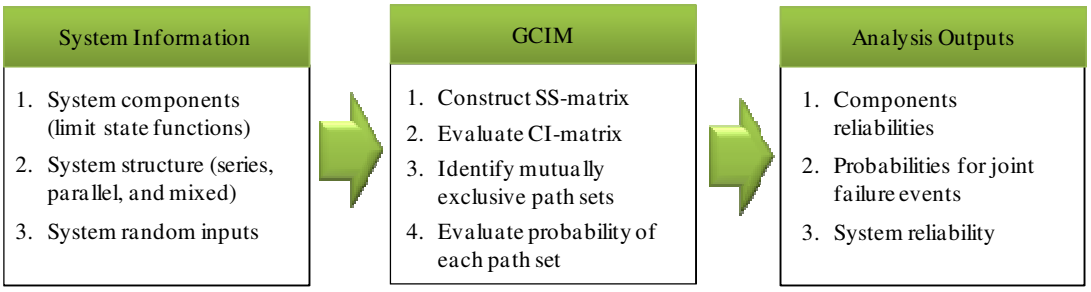

Figure 3-3: A generalized CIM framework for system reliability analysis

3.6 Case Studies

This section attempts to demonstrate the feasibility of the proposed CIM for system reliability analysis. Four engineering case studies are used to demonstrate the numerical efficiency and accuracy of the proposed CIM for system reliability analysis. First of all, the CIM, the first-order system reliability bound methods method and the second-order system reliability bounds method are employed for system reliability analysis. Their results are compared with that from MCS. This study demonstrates how accurately the CIM estimates system reliability for serial

systems. Then, the CI-matrix in the CIM is evaluated using three different reliability methods: FORM, SORM, and the EDR method.

3.6.1 Series System: Vehicle Side Impact Problem

The vehicle side crash analysis example is employed here for system reliability analysis. In this study, the response surfaces for the vehicle side impact model (10 constraints and 11 random variables) are employed in this study and they are found in Appendix B. Random variables and their random properties are summarized in Table 3-1. System reliability analyses are performed at the eight different design points listed in Table 3-2. These design points are the optimum designs from RBDO using FORM with eight different target reliability levels. As what has been done in the previous example, the study on mathematical errors in the formula of different system reliability methods are first carried out. Then numerical error is investigated with different numerical methods for reliability assessment.

First, three different system reliability analysis are compared to observe mathematical errors in their formulae for system reliability assessment. This study employs the first-order bounds method, the second-order bounds method, and the CIM To minimize numerical errors in system reliability estimates, the MCS with 1,000,000 sample points is employed to evaluate the probabilities of the component safety (or failure), CI, and the second-order joint events. Results for system reliability assessment are summarized in Table 3-3 and shown in Fig. 3-4. It is found that the second-order bounds method gives much narrower bounds than the first-order regardless of the reliability levels. The reliability bounds become narrower as

reliability level increases. In summary, the CIM provides more accurate results at all reliability levels, compared to the first- and second-order bounds methods.

Second, this study attempts to observe numerical error in system reliability that is given by numerically evaluating the system reliability formula of the CIM in Eq. (3.18). The system reliability formula is numerically computed using three different numerical methods: FORM, SORM and the EDR method. Again, system reliabilities are evaluated at eight different designs. The results from FORM, SORM, and the EDR method are also compared with those from MCS with one million sample points, as shown in Table 3-4 and Fig. 3-5. The MCS results are reported with confidence intervals MCS low bound (MCS_LB) and MCS upper bound (MCS_UB) according to the discussion in Chapter 2. Tables 3-4 and 3-5 summarize the results of numerical accuracy and efficiency, respectively. It is also found that the EDR method is much more accurate and efficient than MPP-based methods (FORM/SORM) for system reliability assessment because of highly nonlinear behavior of the CI events. Again, the CIM results using the EDR method is least influenced by the reliability levels unlike using FORM or SORM, as shown in Fig. 3-5. The CIM using the EDR method appears to be very accurate and efficient method for system reliability prediction.

Table 3-1: Properties of random variables in vehicle side impact example

Random Variables	Distr. Type	Std Dev.
X_1 (B-pillar inner) [mm]	Normal	0.050
X_2 (B-pillar reinforce) [mm]	Normal	0.050
X_3 (Floor side inner) [mm]	Lognormal	0.050
X_4 (Cross member) [mm]	Lognormal	0.050
X_5 (Door beam) [mm]	Uniform	0.050
X_6 (Door belt line) [mm]	Uniform	0.050
X_7 (Roof rail) [mm]	Uniform	0.050
X_8 (Mat. B-pillar inner) [GPa]	Gumbel	0.006
X_9 (Mat. Floor side inner) [GPa]	Gumbel	0.006
X_{10} (Barrier height) [mm]	Normal	10.00
X_{11} (Barrier hitting) [mm]	Normal	10.00

Table 3-2: Eight different design points for system reliability for VSI example

Optimum design points	Mean Values for Random Variables										
	X_1	X_2	X_3	X_4	X_5	X_6	X_7	X_8	X_9	X_{10}	X_{11}
1	0.5	1.2669	0.5	1.2298	0.5532	1.5	0.5	0.345	0.1920	0	0
2	0.5	1.2786	0.5	1.2364	0.5680	1.5	0.5	0.345	0.1920	0	0
3	0.5	1.2918	0.5	1.2438	0.5840	1.5	0.5	0.345	0.1920	0	0
4	0.5	1.3071	0.5	1.2524	0.7097	1.5	0.5	0.345	0.1920	0	0
5	0.5	1.3264	0.5	1.2634	0.7389	1.5	0.5	0.345	0.1920	0	0
6	0.5	1.3551	0.5	1.2801	0.8149	1.5	0.5	0.345	0.1920	0	0
7	0.5	1.3876	0.5	1.2998	0.8548	1.5	0.5	0.345	0.1921	0	0
8	0.5	1.4094	0.5	1.3140	0.9945	1.5	0.5003	0.345	0.2511	0	0

Table 3-3: Results of different system reliability analysis methods for VSI example: (1) MCS, (2) First-Order Bounds (FOB) using MCS, (3) Second-Order Bounds (SOB) using MCS, (4) CIM using MCS (N=1,000,000)

Methods		System Reliability at each point							
		1	2	3	4	5	6	7	8
FOB	Lower	0	0.0961	0.2395	0.4606	0.5867	0.7267	0.8319	0.8748
	Upper	0.4763	0.5269	0.5799	0.6378	0.7055	0.788	0.8589	0.8937
SOB	Lower	0.2307	0.3036	0.3869	0.5248	0.6225	0.7415	0.8379	0.8812
	Upper	0.2992	0.3491	0.4146	0.5267	0.6235	0.7424	0.8382	0.8822
CIM		0.2511	0.3158	0.3935	0.5257	0.6226	0.7416	0.8379	0.8814
MCS		0.2621	0.326	0.4017	0.5267	0.6227	0.7417	0.838	0.8815
MCS_LB		0.2608	0.3246	0.4002	0.5252	0.6212	0.7404	0.8369	0.8805
MCS_UB		0.2634	0.3274	0.4032	0.5282	0.6242	0.743	0.8391	0.8825

Table 3-4: Results of system reliability analysis using CIM with different numerical reliability methods for VSI example: (1) FORM, (2) SORM, and (3) EDR

Analysis	System Reliability							
Methods	1	2	3	4	5	6	7	8
CIM-FORM	0.4331	0.52	0.637	0.747	0.8276	0.9177	0.9648	0.9809
CIM-SORM	0.4022	0.4824	0.5721	0.6963	0.7585	0.8581	0.929	0.9569
CIM-EDR	0.2659	0.3288	0.4013	0.5135	0.614	0.7253	0.8271	0.8772
MCS	0.2621	0.3260	0.4017	0.5267	0.6227	0.7417	0.8380	0.8815
MCS_LB	0.2608	0.3246	0.4002	0.5252	0.6212	0.7404	0.8369	0.8805
MCS_UB	0.2634	0.3274	0.4032	0.5282	0.6242	0.7430	0.8391	0.8825

Table 3-5**:** Efficiency of system reliability analysis using CIM with different numerical reliability methods for VSI example: (1) FORM, (2) SORM, and (3) EDR

Methods	EDR	FORM	SORM	MCS
Total number of function evaluation	23	280	280	1,000,000
Total number of sensitivity evaluation	0	280	280	0
Hessian Matrix Evaluation	0	0	55	0

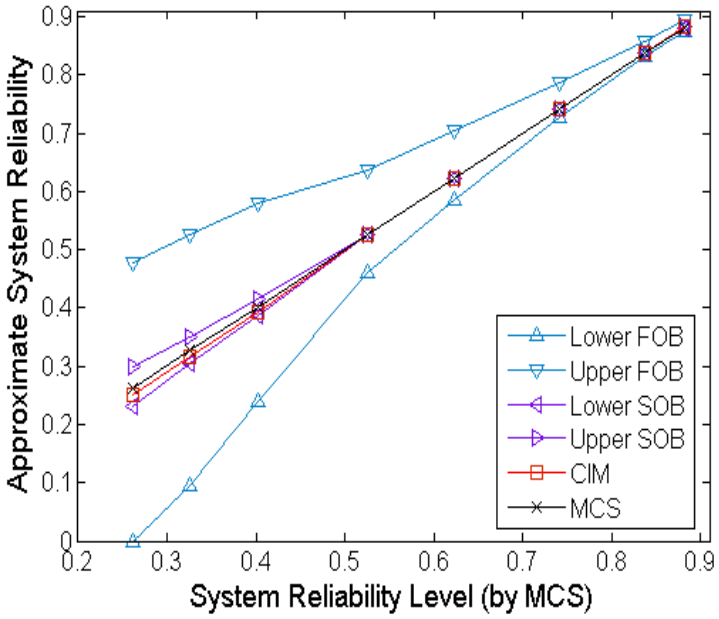

Figure 3-4: Accuracy of system reliability analysis at eight design points for VSI Example

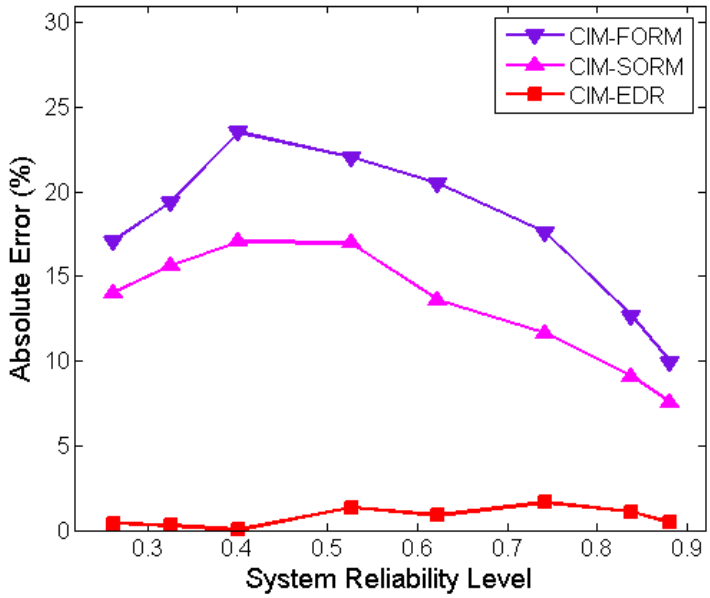

Figure 3-5: Absolute errors in system reliability [%] for VSI example

3.6.2 Series System: Probabilistic Fatigue Analysis for Large Sea Vessel

Fatigue failure is commonly found in maritime ship structures and spectral fatigue analyses are often used for predicting the structural lives of maritime ship structures. In this study, fatigue lives of large sea vessel connection ends are considered and the fatigue system reliability is determined by using CIM with EDR method. It has been reported that the most critical spot for fatigue failure are longitudinal and Transverse Connection as shown in Fig. 3-6. The finite element (FE) model for this study is shown in Fig. 3-7 with the model information in Table 3-6. In this study 4 end connections with totally 8 weld hot-spots (each end has one weld heel and weld toe) are considered as a series system as shown in Fig. 3-8, and the end connection in this model is shown in Fig. 3-9.

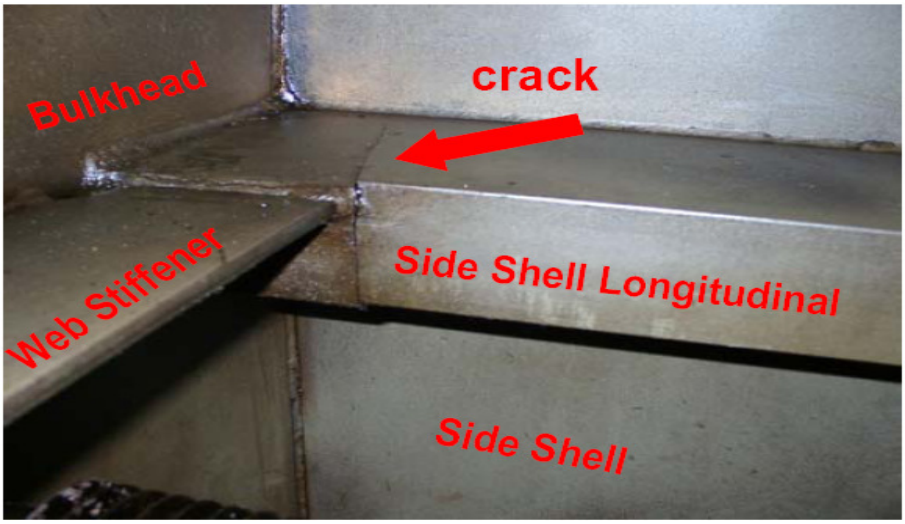

Figure 3-6: Large Sea Vessel End Connections

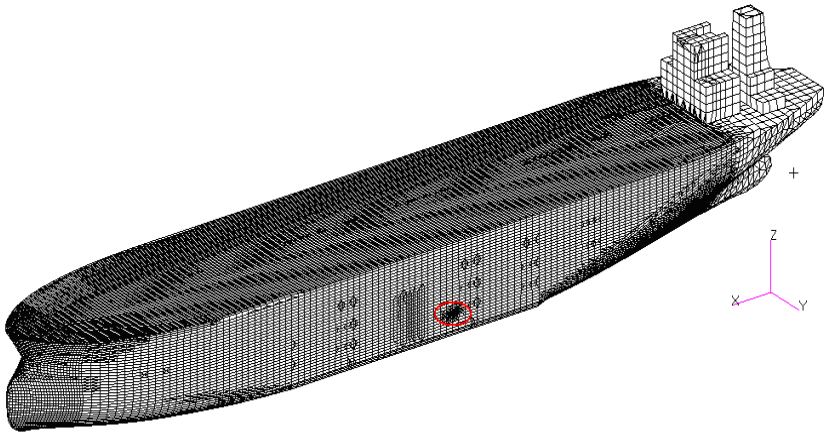

Figure 3-7: FE model for a large sea vessel

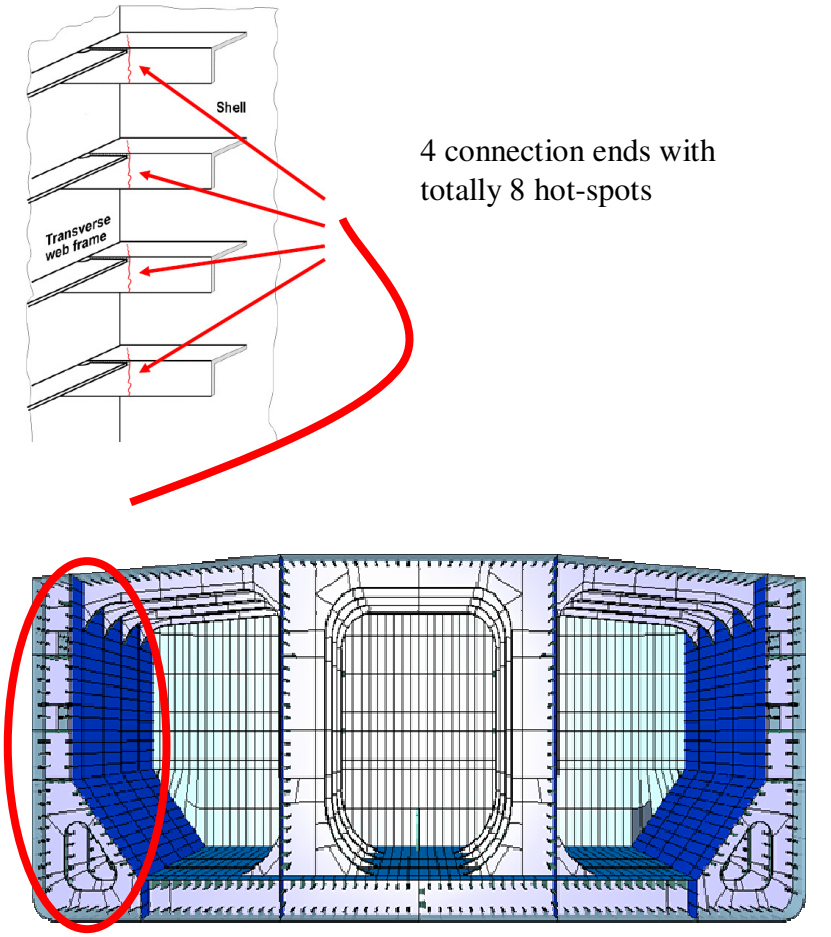

Figure 3-8: Definition of system components

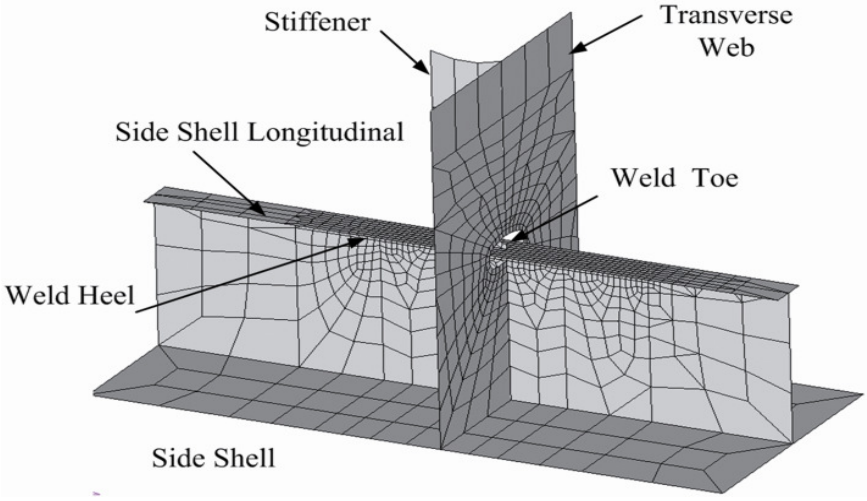

Figure 3-9: Longitudinal end connections

Table 3-6: Model information (DOF = 789,000)

Model Component		Amount
Node		131,511
Elements	QUAD4	137,387
	TRIA3	18,959
	BAR	65,697
	ROD	68,157

The uncertainties present in this analysis are the loading factors (e.g., wave height and period) and material properties. The variability of the loading factors is accounted for in the development of the stress response spectrum [Youn et al. 2007]. Even if geometric tolerances are uncertain, small variances in the geometric tolerances of a large vessel will not be a significant contributor to the overall reliability of the welded components. On the other hand, the uncertainties of the S/N curve can be taken into consideration in the fatigue model after the FE analysis. A total of four parameters of the S/N curve can be considered, c, the S-N curve life intercept, m_1, the negative inverse slope preceding the transition point, m_2, the negative inverse slope following the transition point, T_p and the location of the transition point. The statistical information of these random variables is located in Table 3-7. The response value being attained through this fatigue analysis is cumulative fatigue damage ratios, D, (= designed life/fatigue life), where the designed life is 20 years. The structure is safe for fatigue when D is less than one. In order to determine the reliability, the EDR method is used with a 4N+1 eigenvector samples. Using EDR method, the CI-matrix is obtained as shown in Fig. 3-10 and accordingly

the system reliability for fatigue is obtained through CIM as 03877. Based on this calculation, we can also obtain the approximated first-order system reliability bounds as: $0.3456 \leq R_s \leq 0.3975$. In order to verify the fatigue system reliability result, a Monte Carlo simulation (MCS) is performed, using 1,000 samples. Both the EDR and MCS results are shown in Table 3-8. It is found that the EDR method with 17 fatigue analyses gives a good agreement with the MCS in reliability prediction.

Table 3-7: Statistical parameters of S/N curve

Variable	c	m_1	m_2	T_p
Distribution	~N(1.52e12,7.6e10^2)	~N(3,0.075^2)	~N(5,0.25^2)	~N(1e7,5e5^2)

$$CI_{fatigue} = \begin{bmatrix} 0.3975 & 0.5736 & 0.6093 & 0.6092 & 0.6114 & 0.6090 & 0.5986 & 0.6109 \\ & 0.9564 & 0.0430 & 0.0430 & 0.0419 & 0.0431 & 0.0395 & 0.0421 \\ & & 1 & 1.5E-6 & 4.7E-5 & 9.4E-7 & 0.0085 & 2.2E-5 \\ & & & 1 & 4.2E-5 & 6.5E-7 & 0.0085 & 1.9E-5 \\ & & & & 0.9999 & 3.5E-5 & 0.0089 & 0.0001 \\ & & & & & 1 & 0.0084 & 1.6E-5 \\ & & & & & & 0.9918 & 0.0086 \\ & & & & & & & 1 \end{bmatrix}$$

Figure 3-10: CI-matrix for the sea vessel fatigue reliability analysis

Table 3-8: Comparison of results from EDR and MCS

	System Reliability	Error	Analysis
CIM_EDR	0.3877	1.09%	17
CIM_MCS	0.3960	0.00%	1,000
MCS	0.3960 (0.3496 ~ 0.4424)	N/A	

3.6.3 Parallel System: A Brittle Ten-Bar System

The following ten-bar system example is used to demonstrate the effectiveness of the CIM framework for parallel systems. As shown in Fig. 3-11, ten brittle bars are connected in parallel to sustain a load applied at one end. This case study is modified from the example employed in the work [Mahadevan et al. 2001] by increasing the total number of bars from 2 to 10. Ten bars are all brittle with different fracture strain limits ε_{fi}, $1 \le i \le 10$, which are sorted in an ascending order. If the exerted strain ε is between the $(i-1)^{th}$ and i^{th} fracture strain limits, i.e., $\varepsilon_{f(i-1)} \le \varepsilon < \varepsilon_{fi}$, , bar components with fracture strains below ε_{fi} will fail, and the allowable load is then the sum of the strength of components with fracture strains equal to or above ε_{fi}. Therefore, the strain level corresponding to the overall maximum allowable load is among the ten fracture strain limits. As the overall maximum allowable load, the system strength R_T can be formulated in Eq.(3.24).

$$R_T = \max_{1\le i\le 10}\left\{\sum_{j=i}^{10} R_j(\varepsilon_{fi})\right\} = \max\left\{\sum_{j=1}^{10} R_j(\varepsilon_{f1}),\quad \sum_{j=2}^{10} R_j(\varepsilon_{f2}),\quad \cdots,\quad R_{10}(\varepsilon_{f10})\right\} \tag{3.24}$$

For example, if the exerted strain ε is equal to the fracture strain ε_{f2}, the 1^{st} brittle bar fails due to the fracture and no longer contributes to the overall system strength. Thus, the system strength R_T at this fracture strain is the sum of strength of the other nine brittle bars. The brittle bar system fails to sustain the load F only if the system strength at any of the ten fracture strains is smaller than the load F. This is a parallel system with ten components, corresponding to the ten fracture strains. The component safety events can be expressed in terms of several random variables.

$$G_i = F - \sum_{j=i}^{10} R_j(\varepsilon_{fi}) = F - \sum_{j=i}^{10} (E_j A_j)\cdot \varepsilon_{fi}, \qquad 1 \le i \le 10 \tag{3.25}$$

where R_j represents the allowable load that can be sustained by the j^{th} brittle bar, A_j the cross section area of the j^{th} brittle bar, and E_j the Young's modulus of the j^{th} brittle bar.

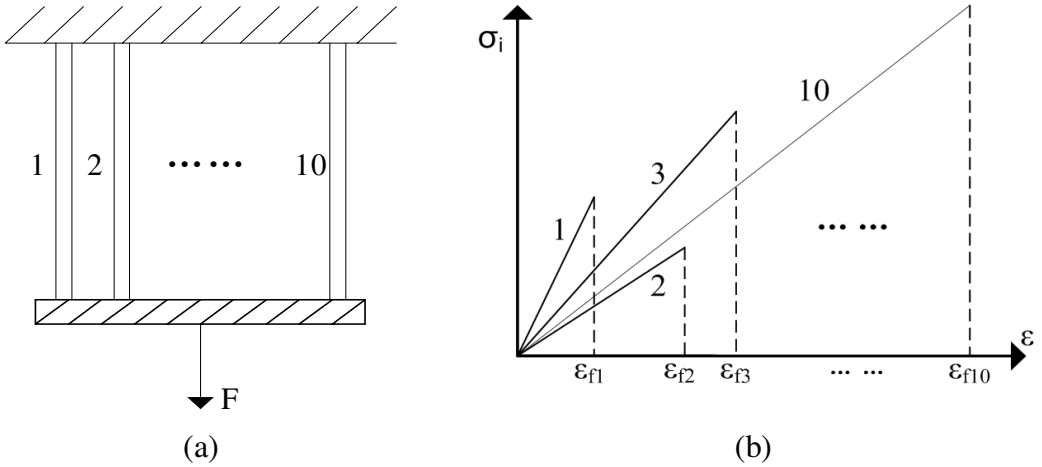

Figure 3-11: Ten brittle bar parallel system:
(a) system structure model; (b) brittle material behavior in parallel system

Random variables and their random properties are summarized in Table 3-9. Ten different system reliability levels are used for comparison with ten different loading conditions (F). These loading points are used to validate the CIM method at different reliability levels. Table 3-10 summarizes the results of system reliability analyses which are illustrated in Fig. 3-12. It can be seen that the first-order bounds are too wide to be of practical use. Whereas, the second-order bounds method gives tighter system reliability bounds compared with the first order bounds method. The CIM method provides more accurate results at all reliability levels and its high accuracy is maintained at high reliability levels, which are often encountered in engineering practices. Similar to the first case study, only the first and second order CI events were considered and the error for the CIM comes from the effects of the third- or

higher-order CI events. However, for a parallel system these effects tend to decrease as the system reliability decreases, thus the error at a low system reliability level is smaller than that at a higher system reliability level, as observed from Fig. 3-12.

Table 3-9: Statistical information of input random variables for the ten bar system

Random Variable	Mean	Standard eviation	Distribution Type
E_1-E_{10} (GPa)	200.0	10.0	Gumbel
A_1 (mm^2)	100.0	5.0	Lognormal
A_2 (mm^2)	120.0	5.0	Lognormal
A_3 (mm^2)	140.0	5.0	Lognormal
A_4 (mm^2)	140.0	10.0	Lognormal
A_5 (mm^2)	140.0	10.0	Lognormal
A_6 (mm^2)	150.0	10.0	Lognormal
A_7 (mm^2)	150.0	15.0	Lognormal
A_8 (mm^2)	150.0	15.0	Lognormal
A_9 (mm^2)	200.0	15.0	Lognormal
A_{10} (mm^2)	300.0	25.0	Lognormal
ε_{f1}	0.0010	0.0002	Uniform
ε_{f2}	0.0012	0.0003	Uniform
ε_{f3}	0.0018	0.0004	Uniform
ε_{f4}	0.0025	0.0005	Uniform
ε_{f5}	0.0027	0.0006	Uniform
ε_{f6}	0.0030	0.0007	Uniform
ε_{f7}	0.0033	0.0008	Uniform
ε_{f8}	0.0036	0.0009	Uniform
ε_{f9}	0.0040	0.0010	Uniform
ε_{f10}	0.0050	0.0011	Uniform
F (kN)	---	30.0	Normal

Table 3-10: Results of system Reliability analysis with MCS, FOB using MCS, SOB using MCS, and CIM using MCS (N=1,000,000)

Analysis Method		System Reliability Level at Each Design									
		1	2	3	4	5	6	7	8	9	10
FOB	Upper	0.4133	0.5639	0.7331	0.9216	1	1	1	1	1	1
	Lower	0.1594	0.2054	0.2507	0.2974	0.3444	0.4395	0.4865	0.5334	0.5803	0.9705
SOB	Upper	0.3537	0.467	0.5854	0.7065	0.8293	1	1	1	1	1
	Lower	0.3192	0.4062	0.4849	0.5507	0.6068	0.6917	0.7161	0.7459	0.7897	0.9943
CIM		0.3417	0.4456	0.549	0.6482	0.7388	0.8714	0.9017	0.9069	0.9051	0.9943
MCS		0.3301	0.4272	0.5226	0.6131	0.6961	0.8314	0.8813	0.9192	0.9476	0.9998
MCS_LB		0.3287	0.4257	0.5211	0.6116	0.6947	0.8303	0.8803	0.9184	0.9469	0.9998
MCS_UB		0.3315	0.4287	0.5241	0.6146	0.6975	0.8325	0.8823	0.92	0.9483	0.9998

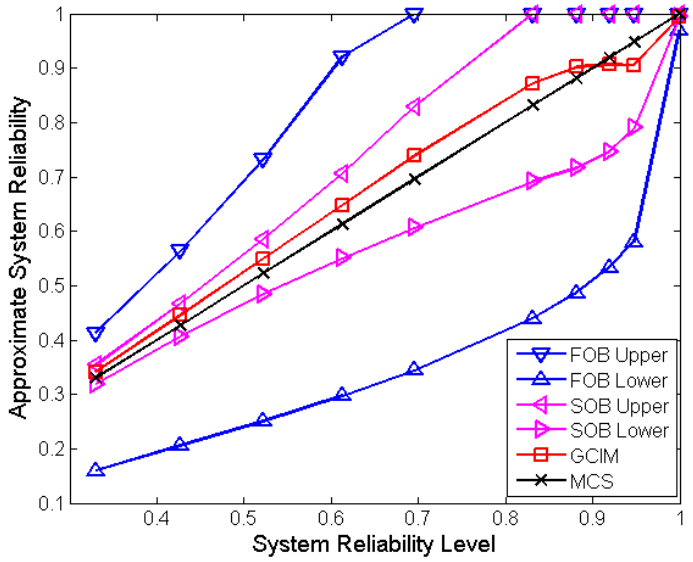

Figure 3-12: Results of system reliability analysis at ten different reliability levels

3.6.4 Mixed System: Power Transformer Winding Joint System

Power transformers are among the most expensive elements of high-voltage power systems [Rivera et al. 2000]. The power transformer vibration induced by the magnetic field loading will cause the windings support joint loosening or the fatigue failures, which will gradually increase the vibration amplitude of the winding and eventually damage the core [Kim et al. 2009]. In this case study the proposed CIM is applied for the system reliability analysis of the power transformer winding support joints. We considered four failure modes, which are the fatigue failures at the four winding support joints. A power transformer simulation model was built using the finite element analysis tool ANSYS 10 (see Fig. 3-13). Figure 3-14 shows the detail of the winding bolt joint, which assembles the windings of the power transformer with the bottom fixture. The transformer is fixed at the bottom and the vibration load

is applied to the magnetic core with the frequency of 120 Hz. This case study employed ten random variables, as listed in Table 3-11, which include the geometric tolerances and material properties

This winding support system with the four joints was treated as a 3-out-of-4 system as shown in Fig. 3-15, which means that the system becomes safe only if at least three out of the four support joints survive. The CI-matrix for this case study was evaluated using the MCS (with 1000 samples), as shown in Fig. 3-16. Figure 3-17 shows the system reliability block diagram and Table 3-12 displays the SS-matrix for this transformer joint system. The mutually exclusive path sets can be determined using the BBD (see Fig. 3-18) as

$$\text{Pathset} = \left\{ E_1 E_2 E_3,\ \overline{E}_1 E_2 E_3 E_4,\ E_1 \overline{E}_2 E_3 E_4,\ E_1 E_2 \overline{E}_3 E_4 \right\}$$

These path sets are mutually exclusive with the series system structure, as discussed in Section 3.4. As shown in Table 3-13, the reliabilities for these mutually exclusive path sets can be obtained and the system reliability for this transformer joint system can be estimated using Eq. 17. It is found that the CIM accurately assesses system reliability compared with the MCS. This demonstrates the feasibility and great capability of the CIM for system reliability analysis with any system structure.

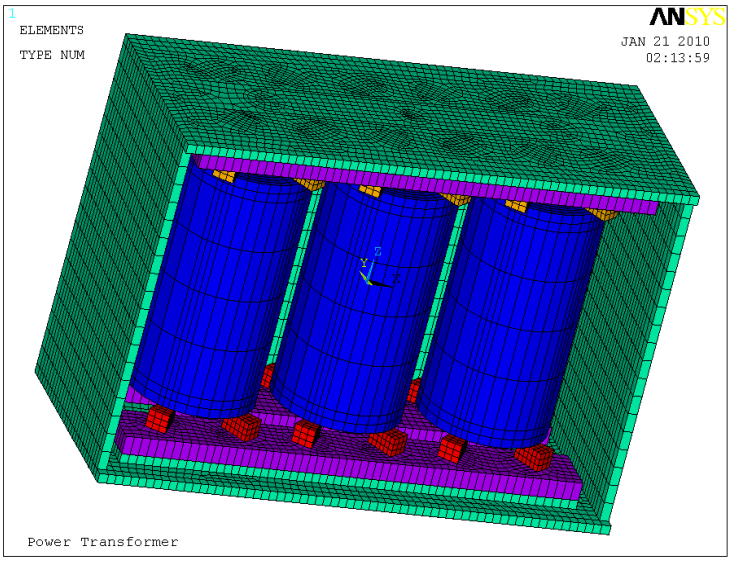

Figure 3-13: A power transformer FE model (without the covering wall)

Table 3-11: Random property of input variables for the power transformer

Random Variable	Physical Meaning	Mean	Standard Deviation	Distribution Type
X_1	Wall Thickness	3	0.06	Normal
X_2	Angular width of joints	15	0.3	Normal
X_3	Height of support joints	6	0.12	Normal
X_4	Young's modulus of joints	2e12	4e10	Normal
X_5	Young's modulus of loosening joints	2e10	4e8	Normal
X_6	Young's modulus of winding	1.28e12	3e10	Normal
X_7	Poisson ratio of joints	0.27	0.0054	Normal
X_8	Poisson ratio of winding	0.34	0.0068	Normal
X_9	Density of joints	7.85	0.157	Normal
X_{10}	Density of windings	8.96	0.179	Normal

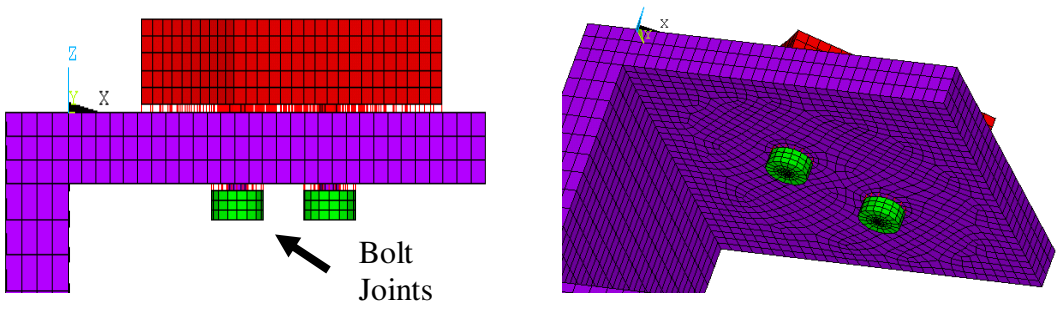

(a) Side view of one joint (b) Bottom view of the bolt joint

Figure 3-14: Winding support bolt joint: (a) side view, (b) bottom view

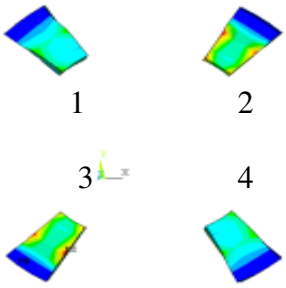

Figure 3-15: 3 out of 4 system with 4 support joints

$$\text{CI-matrix} = \begin{bmatrix} 0.999 & 0.000 & 0.238 & 0.242 \\ 0.000 & 0.999 & 0.238 & 0.242 \\ 0.000 & 0.000 & 0.761 & 0.008 \\ 0.000 & 0.000 & 0.000 & 0.757 \end{bmatrix}$$

Figure 3-16: CI-matrix for the power transformer case study

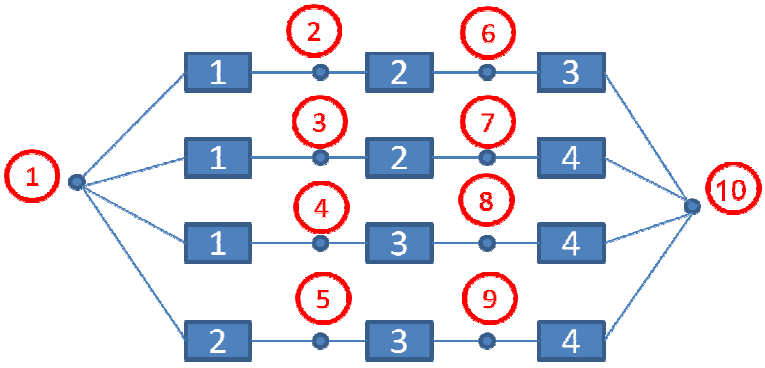

Figure 3-17: System reliability block diagram for power transformer case study

Table 3-12: System structure matrix for the power transformer case study

Component No.	1	1	1	2	2	2	3	3	3	4	4
Starting node	1	1	1	1	2	3	4	5	6	7	8
End node	2	3	4	5	6	7	8	9	10	10	10

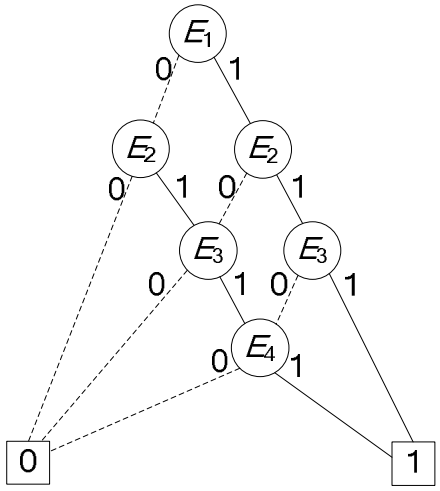

Figure 3-18: BDD for the power transformer case study

Table 3-13: Results of CIM for power transformer case study comparing with MCS (1,000 samples):

Analysis Method	Reliability of Path Set (Series System)				System Reliability
	$E_1E_2E_3$	$\bar{E}_1E_2E_3E_4$	$E_1\bar{E}_2E_3E_4$	$E_1E_2\bar{E}_3E_4$	
CIM	0.761	0.000	0.000	0.002	0.763
MCS	-	-	-	-	0.763 (0.7227~ 0.8033)

3.7 Summary

In this chapter, the CIM was proposed to evaluate system reliability for series system, parallel and mixed systems. The proposed method makes the five technical contributions as:

(1) Definition of the CI event: The key idea of the proposed method is the definition of the CI event. This definition enables the decomposition of the probability of an N^{th}-order joint safety event into the probabilities of the first to N^{th}-order CI events;

(2) Analytic expression for the probability of any higher-order joint event by the probability decomposition theorem: The probability of any second or higher-order joint event can be analytically expressed in terms of the probabilities of the CI events.

(3) Easy numerical assessment of system reliability: Through the analytic expression for system reliability, it can be assessed by simply evaluating the probabilities of the CI events using advanced reliability analysis methods (e.g., Dimension Reduction (DR), polynomial chaos expansion (PCE), stochastic collocation method).

(4) A general framework of system reliability analysis: Regardless of a system structure (e.g., series, parallel, and mixed), the CIM can execute system reliability analysis in a generic manner;

(5) The CI-matrix facilitates to compute system reliability for large-scale system applications.

Chapter 4: Bayesian Approach to Reliability-Based Design Optimization

This chapter presents the research solution to the second challenging question which is how limited data for input manufacturing variability can be used in RBDO to ensure a high reliability of an engineered system in the early design stage. In practice, the amount of data to characterize random variables is limitedly given due to the lack of resources (e.g., time, budget, facility, and human). This chapter presents a Bayesian reliability-based design optimization (Bayesian RBDO) framework as a detail design tool for an engineered system when the amount of the data is lacking. Section 4.1 presents the Bayesian updating technique and the Bayesian binomial inference model for reliability modeling. Section 4.2 presents the Bayesian reliability analysis with lack of data and Section 4.3 derives the sensitivity of Bayesian reliability with respect to random input variables. The Bayesian RBDO is formulated in Section 4.4 and case studies are presented in Section 4.5. Section 4.6 summarizes this chapter.

4.1 Bayesian Updating and Binomial Inference

This section gives an introduction of the Bayesian updating technique and the Bayesian binomial inference model.

4.1.1 Bayesian updating

Let X be a random variable with a probability density function $f(x,\theta)$, $\theta \in \Omega$. From the Bayesian point of view, θ is interpreted as a realization of a random

variable Θ with a probability density $f_\Theta(\theta)$. The density function expresses what one thinks about the occurring frequency of Θ before any future observation of X is taken, that is, a prior distribution. Based on Bayes' theorem, the posterior distribution of Θ given a new observation X can be expressed as

$$f_{\Theta|X}(\theta \mid x) = \frac{f_{X,\Theta}(x,\theta)}{f_X(x)} = \frac{f_{X|\Theta}(x \mid \theta) \cdot f_\Theta(\theta)}{f_X(x)} \tag{4.1}$$

The Bayesian approach is used for updating information about the parameter θ. First, a prior distribution of Θ must be assigned before any future observation of X is taken. Then, the prior distribution of Θ is updated to the posterior distribution as the new data for X is employed. The posterior distribution is set to a new prior distribution and this process can be repeated with an evolution of data sets. In Bayesian probability theory, a class of prior probability distributions $f_\Theta(\theta)$ is said to be conjugate to a class of likelihood functions $f_{X|\Theta}(x|\theta)$ if the resulting posterior distributions $f_{\Theta|X}(\theta|x)$ are in the same family as $f_\Theta(\theta)$. For example, if the likelihood function is Gaussian, choosing a Gaussian prior ensures that the posterior distribution is also Gaussian. A Bayesian inference model is called a conjugate model if the conjugate prior distribution is used. For conjugate Bayesian inference models, the updating results are independent of the sequence of data sets. Conjugate models of Bayesian updating are quite useful for uncertainty modeling with evolving data sets, since the prior and posterior distributions are given in a closed form. However, it is found that the Bayesian updating results often depend on the selection of a prior distribution in the conjugate models. Besides, the available conjugate Bayesian models are limited. To eliminate the dependency and the limitation, non-conjugate

Bayesian updating models can be developed using Markov Chain Monte Carlo (*MCMC*) methods. This is, however, more computationally intensive.

4.1.2 Bayesian Binomial inference model

In many engineering applications, outcomes of events from repeated trials can be a binary manner, such as occurrence or nonoccurrence, success or failure, good or bad, etc. In such cases, random behavior can be modeled with a discrete probability distribution model. In addition, if the events satisfy the additional requirements of a Bernoulli sequence, that is to say, if the events are statistically independent and the probability of occurrence or nonoccurrence of events remains constant, they can be mathematically represented by the binomial distribution. In other words, if the probability of an event occurrence in each trial is r and the probability of nonoccurrence is $(1-r)$, then the probability of x occurrences out of a total of N trials can be described by the probability mass function (PMF) of a Binomial distribution as

$$\Pr\left(X = x, N \mid r\right) = \binom{N}{x} r^{x} \left(1-r\right)^{N-x} \quad x = 0,1,2,\ldots,N \tag{4.2}$$

where the probability of success identified in the previous test, r, is the parameter of the distribution.

In Eq.(4.2), the probability of x/N (x occurrences out of N trials) can be calculated when a prior distribution on r is provided. This inference process seeks to update r based on the outcomes of the trials. Given x occurrences out of a total of N trials, the probability distribution of r can be calculated using Bayes' Rule as

$$f\left(r \mid x\right) = \frac{f\left(x \mid r\right) f\left(r\right)}{\int_0^1 f\left(x \mid r\right) f\left(r\right) dr} \tag{4.3}$$

where $f(r)$ is the prior distribution of r, $f(r \mid x)$ is the posterior distribution of r and $f(x \mid r)$ is the likelihood of x for a given r. The integral in the denominator is a normalizing factor to make the probability distribution proper. The prior distribution is known for r, prior to the current trials. In this study, a uniform prior distribution is used to model r bounded in [0, 1]. However, it is possible to obtain a posterior distribution with any type of a prior distribution.

For use of this Bayesian inference model, both a prior reliability distribution (r) and the number (x) of safety occurrences out of the total number of test data sets N must be known. If the prior reliability distribution (r) is unavailable, it will be simply modeled with a uniform distribution, $r \sim U(a, b)$ where $a < b$ and $a, b \in [0, 1]$. Bayesian binomial inference model can be used to update the prior knowledge of reliability (r), which is a parameter of a binomial distribution. In this inference model, the binomial distribution likelihood function is used for test data, whereas the conjugate prior distribution of this likelihood function is used for reliability (r), which is a Beta distribution. The PDF of the Beta distribution is expressed as

$$f(r) = \frac{1}{B(\alpha, \beta)} r^{\alpha-1} (1-r)^{\beta-1}, \quad \left(B(\alpha, \beta) = \int_0^1 t^{\alpha-1} (1-t)^{\beta-1} dt \right) \tag{4.4}$$

where α and β are two parameters. For a simple case, $\alpha = \beta = 1$ represents a uniform distribution over [0, 1]. If this uniform distribution is used as a prior distribution for r, the likelihood function $f(x|r)$ can be obtained using Eq. (4.3)and the posterior distribution $f(r|x)$ using Eq.(4.4). It follows a Beta distribution with $\alpha = x + 1$ and $\beta = N - x + 1$. This posterior distribution represents the probability distribution of reliability, which is a function of x and N. With k sets of evolving testing data sets, the final updating result for r is also a Beta distribution with

$$\alpha = 1 + \sum_{i=1}^{k} x_i \quad \text{and} \quad \beta = 1 + \sum_{i=1}^{k} \left(N_i - x_i \right) \tag{4.5}$$

As it is a conjugate Bayesian inference model, there is also no data-sequence effect on updating results.

4.2 Bayesian Reliability Analysis

When only epistemic uncertainties are used in the reliability assessment, the PDF of the reliability can be modeled using the Beta distribution in Eq. (4.4) by counting the number of safety occurrences, x. In general, both aleatory and epistemic uncertainties appear in most engineering design problems. In such situations, the PDF of reliability can be similarly obtained through Bayesian reliability analysis. To build the PDF of reliability, reliability analysis must be performed at every data point for epistemic uncertainties while considering aleatory uncertainties. Different reliability measures, $R_k = R(x_{e,k})$, are obtained at different sample points for epistemic uncertainties. In Eq.(4.5), $\alpha = x + 1$ and $\beta = N - x + 1$, where $x = \sum R_k$. Then, the PDF of reliability r with a uniform prior distribution is updated to $R(\mathrm{X}_a, \mathrm{X}_e; \mathrm{d})$ as

$$\begin{gathered} R\left(\mathbf{X}_a, \mathbf{X}_e; \mathbf{d}\right) = f\left(r \mid \bar{\mathbf{x}}\right) = \frac{1}{Beta(\alpha, \beta)} r^{a-1} (1-r)^{\beta-1} \\ \text{where } \alpha = 1 + x, \quad \beta = N - x + 1, \quad \bar{\mathbf{x}} = \left\{ \mathbf{x}_{e,1}, \cdots, \mathbf{x}_{e,N} \right\} \\ x = \sum R_k, \text{ and } R_k = \Pr\left[g(X_a) \le 0 \mid \mathbf{x}_{e,k} \right] \end{gathered} \tag{4.6}$$

N is the number of finite data sets for epistemic uncertainties. Figures 4-1 and 4-2 show such a functional relationship between the reliability distribution and its parameters, x and N. Figure 4-1 demonstrates the dependence of the reliability PDF on the number of safety occurrences, x, out of the given N trials (e.g., N = 40 in Fig. 4-1). The larger the number of safety occurrences for a given N trials, the greater the

mean of reliability. The PDF of reliability appears to be feasible, since the mean of the PDF is close to x/N, which is a Frequentist estimate of reliability (e.g., $\mu_{\text{Beta}(5,37)} \approx 4/36$). Figure 4-2 exhibits the dependence of the reliability PDF on the total number of trials (N) with the same ratio of x to N. As the total number of trials is increased, the variation of reliability is decreased, such as $\sigma_{\text{Beta}(451,151)} < \sigma_{\text{Beta}(151,51)} < \sigma_{\text{Beta}(46,16)} < \sigma_{\text{Beta}(16,6)}$. In other words, the PDF of reliability asymptotically converges to the exact reliability with the increase of the number of trials.

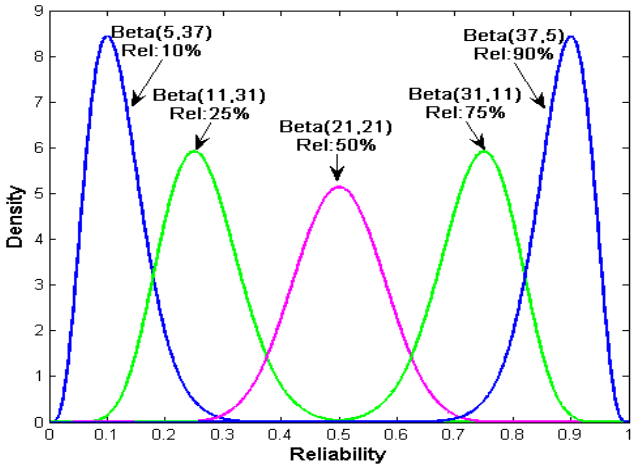

Figure 4-1: Dependence of the PDF of reliability on the number of safety occurrences, x/N

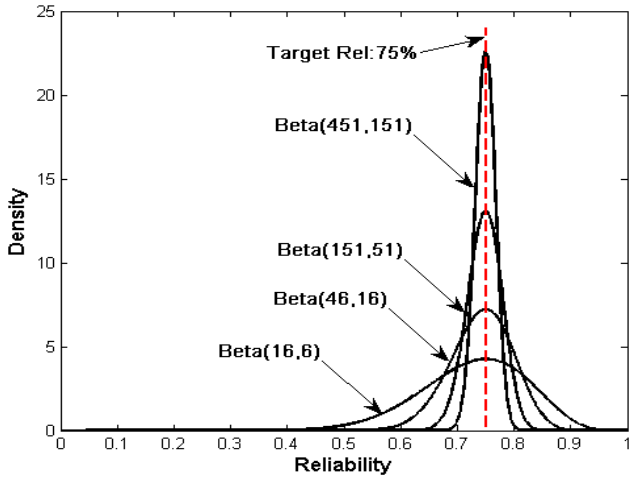

Figure 4-2: Dependence of the PDF of reliability on the total number of trials, N

For design optimization, reliability must satisfy two requirements: (a) sufficiency and (b) uniqueness. The sufficiency requirement means that the reliability must be conservative or no larger than an exact reliability realized with a sufficient amount of data for the input uncertainties. As this reliability is an estimated reliability based on the posterior reliability distribution obtained through the Bayesian updating of the prior reliability distribution, thus it is referred to as "Bayesian reliability". Then, Bayesian RBDO based on Bayesian reliability measure will provide an optimum design with higher reliability than target reliability, regardless of the data size. Depends on different applications, the designer may be desired with different confidence level of realized Bayesian reliability. This requires that Bayesian reliability can be flexibly defined based on the user-defined confidence level. Suppose that the user-defined confidence level of Bayesian reliability as C_L, and the sample size of epistemic uncertainty is N, then Bayesian reliability can be uniquely justified as

$$1-C_L=\int_0^{R_B} f_R(r)\,dr \tag{4.7}$$

This will gives the Bayesian reliability definition with the user-defined confidence level as

$$R_B=F_R^{-1}\left[1-C_L\right] \tag{4.8}$$

In the case studies of this dissertation, the confidence level in Eq. (4.8) for defining Bayesian reliability is chosen to be $\sqrt[N]{0.5}$ where N is the number of sample size. By choosing the confidence level in such a way, Bayesian reliability is exactly the median value of the extreme distribution for the smallest value derived from the Beta distribution in Eq.(4.6).

Based on the extreme distribution theory, the extreme distribution for the smallest reliability value is constructed from the reliability distribution, Beta distribution. For random reliability R with the Beta distribution function, $F_R(r)$, let ${}^1R$ be the smallest value among N data points for random reliability, R. Then the Cumulative Distribution Function (CDF) of the smallest reliability value, ${}^1R$, can be expressed as [Rao 1992]

$$\begin{aligned} 1-F_{{}^1R}(r) &= P\left({}^1R > r\right) \\ &= P\left({}^1R > r, {}^2R > r, \cdots, {}^NR > r\right) \end{aligned} \tag{4.9}$$

Since the i^{th} smallest reliability values, ${}^iR$ (i = 1,…, N), are identically distributed and statistically independent, the CDF of the smallest reliability value becomes

$$F_{{}^1R}(r) = 1-\left[1-F_R(r)\right]^N \tag{4.10}$$

Bayesian reliability, R_B, is defined as the median value of the reliability distribution. That is to say, Bayesian reliability is the solution of the nonlinear equation in Eq. (4.10) by setting $F_{{}^1R}\left(R_B\right) = 0.5$.

$$R_B = F_R^{-1}\left[1-\sqrt[N]{1-F_{{}^1R}\left(r^m\right)}\right] = F_R^{-1}\left[1-\sqrt[N]{0.5}\right] \tag{4.11}$$

Based on this definition, the confidence level o f the Bayesian reliability can be calculated as

$$C_L^B = 1-F_R\left(R_B\right) = 1-F_R\left(F_R^{-1}\left[1-\sqrt[N]{0.5}\right]\right) = \sqrt[N]{0.5} \tag{4.12}$$

Based on the above definition, Bayesian reliability analysis can be conducted using the following numerical procedure as:

STEP1 Collect a limited data set for epistemic uncertainties where the data size is N.

STEP2 Calculate reliabilities (R_k) with consideration of aleatory uncertainties at all epistemic data points.

STEP3 Build a distribution of reliability using the Beta distribution in Eq.(4.6) with aleatory and/or epistemic uncertainties.

STEP4 Construct the extreme distribution in Eq. (4.10) with the Beta distribution obtained in Step 3.

STEP5 Determine the Bayesian reliability using Eq.(4.11).

A mathematical example is used to help understand the numerical procedure of Bayesian reliability analysis.

4.3 Sensitivity Analysis of Bayesian Reliability

The sensitivity analysis for Bayesian reliability with respect to design variables must also be carried out for Bayesian RBDO. Direct calculation of the sensitivities of Bayesian reliability follows a complicated mathematical derivation and implementation and may encounter numerical singularity [Youn and Wang 2008a], thus a more simple way is sought. The idea comes from a one-to-one mapping between Bayesian reliability and the mean value of the Beta distribution (the posterior distribution) for reliability for a given sample size, $R_i^B=R_i^B(M_i)$ or $M_i=M_i(R_i^B)$. The transform between these two values is shown in the equation

$$1-C_L=\int_0^{R_B}\frac{1}{B(p,q)}\theta^p(1-\theta)^q\,d\theta \tag{4.13}$$

where $p=(N+2)M_i$, $q=(N+2)(1-M_i)$. Instead of Bayesian reliability, the corresponding mean value of the beta distribution for reliability and the sensitivity of the mean value with respect to the design variables will be used for design optimization. For a given

sample size, the one-to-one mapping relates a target Bayesian reliability to a single-valued target mean value of the beta distribution for reliability. Thus, satisfaction of the target mean value of the beta distribution for reliability always ensures satisfaction of the target Bayesian reliability.

Suppose that the Beta distribution Beta (α, β) is used to model reliability and its mean value, $M_i = M_i(R_i^B)$, can be expressed as

$$M_i = \frac{\alpha_i}{\alpha_i + \beta_i} = \frac{\alpha_i}{N+2} \tag{4.14}$$

The sensitivity of its mean value to design variable, d_j, can be expressed as

$$\frac{\partial M_i}{\partial d_j} = \frac{1}{N+2}\frac{\partial \alpha_i}{\partial d_j} \tag{4.15}$$

From Eq.(4.6), Eq. (4.15) can be expressed as

$$\frac{\partial M_i}{\partial d_j} = \frac{1}{N+2}\left(\frac{\partial R_1}{\partial d_j} + \frac{\partial R_2}{\partial d_j} + \cdots + \frac{\partial R_N}{\partial d_j}\right) \tag{4.16}$$

The mean value of the reliability, $M_i = M_i(R_i^B)$, can be converted to a reliability index. Then, the sensitivity can be developed for the format of the reliability index β_i^B, where $\beta_i^B = \Phi^{-1}(M_i)$. Correspondingly, all reliabilities, $P_i, i = 1, 2, ..., N$, can be transformed into the reliability indices, β_i. The sensitivity of Bayesian reliability index can be expressed as

$$\frac{\partial \beta_i^B}{\partial d_j} = \frac{\partial M_i}{\partial d_j} \Big/ \frac{\partial M_i}{\partial \beta_i^B} \tag{4.17}$$

where

$$\frac{\partial M_i}{\partial \beta_i^B} = \frac{1}{\sqrt{2\pi}} e^{-\frac{\left(\beta_i^B\right)^2}{2}} \tag{4.18}$$

Similarly,

$$\frac{\partial M_i}{\partial d_j} = \frac{1}{N+2}\left(\frac{\partial R_1}{\partial \beta_1}\frac{\partial \beta_1}{\partial d_j} + \cdots + \frac{\partial R_N}{\partial \beta_N}\frac{\partial \beta_N}{\partial d_j} \right) \tag{4.19}$$

where

$$\frac{\partial R_i}{\partial d_j} = \frac{\partial R_i}{\partial \beta_i}\frac{\partial \beta_i}{\partial d_j} = \frac{1}{\sqrt{2\pi}} e^{-\frac{\beta_i^2}{2}} \frac{\partial \beta_i}{\partial d_j} \tag{4.20}$$

By substituting the sensitivity of reliability index, $\partial \beta_i / \partial d_j$ into Eq.(4.20), the sensitivity of Bayesian reliability, $\partial \beta_i^B / \partial d_j$, can be obtained as

$$\frac{\partial \beta_i^B}{\partial d_j} = \frac{e^{\frac{\left(\beta_i^B\right)^2}{2}}}{N+2} \sum_{k=1}^{N} e^{-\frac{\beta_k^2}{2}} \frac{\partial \beta_k}{\partial d_j} \tag{4.21}$$

4.4 Bayesian Reliability-Based Design Optimization

4.4.1 Guideline of target Bayesian reliability

This section provides a guideline to set target reliability in Bayesian RBDO, which depends on a data size of epistemic uncertainties. Based on this definition, Bayesian reliability is then a function of user-defined confidence level and the reliability distribution, which is a function of the sample size of the epistemic uncertainties, *N*. To enable Bayesian RBDO with this flexibly defined Bayesian reliability, the target Bayesian reliability must be determined appropriately. Target reliability must depend on the data size of epistemic uncertainties. With few data for uncertainties, setting target reliability to 99.9% is not possible. Although high reliability is achieved through RBDO, the confidence of reliability will be extremely

low. To determine the appropriate target Bayesian reliability for the design optimization purpose, the maximum Bayesian reliability which can be possibly obtained has the following relationship with the user-defined confidence level C_L and sample size N as

$$1-C_L=\int_0^{R_B^{\max}}\frac{1}{Beta(1+N,1)}r^N(1-r)^0dr \tag{4.22}$$

Thus, the maximum Bayesian reliability is a function of user-defined confidence level and the sample size N as

$$R_B^{\max}=F_R^{-1}\left(1-C_L\right)\quad \text{where } R\sim Beta\left(1+N,1\right) \tag{4.23}$$

Figure 4-3 shows the maximum Bayesian reliability with respect to different sample size and confidence levels.

If the confidence level in Eq. (4.23) is chosen to be $\sqrt[N]{0.5}$, the maximum Bayesian reliability can be defined for a given sample size as

$$R_B^{\max}=F_R^{-1}\left(1-\sqrt[N]{0.5}\right)=\text{median}\left[F_{1_R}\left(r\right)\right] \tag{4.24}$$

As shown in Fig. 4-4, with the increase of the sample size, $P_B{}^{\max}$ rapidly rises to 90% and then slowly increases. Target reliability must be set lower than the maximum Bayesian reliability for a given data size. For example, the target reliability with 50 data for epistemic uncertainties must be lower than 92%.

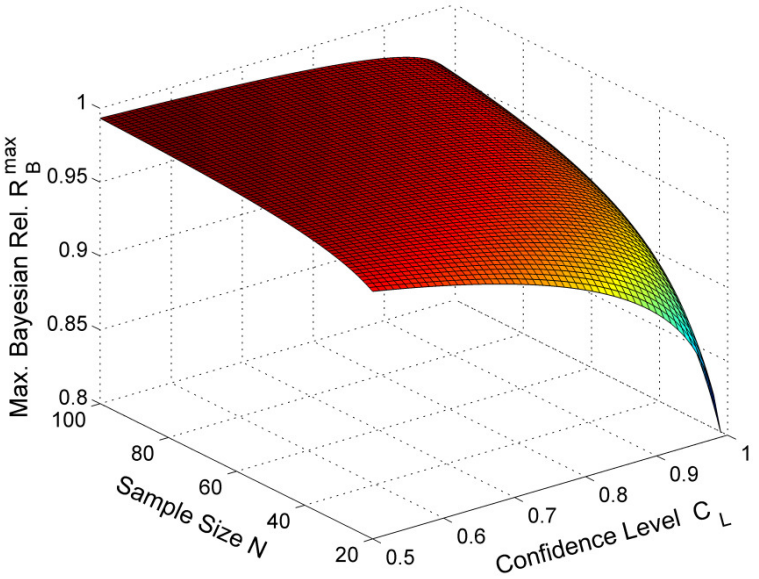

Figure 4-3: Maximum Bayesian reliability with confidence level C_L and sample size, N

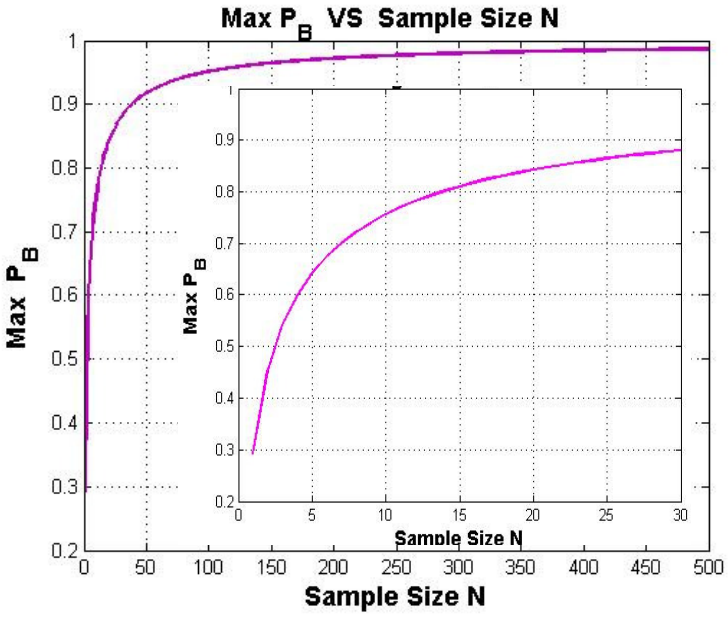

Figure 4-4: Maximum Bayesian reliability with confidence level $C_L = \sqrt[N]{0.5}$

4.4.2 Formulation and procedure of Bayesian RBDO

Knowing that both aleatory and epistemic uncertainties exist in the system of interest, Bayesian RBDO can be formulated as

$$\begin{aligned} &\text{minimize} \quad C(\mathbf{X}_a, \mathbf{X}_e; \mathbf{d}) \\ &\text{subject to} \quad P_B(G_i(\mathbf{X}_a, \mathbf{X}_e; \mathbf{d}) \le 0) \ge \Phi(\beta_{t_i}), \quad i = 1, \cdots, np \\ &\qquad \mathbf{d}^{\mathrm{L}} \le \mathbf{d} \le \mathbf{d}^{\mathrm{U}}, \quad \mathbf{d} \in R^{nd} \text{ and } \mathbf{X}_a \in R^{na}, \mathbf{X}_e \in R^{ne} \end{aligned} \tag{4.25}$$

where $P_B(G_i(\mathbf{X}_a, \mathbf{X}_e; \mathbf{d}) \le 0) = R_{B,i}$ is Bayesian reliability where $G_i(\mathbf{X}_a, \mathbf{X}_e; \mathbf{d}) \le 0$ is defined as a safety event; $C(\mathbf{X}_a, \mathbf{X}_e; \mathbf{d})$ is the objective function; $\mathbf{d} = \boldsymbol{\mu}(\mathbf{X})$ is the design vector; $\mathbf{X}_a$ and $\mathbf{X}_e$ are the aleatory and epistemic random vectors, respectively; β_{ti} is a prescribed target Bayesian reliability index; and *np*, *nd*, *na*, and *ne* are the numbers of probabilistic constraints, design variables, aleatory random variables, and epistemic random variables, respectively.

Based on the discussion in the previous sections, the procedure of Bayesian RBDO is presented in Fig. 4-5. The Bayesian reliability analysis in the left shaded box calculates the Bayesian reliabilities as well as their sensitivities, which require reliability analyses at all epistemic sample points. For instance, the probabilistic constraints at any data point for epistemic uncertainties become functions of only aleatory uncertainties and then the existing reliability analysis methods (FORM, SORM or EDR method, etc.) could be used for reliability and its sensitivity analyses. Thus, one Bayesian reliability analysis engages reliability and its sensitivity analyses *N* times. This is why Bayesian RBDO could become expensive and thus more investigation must be made to reduce its computational effort. Once the cost function, Bayesian reliability, and their sensitivities are computed, design optimization is

conducted in the right shaded box in Fig. 4-5. It is clear from the flowchart that Bayesian RBDO completely integrates Bayesian reliability analysis to RBDO.

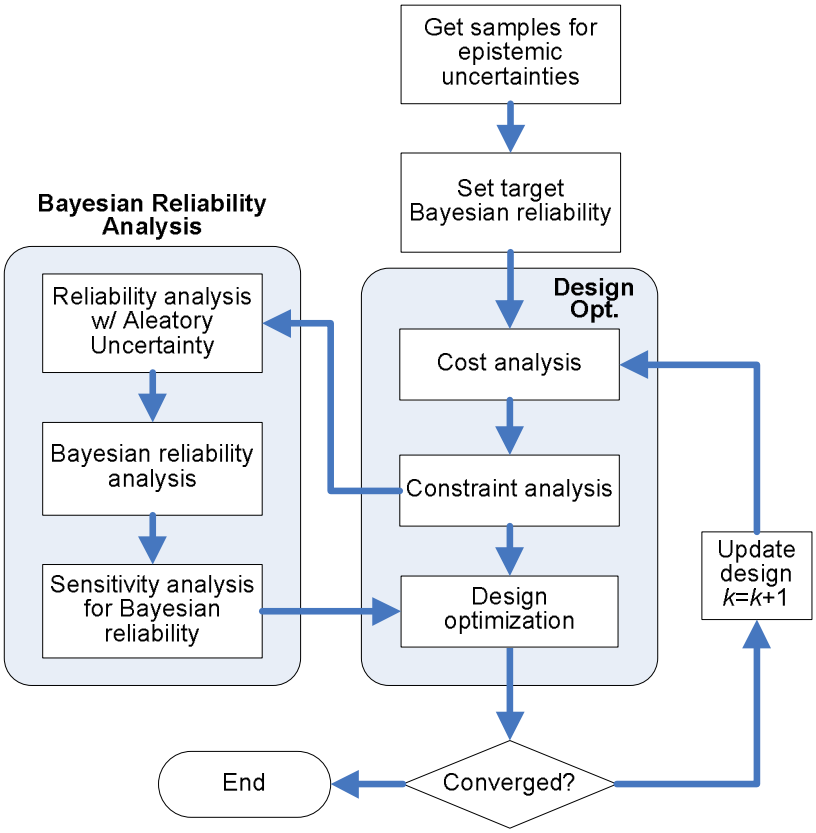

Figure 4-5: Bayesian RBDO flowchart

4.5 Case Studies

In this section, three case studies are presented to demonstrate the proposed Bayesian reliability analysis and Bayesian RBDO. The first case study is the Bayesian reliability analysis for a vehicle door system with consideration of customer satisfaction of door closure performance and the epistemic random input variables. In the second and third case studies, the vehicle lower control arm and the power

transformer winding joint are designed with consideration of epistemic loading variables.

4.5.1 Bayesian reliability analysis for a vehicle door system

The problem used in this case study is the body-door system of a passenger vehicle, as illustrated in Fig. 4-6. The vehicle door system is of special concern due to its frequency of use and its engineering challenge with respect to design, assembly, and operation. Variation exists in the CLD (Compression Load Deflection) response of the seal, the gap between the body and door, as well as in attaching the door to the car body. Besides the presence of variation, the complexity of the system is high due to the nonlinear seal behavior and the dynamics of door closing. The detail of vehicle door system regarding the problem description, failure mechanism specification, physical model creation and response surface construction can be found from Ref. [Kloess et al. 2004]. The performance measure selected in this study to assess one aspect of door system design is the door closing effort. The measurable quantity for this performance measure is the door closing velocity. A response surface for door closing velocity was created based on results from physics-based models and the performance evaluation criteria were deduced from both expert opinions and voice of the customer information.

For the door system example in this study, 26 random input variables are used to specify the uncertainty of the system. Within these 26 random input variables, listed in Table 4-1, X_5, X_6, X_7, X_{25} and X_{26} are aleatory variables which, for this example, are assigned uniform distributions on different threshold values as shown in the table. Except for these five random input variables, all others are epistemic variables with a

total of 79 sets of measurement data. For illustrative purpose, these epistemic data are partially listed in Table 4-2.

Table 4-1: Random variables and descriptions for a vehicle door system

Variable Name	Description	Variable Type
X_1	UHCC- Upper hinge location in cross-car direction	Epistemic
X_2	LHCC- Lower hinge location in cross-car direction	Epistemic
X_3	LATCC-Latch location in cross-car direction	Epistemic
X_4	LATUD-Latch location in up-down direction	Epistemic
X_5	Primary seal CLD property factor	U(0.7, 1.3)
X_6	Auxiliary seal CLD property factor	U(0.7, 1.3)
X_7	Cutline seal CLD property factor	U(0.7, 1.3)
X_8~X_{24}	Primary Seal Margin Regions 1~17	Epistemic
X_{25}	Auxiliary Seal Margin	U(-1, 1)
X_{26}	Cutline Seal Margin	U(-1, 1)

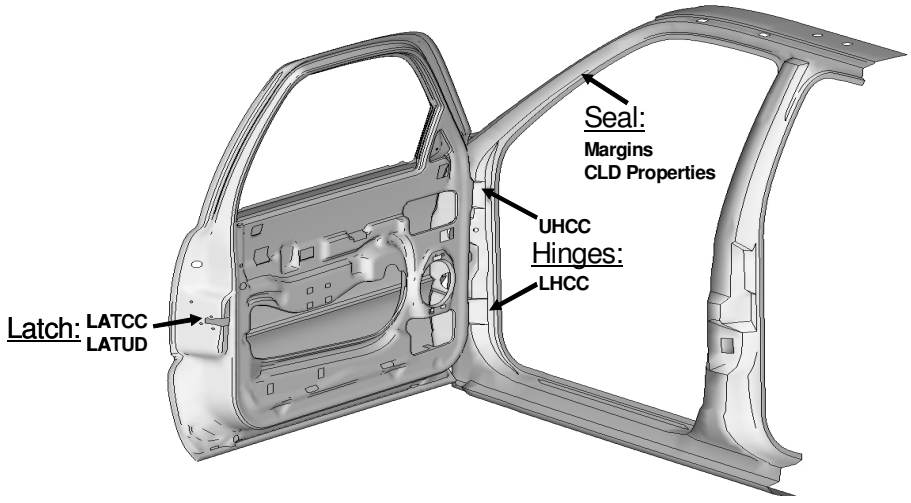

Figure 4-6: Vehicle Door system

Table 4-2: Data for epistemic random variables of the vehicle door system

Variables	Data						
	Set 1	Set 2	Set 3	Set 4	Set 5	…	Set 79
X_1	1.62	2.29	1.58	1.58	1.19	…	2.16
X_2	2.82	2.49	1.8	2.1	2.03	…	1.355
X_3	2.555	2.1	1.82	1.67	1.75	…	1.35
X_4	-0.38	-0.35	-0.01	-0.01	0.61	…	-0.61
X_8	1.655	1.235	1.015	0.715	0.71	…	0.559167
X_9	1.0775	0.7725	0.5925	0.2825	0.115	…	0.39875
X_{10}	0.5	0.31	0.17	-0.15	-0.48	…	0.238333
X_{11}	1.24	0.74	0.426667	0.113333	-0.23	…	0.955
X_{12}	-0.27	-0.31	-0.28	-0.66	-1.29	…	0.278333
X_{13}	0.03	0.16	-0.205	-0.29	-1.02	…	0.1125
X_{14}	0.33	0.63	-0.13	0.08	-0.75	…	-0.05333
X_{15}	0.5	0.79	0.06	0.22	-0.76	…	0.135
X_{16}	0.89	1.01	0.87	0.27	-0.63	…	0.24
X_{17}	0.27	0.51	-0.01	-0.21	-1.565	…	0.233333
X_{18}	-0.35	0.01	-0.89	-0.69	-2.5	…	0.226667
X_{19}	-0.35	0.01	-0.89	-0.69	-2.5	…	0.226667
X_{20}	-0.44	-0.53	-1.27	-1.55	-2.93	…	-0.37667
X_{21}	-0.44	-0.53	-1.27	-1.55	-2.93	…	-0.37667
X_{22}	0.16	-0.03	-0.7125	-0.8625	-1.6825	…	0.12375
X_{23}	0.76	0.47	-0.155	-0.175	-0.435	…	0.624167
X_{24}	1.49	0.91	0.56	0.27	0.91	…	0.535

Modeling of the Marginal Velocity

The marginal velocity which serves as the criteria of the door performance evaluation is modeled by using the Bayesian updating technique based on expert opinion and the customer data. From a hypothetical expert, the door closing velocity values for customer satisfaction should be, for example, within the range of 0 m/s to v_{max} m/s. Customer survey regarding the door closing velocity can be carried out by using the direct customer survey method [Winkler 1967; Spetzler et al. 1975; Wallsten and Budescu 1983] and illustrative results which show the Customer Rejection Rate (CRR) versus the door closing velocity (normalized by v_{max}) are shown in Fig. 4-7. For the modeling of the marginal velocity, CRR can be treated as the probability of the marginal velocity being smaller than a given a or $CRR = P(v_m \leq a)$ where v_m is a random marginal velocity and a is within [0, v_{max}] based on expert opinion.

The procedure of marginal velocity modeling can be briefly summarized into three steps. First, based on the customer data, one Bayesian inference model should be specified. For example, if the Bayesian normal inference model is used, the marginal velocity will be modeled as the mean value of the normal distribution which is the conjugate distribution for this model. Second, based on the selected model, the CDF analysis can be carried out for the CDF/ Velocity data. After completing this analysis, the CDF data are then transferred to parameter data for the distribution. Third, with one prior distribution assumed, Bayesian updating can then be carried out with sets of parameter data. In this study, the Bayesian normal inference model is used and the marginal velocity is modeled as the mean value of a Normal distribution.

Figure 4-8 shows the Bayesian updating process for the modeling of the marginal velocity with three clinic survey data. The detail of the marginal velocity modeling process can be found in Ref. [Youn and Wang 2009]. Through the Bayesian updating, the CDF of the final Bayesian model, N (0.5946, 0.0355^2), is used as the distribution for the marginal velocity.

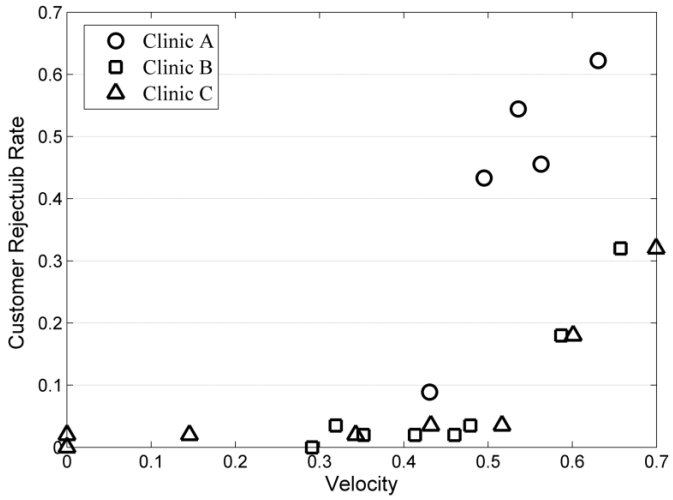

Figure 4-7: Customer rejection rate

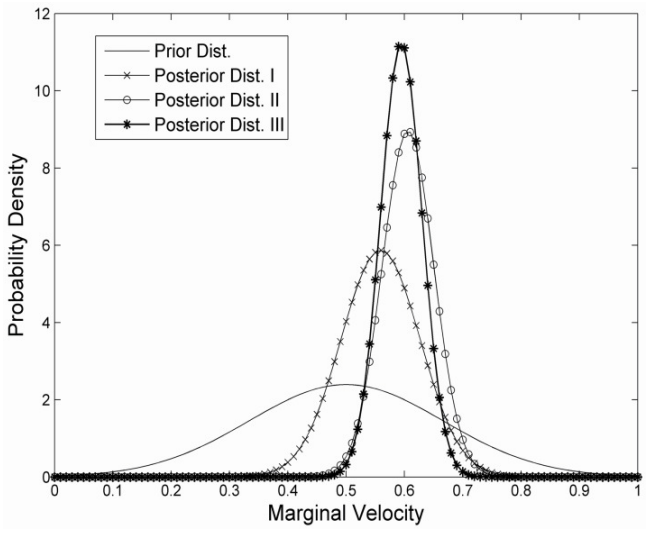

Figure 4-8: Bayesian updating for the marginal velocity using a normal distribution

Bayesian Reliability Analyses for a Vehicle Door System

Based on the marginal velocity PDF created, Bayesian reliability analysis is then carried out for the door closing effort problem with both aleatory and epistemic uncertainties. For a given set of input values, the performance response can be obtained from the response surface created based on the physical model. Since Bayesian reliability analysis requires the probabilistic performance evaluation for each set of epistemic data, two different approaches, MCS and EDR method, are employed to calculate the reliability.

First, for each set of epistemic data, direct MCS is used to carry out the reliability analysis. For each aleatory variable (including the variable of marginal velocity), 10,000 random samples are generated and used for MCS. Table 4-3 shows the 55 reliabilities corresponding to the first 55 sets of epistemic data. Based on Table 4-3, we carried out the Bayesian reliability analysis and obtained the reliability distribution as Beta (53.524, 3.476). Then by the Bayesian reliability definition described in Section 4.2, the extreme distribution of the smallest value for the Beta distribution is constructed and the Bayesian reliability is realized as 0.849185. Figure 4-9 (a) shows the Beta distribution, extreme distribution and the Bayesian reliability value using MCS. With 24 new data sets involved for the epistemic random variables the Bayesian reliability is updated. The updated reliability distribution is Beta (77.1869, 3.8131) and the Bayesian reliability is updated from the original 0.849185 to 0.880935. Table 4-4 shows the reliabilities corresponding to each set of the new involved data. Figure 4-10 (a) shows the updated Beta distribution, extreme distribution and the Bayesian reliability using MCS.

As we can see from the Monte Carlo Simulation method, the reliability analysis for each set of epistemic data can require a large amount of response performance evaluations depending on the simulation sample size (in this case 10,000). In order to make the calculation of the Bayesian reliability more efficient, the EDR method is used for the probability calculation for each set of epistemic data. By using EDR method, the total number of the response performance evaluation is reduced from 10,000 to 2n+1=13. Based on the marginal velocity PDF created in subsection 1, the reliability R_i of a certain design (Xa, Xe^i) can be formulated as $R_i = \Pr [V(X\text{a}, X\text{e}^i) - Vt \leq 0]$ where $V(X\text{a}, X\text{e}^i)$ is the performance velocity variable corresponding to a certain design (Xa, Xe^i), Xa is the aleatory variable set and Xe^i is the ith set of epistemic data, and Vt is the marginal velocity. Totally 55 different reliabilities corresponding to 55 different sets of epistemic uncertainties are realized as shown in Table 4-5. Based on these results, the reliability distribution is obtained as Beta (53.5076, 3.4924) from Bayesian inference. Then by the Bayesian reliability definition, the extreme distribution of smallest value for the Beta distribution is constructed and the Bayesian reliability is realized as 0.848752. Figure 4-9 (b) shows the Beta distribution, extreme distribution and the Bayesian reliability using the EDR method. With 24 new data sets involved, the Bayesian reliability is updated. The updated reliability distribution is Beta (77.1567, 3.8433) and the Bayesian reliability is updated from the original 0.848752 to 0.880363. Table 4-6 shows the reliabilities corresponding to each set of the new involved data. Figure 4-10 (b) shows the updated Beta distribution, extreme distribution and the Bayesian reliability using the EDR method.

A comparison of the results from using the two different probability analysis approaches shows that the EDR method maintains good accuracy and at the same time provides a higher computational efficiency compared with MCS. From the analysis results obtained with both MCS and the EDR method, two points are clear: first, Bayesian reliability increases with the increase of the reliability value corresponding to each set of epistemic data; secondly, the updated Bayesian reliability increases with the addition of more epistemic data into the Bayesian reliability analysis. This is because the Bayesian reliability represents not only the design uncertainty of the system but also the uncertainty due to the limiting information represented by the epistemic uncertainties. As more data is involved, a better understanding of the characteristic of epistemic uncertainties can be expected and consequently a higher Bayesian reliability can be realized. Also, the Bayesian reliability analysis approach proposed in this dissertation offers a convenient and effective method for the performance evaluation of the problems involving several different types of uncertainty and where uncertainty data are continuously collected

Table 4-3: 55 reliabilities corresponding to 55 epistemic data sets (by MCS)

Data Set	Rel.	Data Set	Rel.	Data Set	Rel.	Data Set	Rel.	Data Set	Rel.
1	0.9973	12	1.0000	23	0.9987	34	0.9995	45	0.9988
2	1.0000	13	0.9993	24	0.9970	35	0.9998	46	0.2703
3	0.9993	14	1.0000	25	1.0000	36	0.9999	47	0.9987
4	0.9945	15	1.0000	26	0.9951	37	0.9999	48	1.0000
5	0.8265	16	1.0000	27	0.9970	38	0.9974	49	0.9955
6	0.9996	17	0.9999	28	0.9899	39	0.9977	50	0.9937
7	0.9985	18	0.9991	29	0.9998	40	0.9918	51	0.9918
8	1.0000	19	0.9999	30	1.0000	41	0.9007	52	1.0000
9	1.0000	20	0.9993	31	0.9993	42	0.9976	53	0.9994
10	1.0000	21	1.0000	32	1.0000	43	0.9778	54	0.2109
11	1.0000	22	0.9999	33	0.9963	44	0.9730	55	0.4436

Table 4-4: 24 reliabilities corresponding to 24 new data sets (by MCS)

Data Set	Rel.	Data Set	Rel.	Data Set	Rel	Data Set	Rel	Data Set	Rel	Data Set	Rel
1	0.9929	5	0.9993	9	0.9996	13	0.8864	17	1.0000	21	0.9842
2	0.9999	6	0.9994	10	0.9989	14	1.0000	18	1.0000	22	0.9866
3	0.9995	7	0.9996	11	1.0000	15	0.9963	19	1.0000	23	0.9998
4	0.9993	8	0.9999	12	1.0000	16	0.9240	20	0.8973	24	1.0000

Table 4-5: 55 reliabilities corresponding to 55 epistemic data sets (by EDR)

No. Data Set	Rel.	No. Data Set	Rel.	No. Data Set	Rel.	No. Data Set	Rel.	No. Data Set	Rel.
1	0.9978	12	1.0000	23	0.9991	34	0.9998	45	0.9993
2	1.0000	13	0.9997	24	0.9976	35	0.9998	46	0.2642
3	0.9996	14	1.0000	25	1.0000	36	1.0000	47	0.9992
4	0.9953	15	1.0000	26	0.9963	37	1.0000	48	1.0000
5	0.8243	16	1.0000	27	0.9977	38	0.9982	49	0.9963
6	0.9998	17	0.9999	28	0.9893	39	0.9984	50	0.9944
7	0.9991	18	0.9995	29	0.9998	40	0.9917	51	0.9915
8	1.0000	19	1.0000	30	1.0000	41	0.8938	52	1.0000
9	1.0000	20	0.9996	31	0.9996	42	0.9984	53	0.9997
10	1.0000	21	1.0000	32	1.0000	43	0.9755	54	0.2070
11	1.0000	22	0.9999	33	0.9971	44	0.9702	55	0.4394

Table 4-6: 24 reliabilities corresponding to 24 new data sets (by EDR)

Data Set	Rel.	Data Set	Rel.	Data Set	Rel.	Data Set	Rel.	Data Set	Rel.	Data Set	Rel.
1	0.9928	5	0.9996	9	0.9998	13	0.8814	17	1.0000	21	0.9835
2	0.9999	6	0.9997	10	0.9993	14	1.0000	18	1.0000	22	0.9867
3	0.9997	7	0.9998	11	1.0000	15	0.9969	19	1.0000	23	0.9999
4	0.9996	8	0.9999	12	1.0000	16	0.9190	20	0.8915	24	1.0000

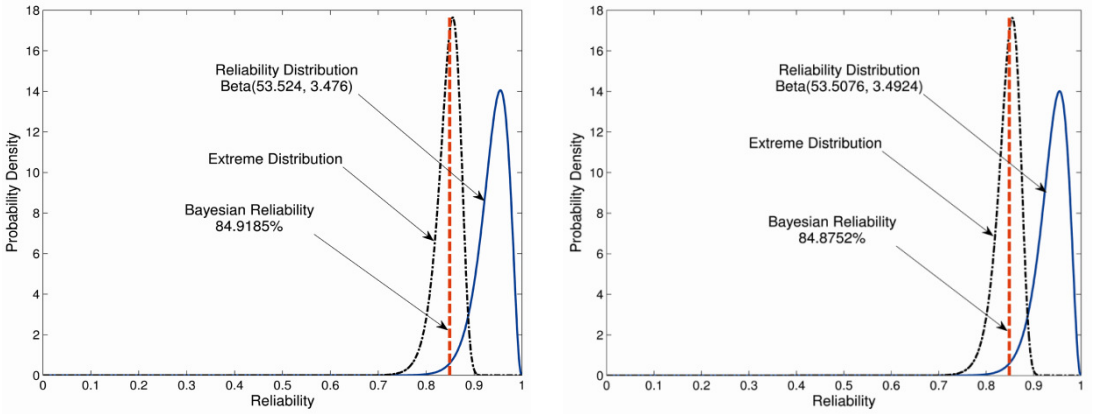

(a) (b)

Figure 4-9: Bayesian reliability with 55 sets data: (a) by MCS, (b) by EDR

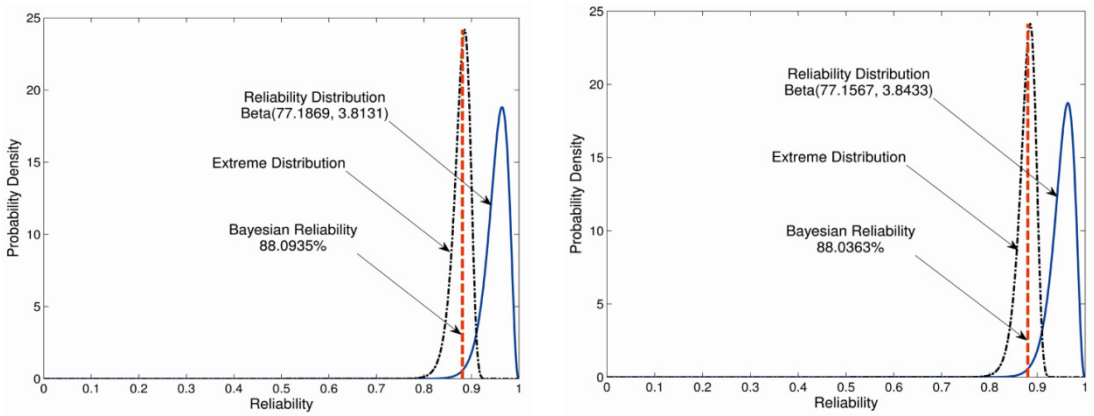

(a) (b)

Figure 4-10 Updated Bayesian reliability with 24 new data sets:

(a) by MCS, (b) by EDR

4.5.2 Lower control arm design problem

In this case study, Bayesian RBDO is performed on a lower control arm for the High Mobility Multipurpose Wheeled Vehicle (HMMWV). Vehicle suspension

systems experience intense loading conditions throughout their service lives. For the purpose of validating the Bayesian RBDO method, a HMMWV lower control arm is presented as a case study.

The lower control arm is modeled with plane stress elements using 54,666 nodes, 53,589 elements, and 327,961 DOFs, where all welds are modeled using rigid beam elements. For FE and design modeling, HyperWorks 7.0 is used. The loading and boundary conditions for this case study are shown in Fig. 4-11, where loading is applied at the ball-joint (Point D) in 3 directions, and the boundary conditions are applied at the bushings (Points A and B) and the shock-absorber/Spring Assemble (Point C). Due to a lack of data, the loads are considered as epistemic random variables. The design variables for this problem are the thicknesses of the seven major components of the control arm, as shown in Fig. 4-12. The statistical information of these components, shown in Table 4-7, is well known, and these random parameters are therefore considered as aleatory variables in Bayesian RBDO.

To determine the hot spots (high stress concentrations) in the model, which are used to determine the constraints, a worst case scenario analysis of the control arm is performed. For this worst case scenario, all the design variables are set at their lower bounds as shown in Table 4-8, and all the loads are set at their highest values attained from the epistemic data points.

From the worst case scenario, thirty nine constraints (G_1 to G_{39}) are defined on several critical regions using the von Mises stress in Fig. 4-13. For those constraints, Bayesian reliabilities are defined as

$$R_i^B(\mathbf{X}_a, \mathbf{X}_e; \mathbf{d}) = P_B(G_i(\mathbf{X}) = \frac{s_i(\mathbf{X})}{s_U} - 1 \le 0) \tag{26}$$

The PDFs for reliabilities at the critical spots are estimated using Bayesian inference. Four representative PDFs (G_1, G_{24}, G_{35} and G_{38}) are plotted in the dotted curve in Fig. 4-14 to Fig. 4-17. The extreme distributions (solid curves) of the reliability PDFs are presented in the figures. The median values of the extreme distribution are then defined as the Bayesian reliabilities for different constraints which are also plotted in Fig. 4-14 to Fig. 4-17 as vertical dash lines. As illustrated in these figures, G_1 and G_{35} (the most critical spots at the current design point) are much less reliable than G_{24} and G_{38}. This observation is consistent with a stress contour in Fig. 4-13, since the stresses in G_1 and G_{35} are extremely high. When a target Bayesian reliability is set to 90%, G_1 and G_{35} are violated but others are inactive.

Table 4-7: Random properties in lower control Arm model

Random Variable	Lower Bound of Mean	Mean	Std. Dev.	Dist. Type
X_1	0.1	0.12	0.006	Normal
X_2	0.1	0.12	0.006	Normal
X_3	0.1	0.18	0.009	Normal
X_4	0.1	0.135	0.00675	Normal
X_5	0.15	0.25	0.0125	Normal
X_6	0.1	0.18	0.009	Normal
X_7	0.1	0.135	0.00675	Normal

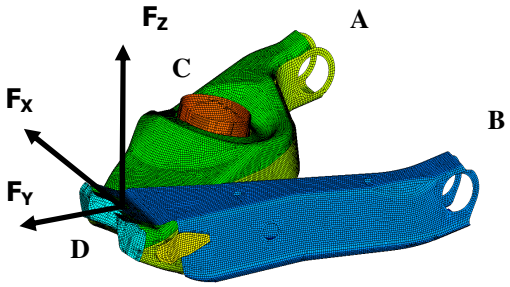

Figure 4-11: Three loading variables (Epistemic)

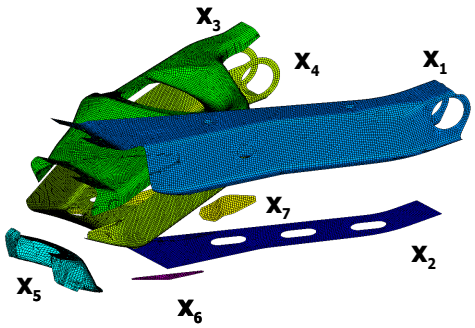

Figure 4-12: Seven thickness variables (Aleatory)

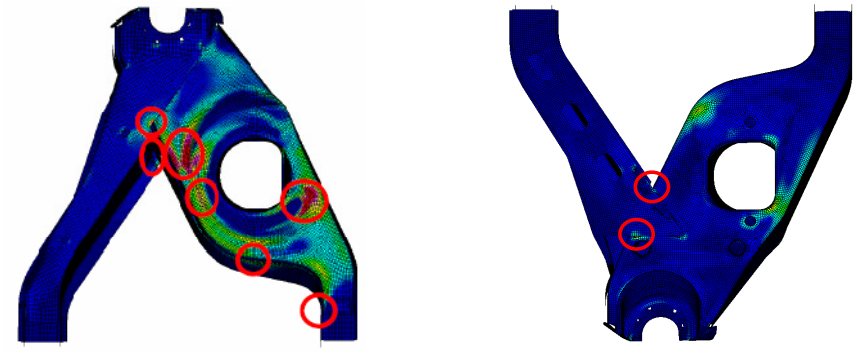

Figure 4-13: 39 Critical constraints of the lower control A-Arm model

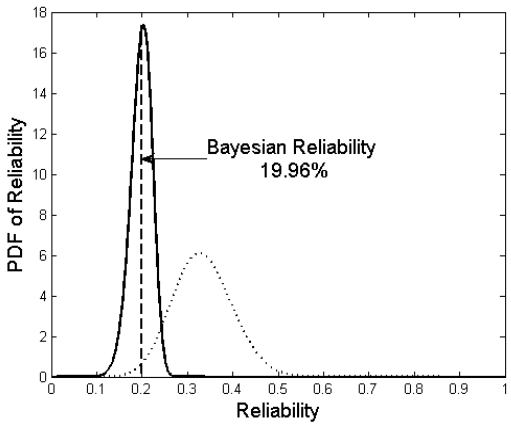

Figure 4-14: Bayesian reliability for G_1

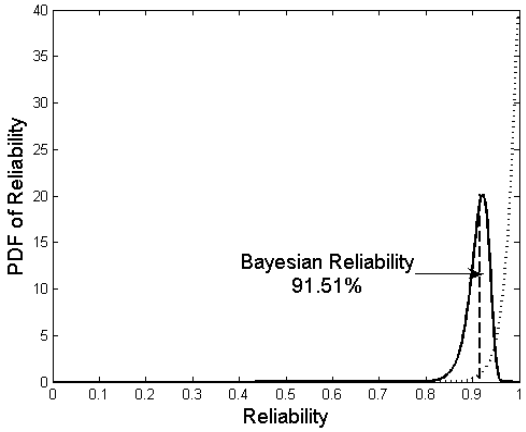

Figure 4-15: Bayesian reliability for G_{24}

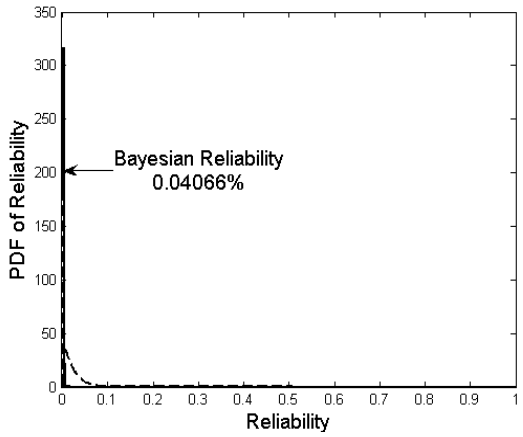

Figure 4-16: Bayesian reliability for G_{35}

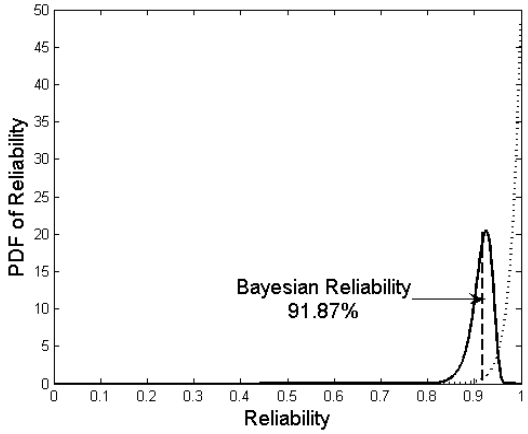

Figure 4-17: Bayesian reliability for G_{38}

The control arm is now used to demonstrate Bayesian RBDO. In this example, seven thickness design variables are considered as aleatory random variables, whereas three load variables (not design variables) are considered as epistemic random variables. 50 data sets are employed for the epistemic loads during Bayesian RBDO. These samples are randomly generated using the assumed distributions shown in Table 4-8. The properties of the design and random variables are shown in Table 4-9.

Table 4-8: Assumed random properties for epistemic uncertainties

Epistemic Variable	Distribution
F_x	~ Normal(1900, 95)
F_y	~ Normal(95, 4.75)
F_z	~ Normal(950, 47.5)

Table 4-9: Random properties in lower control A-Arm model

Random Variable	$\mathbf{d}_L$	$\boldsymbol{\mu}_X=\mathbf{d}$ (Mean)	$\mathbf{d}_U$	Std. Dev.	Dist. Type
X_1	0.1	0.120	0.5	0.00600	Normal
X_2	0.1	0.120	0.5	0.00600	Normal
X_3	0.1	0.180	0.5	0.00900	Normal
X_4	0.1	0.135	0.5	0.00675	Normal
X_5	0.15	0.250	0.5	0.01250	Normal
X_6	0.1	0.180	0.5	0.00900	Normal
X_7	0.1	0.135	0.5	0.00675	Normal

With 39 constraints, Bayesian RBDO is formulated as

$$\begin{aligned} &\text{Minimize } \textit{Mass} \\ &\text{Subject to } P_B(G_i(\mathbf{X}) = \frac{s_i(\mathbf{X})}{s_U} - 1 \le 0) = F_{G_i}^B(0) \ge \Phi(\beta_{t_i}),\ i = 1, \cdots, 39 \end{aligned} \tag{27}$$

In this study, target reliability is set to $R_{B,i}^t = 90\%$. Ten design iterations reach the Bayesian reliability-based optimum design. The histories of the design parameters, objective function, and the Bayesian reliabilities for significant constraints are shown in Table 4-10, Fig. 4-18 and Fig. 4-19. At the optimum design, three constraints, G_1, G_{35} and G_{38}, become active and others are feasible. Figures 4-20 and 4-21 illustrate the reliability PDFs and Bayesian reliabilities at the optimum design for G_1, G_{24}, G_{35} and G_{38}, of which the PDFs at the initial design are shown in Fig. 4-14 to Fig. 4-17. The stress contours and the hot spots for the initial design and optimum designs are shown in Figs.4-22 and 4-23.

Finally, the Bayesian reliability-based optimum design is verified by MCS with 10,000 samples. In this verification, three epistemic load variables are assumed to follow the distributions in Table 4-8. At the optimum design, reliabilities for G_1, G_{35} and G_{38} are 98.85%, 99.15%, and 98.6%. The sufficiency requirement assures higher reliability than the target reliability, 90%.

Table 4-10**:** Bayesian RBDO design history for lower control arm design

Design Iteration	Design							Mass
	X_1	X_2	X_3	X_4	X_5	X_6	X_7	
1	0.12	0.120	0.180	0.135	0.25	0.180	0.135	30.76
2	0.10	0.100	0.109	0.307	0.15	0.500	0.100	37.04
3	0.10	0.143	0.143	0.100	0.15	0.500	0.100	26.70
4	0.10	0.144	0.153	0.107	0.15	0.242	0.500	28.013
5	0.10	0.137	0.153	0.141	0.15	0.500	0.100	29.64
6	0.10	0.138	0.157	0.151	0.15	0.500	0.100	30.51
7	0.10	0.138	0.156	0.156	0.15	0.500	0.100	30.84
8	0.10	0.137	0.156	0.158	0.15	0.500	0.164	31.01
9	0.10	0.137	0.156	0.160	0.15	0.500	0.156	31.11
10 (optimum)	0.10	0.137	0.1559	0.1598	0.15	0.500	0.177	31.13

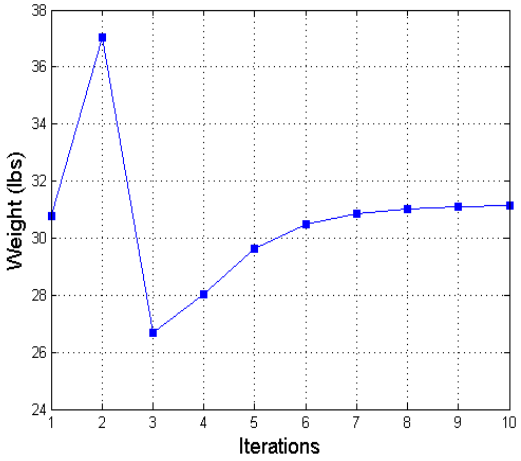

Figure 4-18: Objective function history of lower control arm design

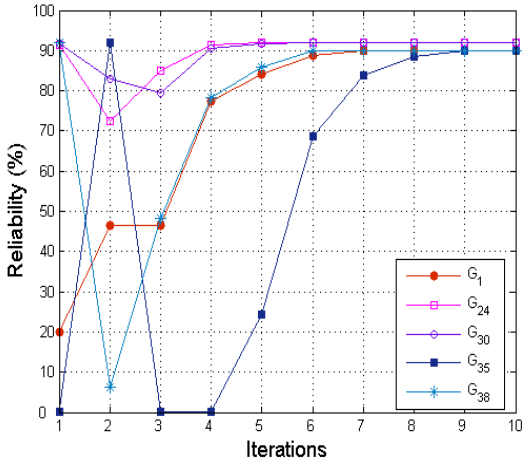

Figure 4-19: Bayesian reliability history of lower control arm design

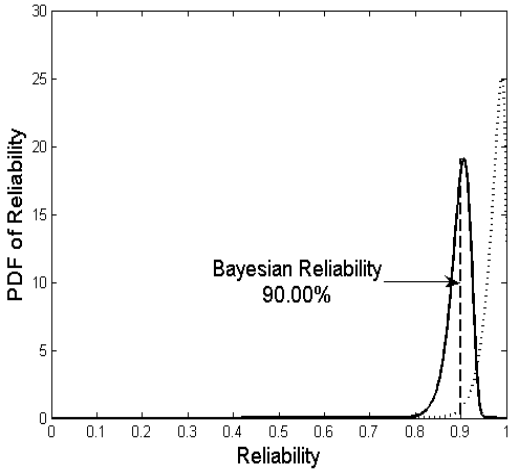

Figure 4-20 Bayesian reliability for G_1, G_{35} and G_{38} at the optimum design

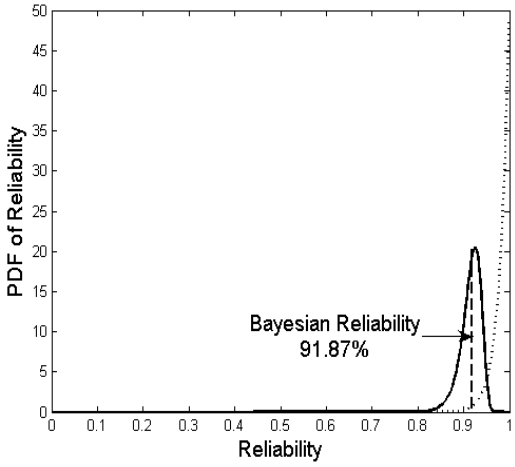

Figure 4-21: Bayesian reliability for G_{24} at the optimum design

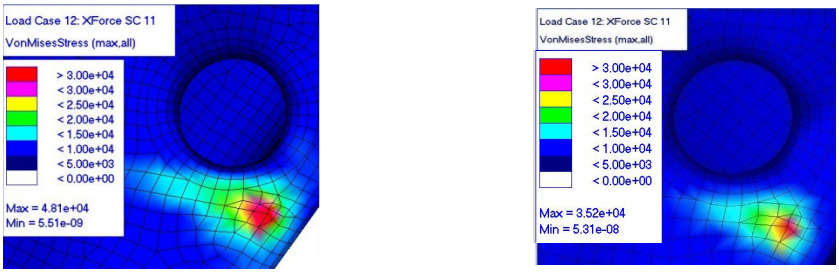

(a) (b)

Figure 4-22: Element stress contour for G_{35}

(a) at the initial design and (b) at the optimum design

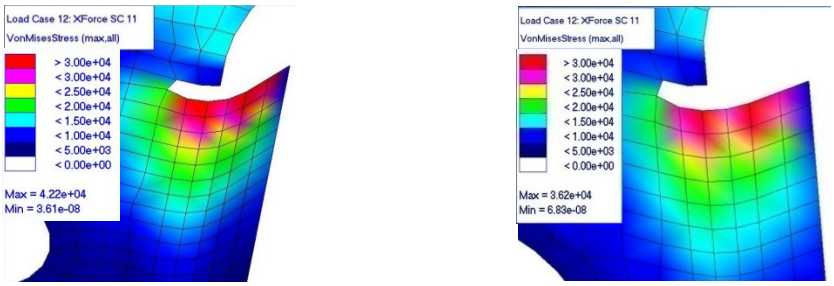

(a) (b)

Figure 4-23: Element stress contour for G_{38}

(a) at the optimum design and (b) at the initial design

4.5.3 Power transformer winding bolt joint design

Power transformers are among the most expensive elements of high-voltage power systems. The power transformer vibration induced by the magnetic field loading will cause the windings support joint loosening or the fatigue failures, which will gradually increase the vibration amplitude of the winding and eventually damage the core. This case study aims at employing the proposed efficient Bayesian RBDO to

design the bolt joints for the power transformer against the fatigue failure. A validated power transformer bolt joint model is accomplished in the finite element analysis tool ANSYS 10 and shown in Fig. 4-24, together with the global power transformer model in which one of outside wall is concealed so that the inner structure can be presented. The detail of the winding bolt joints is shown in Fig. 4-25 from different viewing angles, with which the windings of the power transformer are assembled with the bottom fixture. The transformer is fixed at the bottom and the vibration load is applied to the magnetic core with the frequency of 120 Hz. The random variables and the statistical information for this case study are listed in Table 4-11, with 6 design variables as aleatory uncertainties and 3 epistemic variables.

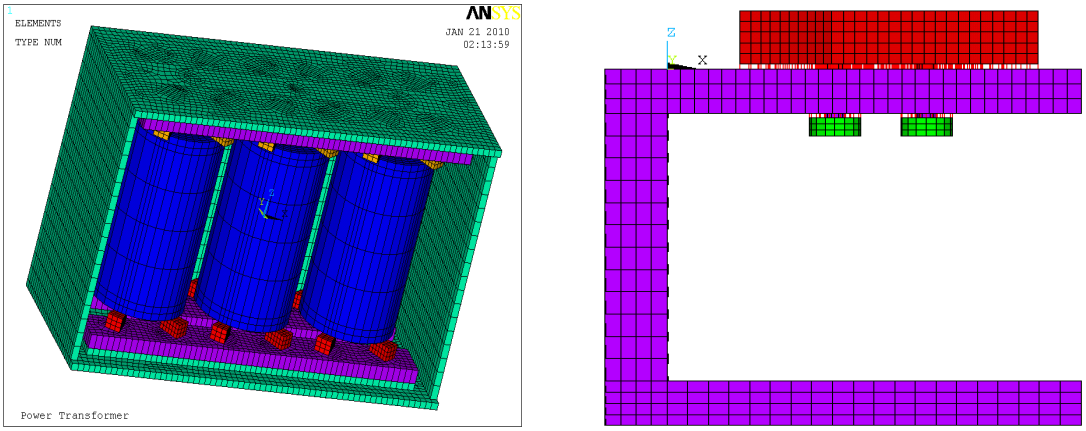

(a) (b)

Figure 4-24: A power transformer and bolt joint FE models

(a) Power Transformer Global Model without Covering Wall, and (b) A Bolt Joint

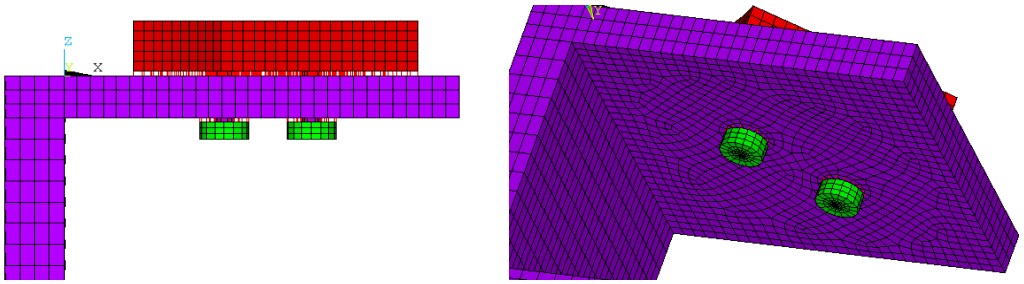

(a) (b)

Figure 4-25: Winding support bolt joint,

(a) side view, (b) bottom view

Table 4-11: Random variables and statistical information for transformer joints

Random variables	Descriptions	Information		
		Dist. Type	Low Bound	Upper Bound
Design Variables (Aleatory Uncertainties)	X_1: I-Beam Thickness	$N(d_1, 0.2^2)$	5	10
	X_2: Support Hinge Height	$N(d_2, 0.2^2)$	5	10
	X_3: Support Hinge Inner Radium	$N(d_3, 2^2)$	40	50
	X_4: Support Hinge Outer Radium	$N(d_4, 2^2)$	65	75
	X_5: Angular width of the Support Hinge	$N(d_5, 0.2^2)$	5	10
	X_6: Bolt Joint Stud Radium	$N(d_6, 0.02^2)$	0.5	1.5
Epistemic Uncertainties	X_7: X directional dynamic loading F_x	50 data samples		
	X_8: Y directional dynamic loading F_y	50 data samples		
	X_9: Z directional dynamic loading F_z	50 data samples		

In this study, the response value being attained through the fatigue analysis is cumulative fatigue damage ratios, D = designed life/fatigue life, where the designed life is 15 years, and the structure is safe for fatigue when D is less than 1. The designed fatigue life is projected to the critical stress range during the cyclic loading due to the magnetic field applied on the winding cores. The power transformer bolt joint contact surface is simulated with the string elements in between two contact surfaces and 27 design constraints are identified through an initial simulation run, as shown in the Fig. 4-26. The objective of this design problem is to minimize the overall weight (Volume) of the transformer joints with 27 fatigue constraints as hot spots identified in Fig. 4-26. The Target Bayesian reliability is set to 90% with a confidence level of 95%. Bayesian RBDO is applied on this design problems and the Bayesian reliability-based optimum design is reached after totally 29 design iterations. The histories of the design parameters, objective function, and the Bayesian reliabilities for significant constraints are shown in Table 4-12, and Figs. 4-27. At the optimum design, two constraints, G_2, and G_{11} which are two hot spots located at the end of two bolt studs, become active and others are inactive.

As is shown in the Table 4-12 and Fig. 4-27 (a), the total volume of the joint has been substantially reduced compared with the initial design. With a user defined confidence level of 95%, the maximum Bayesian Reliability can be reached with 50 data samples is 0.9430. As is shown in Fig. 4-27(b), the Bayesian reliabilities at the optimum design are equal or close to this maximum Bayesian reliability for most of constraints except two active ones. Due to the computational expensiveness, Bayesian RBDO is only carried out with 95% confidence level. However, it can produce

different optimum designs based on different user-defined confidence levels and target Bayesian reliabilities. This case study demonstrates the effectiveness and applicability of the proposed Bayesian RBDO methodology on complex engineering design applications.

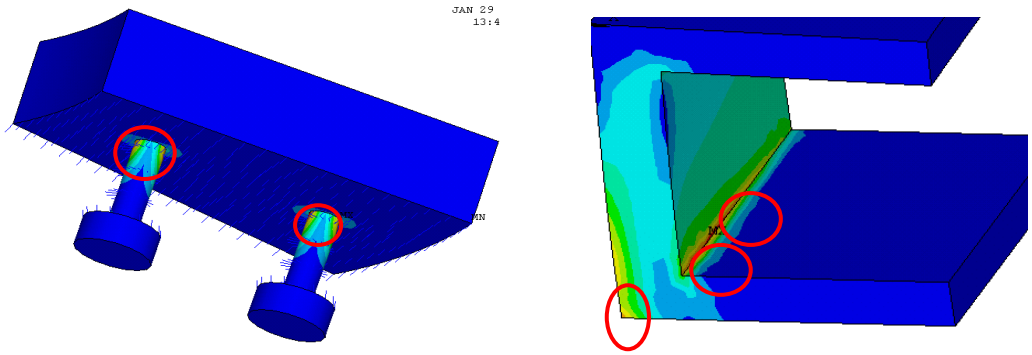

Figure 4-26: 27 Design constraints selected based on the initial simulation results

Table 4-12: Design history of the power transformer joint case study

Design Iteration	d_1	d_2	d_3	d_4	d_5	d_6	Volume
Initial Design	6.000	6.000	45.000	70.000	8.000	1.000	11825.096
1	5.000	7.110	48.000	67.000	5.000	0.500	10854.665
2	5.000	7.091	47.250	67.750	5.750	0.641	11026.164
3	5.000	7.484	48.000	67.000	5.000	0.570	10895.410
…	…	…	…	…	…	…	…
25	5.000	6.702	47.990	67.047	5.010	0.585	10825.283
26	5.000	6.738	47.984	67.047	5.015	0.584	10829.502
27	5.000	6.756	47.982	67.047	5.017	0.584	10831.616
28	5.000	6.765	47.980	67.047	5.019	0.584	10832.673
29(Optimum)	5.000	6.763	47.997	67.047	5.000	0.584	10829.601

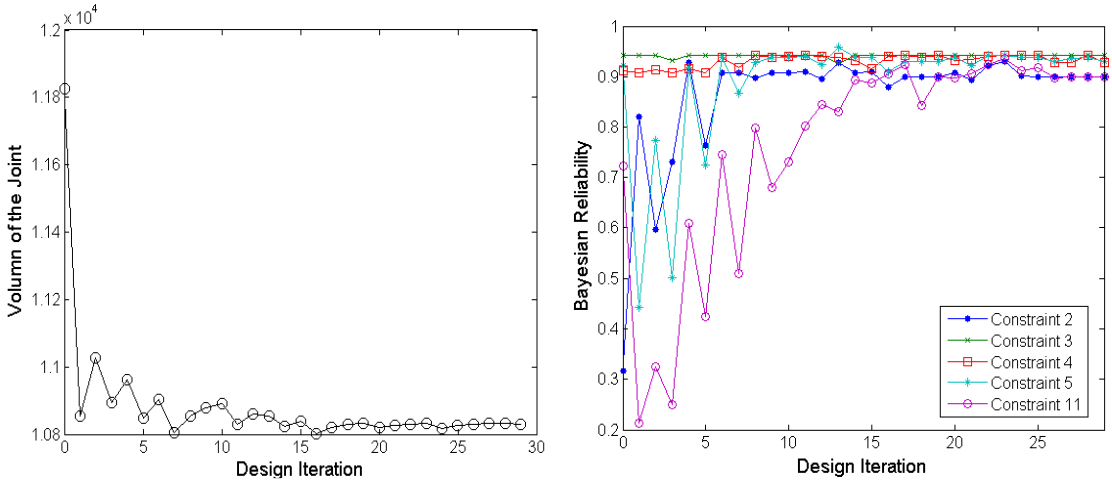

(a) (b)

Figure 4-27: Design process of the power transformer bolt joint case study: (a) objective function, and (b) Bayesian reliabilities for five constraints

4.6 Summary

Practical engineering analysis and design problems involve both sufficient (aleatory) and insufficient (epistemic) data for their random inputs, such as geometric tolerances, material properties, loads, etc. Conventional RBDO methods cannot handle the design problems that involve both aleatory and epistemic uncertainties simultaneously. To tackle such design problems, Bayesian RBDO has been proposed. In this design framework, (1) the Bayesian binomial inference model has been employed for the reliability modeling; (2) Bayesian reliability is uniquely defined for the design purpose with a user provided confidence level; (3) an innovative way of the sensitivity analysis for Bayesian reliability is developed to avoid complicated mathematical derivation and potential numerical singularities; and (4) the EDR method is integrated with Bayesian RBDO for Bayesian reliability analysis to

improve its efficiency and accuracy. Three engineering case studies are employed to demonstrate the Bayesian reliability analysis procedure and the developed Bayesian RBDO methodology. In these case studies, the random parameters related to manufacturing variability and material properties are considered as the aleatory random parameters, whereas the random parameters associated with the load variability are regarded as the epistemic random parameters. It is found that the Bayesian RBDO framework can be generally applied to engineered system design problems in the presences of both aleatory and epistemic uncertainties, where the conventional RBDO model can be viewed as a special case for the developed Bayesian RBDO methodology. In addition, the EDR method enhances numerical efficiency and accuracy for Bayesian RBDO.

Chapter 5: Sensing Function Design for Structural Health Prognostics

With the technical developments presented in previous two chapters, system reliability for a given engineered system can be assessed within a general CIM framework; moreover an engineered system can be designed to satisfy given target reliability levels using the developed Bayesian RBDO technique. So far the work has been mainly focused on addressing the reliability issue in the system design and manufacturing stage. Thus, Ch.5 and Ch.6 will focus on the reliability issue of an engineered system in the system operation stage. This chapter presents the research solution to the third challenging question, as introduced in Chapter 1, which is how sensor networks can be designed to effectively monitor system health degradation under highly uncertain operational conditions. In this chapter, a generic sensor network (SN) design framework based on a probabilistic detectability measure is developed. Section 5.1 defines the detectability measure for a given SN, Section 5.2 presents the detectability analysis, and the generic SN design is proposed in Section 5.3.

5.1 Detectability of a Sensor Network

In the proposed SN design framework, a set of health states, denoted as HS_i, $i = 1, 2,\ldots, N_{HS}$, will first be identified based on critical failure modes for the system under consideration and their combinations. The correct detection of each health state is then defined in a probabilistic form to measure the performance of a given SN design.

This yields a probability of detection (PoD) matrix for a given SN design, from which the SN detectability can be derived.

5.1.1 Probability of Detection Matrix

The general form of a PoD matrix for a given SN design is shown in Table 5-1, where the P_{ij} is defined as the conditional probability that the structural system is detected to be at the HS_j by the SN given the system is at the HS_i. Clearly, P_{ij} represents the probabilistic relationship between the true health state of the system and the detected health state by the SNs. Mathematically, it is expressed as

$$P_{ij} = \Pr(\text{Detected as } HS_j \mid \text{System is at } HS_i) \tag{5.1}$$

The diagonal term in the PoD matrix represents the probability of correct detection for each corresponding system health state.

Table 5-1: Probability of detection (PoD) matrix

Probability		Detected Health State			
		1	2	…	N_{HS}
True Health State	1	P_{11}	P_{12}	…	$P_{1N_{HS}}$
	2	P_{21}	P_{22}	…	$P_{2N_{HS}}$
	…	…	…	…	…
	N_{HS}	$P_{N_{HS}1}$	$P_{N_{HS}2}$	…	$P_{N_{HS}N_{HS}}$

5.1.2 Detectability Measure

Based on the PoD matrix, the detectability measure for the i^{th} system health state HS_i is defined as

$$D_i = P_{ii} = \Pr(\text{Detected as } HS_i \mid \text{System is at } HS_i) \quad (5.2)$$

The above detectability definition provides a probabilistic measure for the SN performance considering uncertainties involved in the SN sensing process, such as material properties for structural systems, loading conditions and operating environments. Based on this definition, the diagonal terms in the PoD matrix, which represent the probabilities of correct detection for predefined health states, will determine the overall SN performance, and thus constitute N_{HS} number of performance constraints on the detectability during the SN design optimization process. Since the detectability measure involves the computation of multiple conditional probabilities, an efficient and accurate method must be developed for the detectability analysis.

5.2 Detectability Analysis

Since the detectability is defined as a probabilistic measure for the performance of a SN, the detectability analysis thus needs to take into account various uncertainties involved in the structural system itself and/or the system operating condition as well. This section will present the detectability analysis method based on the structural simulation and system health state classification. The rest of this section will begin with a mathematical example of detectability calculation. Valuable information will be derived from the discussion of the example, and the detectability analysis method will then be presented.

5.2.1 An Introductory Example

In this example, suppose that only one sensor will be used for the damage detection. For a healthy condition (Health State 1, HS_1), the sensor output is assumed to follow a normal distribution as N (0, 0.5^2), whereas the distribution of sensor output will be changed to N (1, 0.8^2) if there is a minor damage in the system (Health State 2, HS_2). If there is a severe damage in the system (Health State 3, HS_3), the sensor output will further increase and follow a normal distribution as N (5, 1^2). In what follows, we will find out the detectability values for all three defined health states based on the available information.

To calculate the detectability measure for each health state, it is necessary to classify any given sensory data into one of the three health states. This can be accomplished simply by defining the normalized distance between the sensory data and the center data point for each health state, and consequently the given set of sensor point will be classified into the health state which has the smallest normalized distance. In this example, the neutral point $X_{1\text{-}2}$ between HS_1 and HS_2 can be calculated as

$$\frac{X_{1-2}-0}{0.5}=\frac{1-X_{1-2}}{0.8} \tag{5.3}$$

which provides $X_{1\text{-}2} = 0.3846$. Similarly, the neutral point $X_{2\text{-}3}$ between HS_2 and HS_3 can be calculated as

$$\frac{X_{2-3}-1}{0.8}=\frac{5-X_{2-3}}{1} \tag{5.4}$$

which provides $X_{2\text{-}3} = 2.7778$. Figure 5-1 shows the sensor outputs at different health states, $X_{1\text{-}2}$, and $X_{2\text{-}3}$.

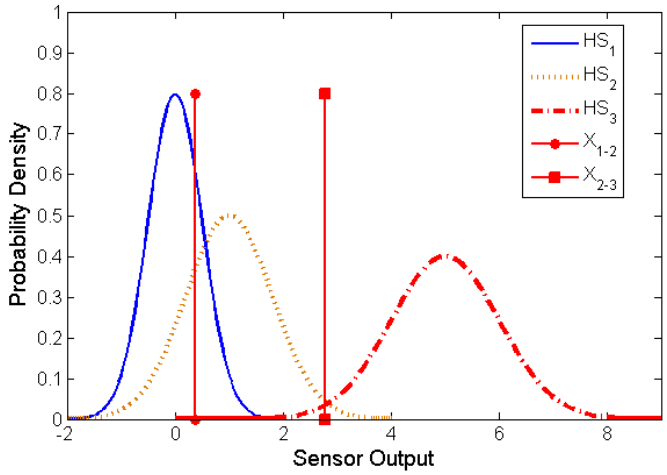

Figure 5-1: Sensor outputs and neutral points between health states

Based on the definition in Eq. (1), the detectability of each health state in this mathematical example can be calculated as

$$\begin{aligned} D_1 = P_{11} &= \Pr(\text{Detected as } HS_1 \mid \text{System is at } HS_1) \\ &= \Pr\left(X \le X_{1-2} \mid X \sim N\left(0, 0.5^2\right)\right) \\ &= 0.7791 \end{aligned} \tag{5.5}$$

$$\begin{aligned} D_2 = P_{22} &= \Pr(\text{Detected as } HS_2 \mid \text{System is at } HS_2) \\ &= \Pr\left(X_{1-2} \le X \le X_{2-3} \mid X \sim N\left(1, 0.8^2\right)\right) \\ &= 0.7660 \end{aligned} \tag{5.6}$$

$$\begin{aligned} D_3 = P_{33} &= \Pr(\text{Detected as } HS_3 \mid \text{System is at } HS_3) \\ &= \Pr\left(X \ge X_{2-3} \mid X \sim N\left(5, 1^2\right)\right) \\ &= 0.9869 \end{aligned} \tag{5.7}$$

From the analytical calculation of the detectability measure in the example above, it is clear that the classification of the health states and the statistical distributions of sensor outputs are crucial for the SN detectability analysis. However, in most engineering applications, an SN is always composed of multiple sensors and required to deal with much more than three different health states. Consequently, the analytical

analysis of SN detectability through the calculation of neutral points between health states becomes practically impossible. Besides, the statistical distributions of all sensors' outputs for all health states are usually not available. Instead, only a finite set of sensory data might be available as training data set to characterize the sensor output for each system health state. Thus, a more sophisticated health state classifier, which should be able to classify any given set of multi-dimensional sensory data into multiple different system health states based on a finite set of training data, is needed for the SN detectability analysis. In this study, the Mahalanobis distance (MD) classifier is employed for this classification purpose.

5.2.2 Mahalanobis Distance Classifier

The Mahalanobis distance provides a powerful method of measuring how similar one set of sensor output data is to another predefined set of training data, and can be very useful for identifying which predefined health state is the most similar one to the current system health state for the purpose of the health state classification. The MD classifier quantitatively measures the similarity between a given sensory data set and the training data sets for the i^{th} system health state through the MD, expressed as

$$MD_i = (X - M_i)^T \Sigma^{-1} (X - M_i) \tag{5.8}$$

where X is the given sensory data set to be classified, M_i is the vector of mean values of the training data set for HS_i, and Σ is the covariance matrix of the training data set for HS_i. The given sensory data set will be classified by the classifier into a predefined system health state that gives the smallest MD, or in other words the highest similarity. The following mathematical example demonstrates the system health state classification using the MD classifier.

In this example, two sensors are used and four system health states including one healthy state HS_1 and 3 faulty states HS_2 to HS_4 are predefined with 10 sets of data for each health state as the training data sets as shown in Table 5-2. To demonstrate the MD classifier, there are 5 sets of sensory data in total, as shown in the first two columns of Table 5-3, need to be classified into one of the four predefined health states. Using the MD classifier, the MDs for each sensory data set can be calculated with the training data set shown in Table 5-2 using Eq. (5.8). The MD values together with the classified system health state for each sensory data set are also shown in Table 5-3.

Based on the above procedure, the PoD matrix can be evaluated as follows. Suppose that there are totally T_i number of testing sensory data sets for HS_i, and in which after the classification process T_{ij} sets classified into HS_j, where $i, j = 1, 2, \ldots, N_{HS}$, then based on the definition of the PoD matrix, the probability of detection P_{ij} can be approximately calculated as

$$P_{ij} \simeq \frac{T_{ij}}{T_i} \tag{5.9}$$

Besides, since one set of sensory signal will definitely be classified into one of the predefined N_{HS} health states, thus,

$$\sum_{j=1}^{N_{HS}} T_{ij} = T_i \tag{5.10}$$

Eq. (5.10) Indicates that the summation of each row of the PoD matrix equals to one. Similarly, the detectability for HS_i can be obtained as

$$D_i = P_{ii} \simeq \frac{T_{ii}}{T_i} \tag{5.11}$$

Table 5-2: Characteristic data for system health states

HS_1		HS_2		HS_3		HS_4	
S_1	S_2	S_1	S_2	S_1	S_2	S_1	S_2
-0.22	-0.09	1.15	-1.20	1.20	-2.51	-1.00	1.28
-0.83	0.36	0.33	-0.66	2.13	-1.69	-1.16	0.87
0.06	-0.29	1.36	-0.59	1.47	-1.75	-0.45	0.81
0.14	1.09	1.81	-0.64	2.71	-1.15	-1.94	0.85
-0.57	-0.07	0.65	-0.35	1.60	-1.70	-0.79	0.26
0.60	0.06	1.43	-0.67	2.26	-2.32	-0.55	0.88
0.59	0.53	1.63	-0.40	2.11	-1.81	-0.63	1.06
-0.02	0.03	0.20	-1.60	1.54	-2.50	-0.71	1.16
0.16	-0.05	0.28	-1.01	0.91	-2.01	-0.98	1.72
0.09	-0.42	1.29	-1.08	1.97	-2.02	-0.66	0.82

Table 5-3: System health states classification using MD classifier

Sensory Data		Mahalanobis Distance				Classified State
S_1	S_2	HS_1	HS_2	HS_3	HS_4	
0.74	-1.05	10.75	0.39	17.68	40.42	HS_2
1.59	-2.12	42.55	18.16	0.20	94.23	HS_3
-0.93	1.22	11.81	64.75	169.94	0.43	HS_4
-0.12	-0.21	0.58	10.63	62.58	12.28	HS_1
1.89	-1.97	44.81	17.91	0.07	96.03	HS_3

5.2.3 Procedure of Detectability Analysis

Based on the preceding discussion, defining the system health states is crucial for the SN design, which will determine the functionality of the SN to be designed. Through defining different type of system health states, SNs can be designed to tackle different failure mechanisms for structural systems. After defining the health states, collecting sample training and testing data sets for each health states are the next step, which can be accomplished through the structural simulation using valid numerical models, such as finite element analysis (FEA). The sample size of the training and testing data sets will determine the accuracy of the detectability evaluation using the proposed MD classifier. With the training and testing data sets available, the detectability for each predefined health state for a given SN design can be evaluated in the same way as we did in the previous example.

The overall procedure of the detectability analysis can be summarized in Table 5-4.

Table 5-4: Procedure for detectability analysis

STEP 1:	Define the problem and system health states;
STEP 2:	Collect characteristic training and testing data sets for each predefined system health state;
STEP 3:	Extract a corresponding subset of training and testing data, for a given SN design, from the characteristic data sets obtained in STEP 2;
STEP 4:	Perform classification using the MD classifier defined by Eq. (5.8);
STEP 5:	Calculate the detectability measure for each health states using Eq. (5.11).

5.3 Sensor network design optimization

The appropriate selection of the sensing devices, such as fiber optics, piezoelectric, MEMS sensors, accelerometers, or acoustic sensors, is determined by the sensor's characteristic attributes, such as full-scale dynamic range, sensitivity, noise floor, and analog-to-digital converter resolution. Thus, the design variables involved in the proposed design framework are the decision variables for the selection of sensing devices, numbers of selected sensing devices, sensing device locations, and the parameters for controlling the sensing process, such as excitation frequency, loading levels. The design constraints are SN probabilistic performance requirements considering various uncertainties presented in the structures as well as the operating conditions. The performance requirements include the SN detectability for each predefined system health state. With all factors considered above, the SN design optimization problem can be formulated as:

$$\begin{aligned} &\text{Minimize} \quad C \\ &\text{subject to} \quad D_i\left(\mathbf{X_T},\ \mathrm{X_N},\ \mathbf{X_{Loc}},\ \mathbf{X_s}\right) \geq D_i^t \\ &\qquad\qquad \left(i = 1, 2, ..., N_{HS}\right) \end{aligned} \tag{5.12}$$

where $\mathrm{X_T}$ is a vector of the binary decision variables for the selection of the types of sensing devices, $\mathrm{X_N}$ is a vector consisting of numbers of each selected type of sensing devices, $\mathrm{X_{Loc}}$ is a 3-D vector of the location of each sensing device, and $\mathbf{X_s}$ is a vector of sensing control parameters; N_{HS} is the total number of predefined health states for the structural system. D_i is the detectability measure of the SN for the i^{th} predefined health state, which is a function of the design variables $\mathrm{X_T}$, $\mathrm{X_N}$, $\mathrm{X_{Loc}}$ and $\mathbf{X_s}$, whereas D_i^t is the target SN detectability for the i^{th} predefined health state. To make the design optimization problem manageable, the design space of sensor locations need to be

properly defined. In this SN design problem, the sensor noise is not considered and the randomness for SN outputs is mainly due to the variability of structural responses.

The SN design optimization problem in Eq. (5.12) contains discrete decision variables for the selection of sensing devices, integer variables for the number of selected sensing devices, as well as continuous variables for the sensor locations. Thus, it is formulated as a mixed-integer nonlinear programming (MINLP) problem [Adjiman et al. 2000], and heuristic algorithms such as Genetic Algorithms (GAs) can be used as the optimizer to for the optimization purpose. In this study, the GA is employed for the example problem that will be detailed in the subsequent section. More alternative algorithms for solving the MINLP problem can be found in references [Adjiman et al. 2000; Wei and Realff 2004].

Figure 5-2 shows the flowchart of the SN design optimization process. As shown in the figure, the process starts from an initial SN design and goes into the design optimization subroutine (the right hand side grey box), which will carry out the SN cost analysis, call the performance analysis subroutine (the left hand side grey box) to evaluate the performance of the SN at the current design, and execute the optimizer to generate the new SN design until an optimal SN design is obtained. In the performance analysis subroutine, the detectability analysis as discussed in the previous section will be carried out. Before solving the optimization problem, valid system simulation models have to be built and structural simulations have to be accomplished so that the training and testing data sets for each predefined health state are available.

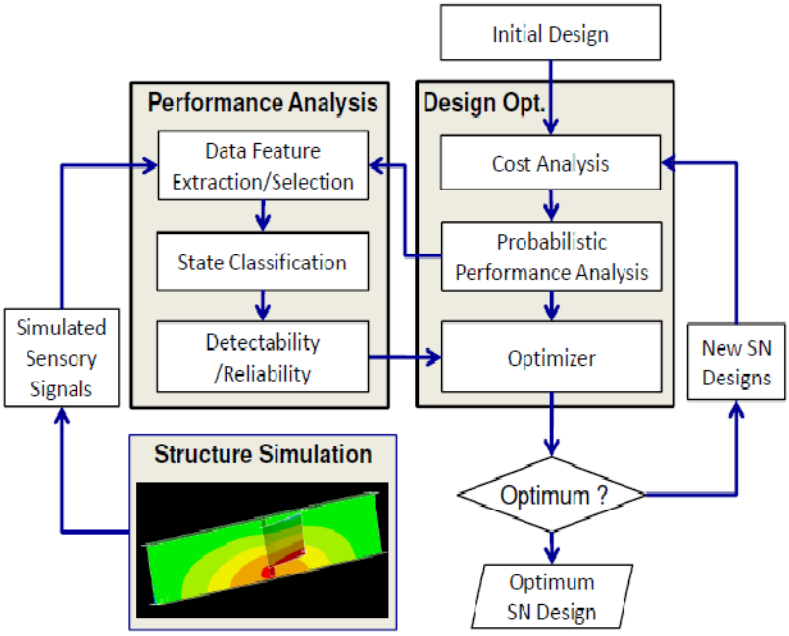

Figure 5-2: Flowchart of the detectability based framework for structural SN design

5.4 Case Studies

This section demonstrates the feasibility of the proposed detectability based sensor network design framework for structural sensor network design. Two examples, one rectangular plate with crack and corrosion failure modes and another power transformer winding joint with joint mechanical failures are used to demonstrate the proposed methodology.

5.4.1 Rectangular Plate Example

In this case study, a two-end fixed rectangular plate (2m x 1m), as shown in Fig.5-3, is employed to demonstrate the developed sensor network design methodology. The plate is assumed to have 6 potential damages as indicated in the figure from D1 to D6, in which D1 and D2 indicate the crack at the fixed ends of the plate, D3 and

D4 indicate the corrosion in the middle field of the plate, whereas D5 and D6 indicate cracks at the middle edges of the plate. With different combinations of these 6 damage locations, 9 health states of the plat are identified for this study as shown in table 5-5. The plate is modeled using the finite element too ANSYS 10 using shell elements with the thickness of each node follows a Gaussian random field variable. The damages of above mentioned crack or corrosion are realized by reducing the Young's modulus of the material. Uncertainties involved in this case study are listed in Table 5-6.

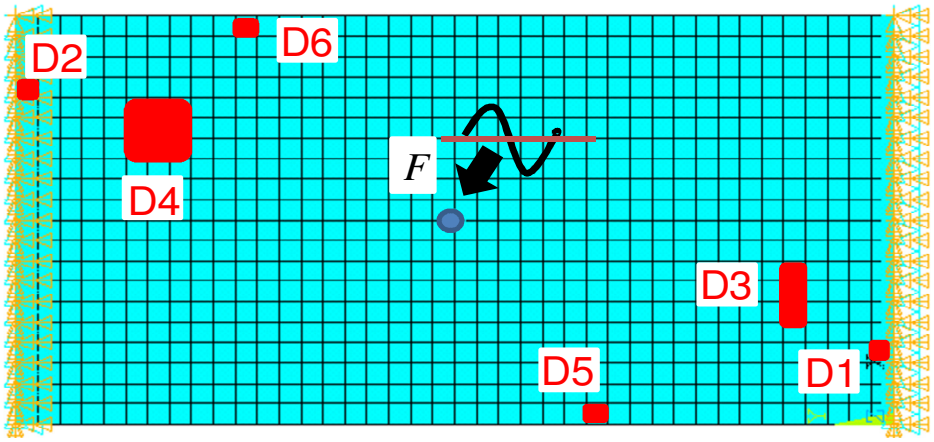

Figure 5-3: Two-end fixed rectangular plate with indicated damages

Table 5-5: Definition of the health states for plate case study

Health State	HS_1	HS_2	HS_3	HS_4	HS_5	HS_6	HS_7	HS_8	HS_9
Damage Combinations	-	D1	D2	D3	D4	D5	D6	D2 & D6	D1 & D4

Table 5-6: Random variables for the plate case study

Random Variables	Descriptions	Statistical Information
h	Plate thickness	Gaussian Random Field: $N(0.4, 0.01^2)$ for each node
ρ	Material property: density	$N(7.8e3, 2e2^2)$
E	Material property: Young's modulus	$N(3e7, 1.5e6^2)$
v	Material property: Poisson ratio	$N(2.7e\text{-}1, 5.4e\text{-}3^2)$
E_{cr}	Young's Modulus for crack failure	$N(3e2, 15^2)$
E_{co}	Young's Modulus for corrosion failure	$N(5e2, 10)$

The plate is modeled using the finite element tool ANSYS 10 with 800 of 3D shell63 elements in total. The thickness of plate is modeled by a Gaussian random field with each node independently follows a normal distribution, as shown in table 5-5. The damages of above mentioned crack or corrosion are realized by reducing the Young's modulus of the material. Uncertainties involved in this case study are also listed in Table 5-5. In this case study, the harmonic analysis with excitation frequencies from 0.1Hz to 1.6 Hz. Figure 5-4 shows the vibration displacement responses for health states HS_1 and HS_2 with excitation frequencies f = 0.3Hz and f = 1.0Hz. As shown in the figure, the change of the vibration responses due to the introduced damage D1 is slight in terms of both locations and magnitudes, whereas the excitation frequency imposes an obvious effect. Thus, the sensors need to be optimally located and the excitation frequencies must be optimally chosen, in order to detect the minor changes for different health states. In this study, 100 sets of random

samples are used for simulation to generate the training data sets, whereas another 100 sets are used as testing data sets.

The objective function of this sensor network design problem is to minimize the total number of used sensors, whereas the constraints are the detectability requirements for each health state. The design variables includes the total number of sensors (accelerometers), each sensor's location (the node number), and excitation frequency for each sensors, as we assume that active sensing approach is employed in this study. Following the flowchart shown in Fig. 5-2 and the detectability analysis procedure listed in Table 5-4, the SN design problem in this case study was solved using the genetic algorithm (GA). To account for the stochastic feature of the GA, the SN design problem is repeatedly solved 1000 times, in which 819 runs successfully converged to the optimum design with a total number of 5 sensors, whereas 181 runs failed. Figure 5-5 shows the detectability measure for each of 9 health states at the optimum SN design versus different total numbers of sensors. As shown in Fig.5-5, 5 sensors are required for the sensor network to satisfy a target detectability of 0.95. The SN with 5 sensors are obtained as the final optimum design and the sensor locations and excitation frequencies for this optimum design are listed in Table 5-7 and shown in Fig. 5-6 as black dots.

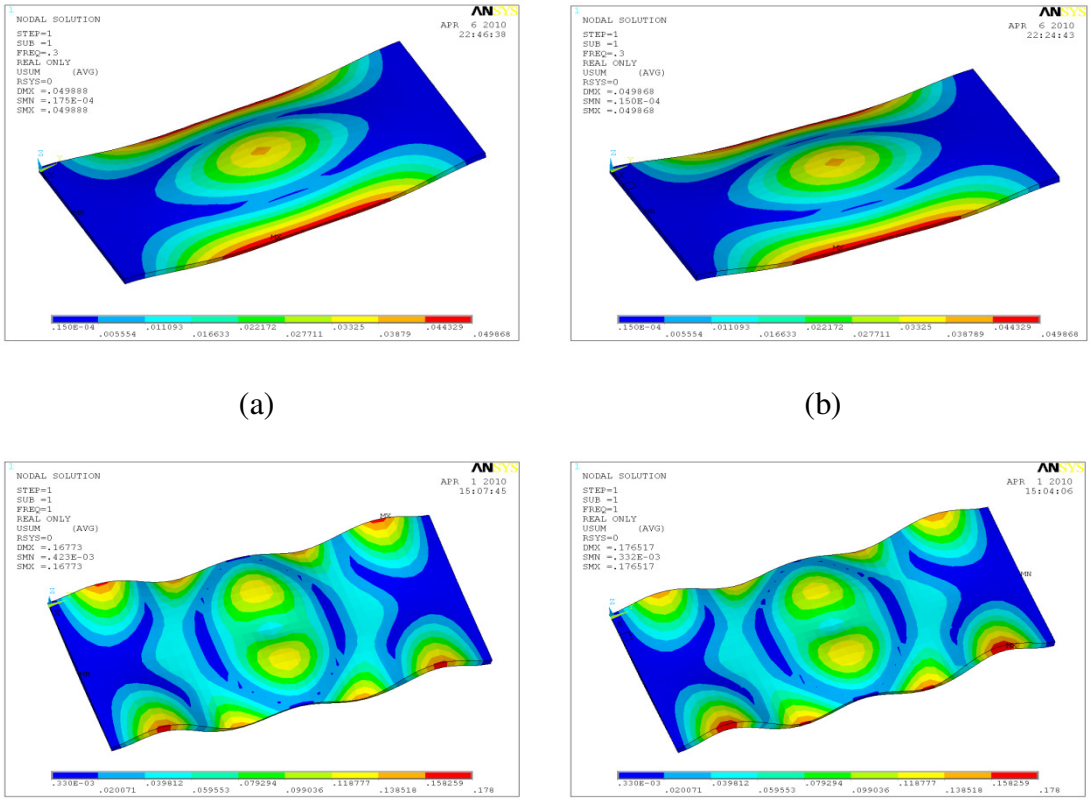

Figure 5-4: Vibration displacement contour of the of the plate

(a) HS_1,with $f = 0.3$, (b) HS_2 with $f = 0.3$, (c) HS_1 with $f = 1.0$, (d) HS_2 with $f = 1.0$

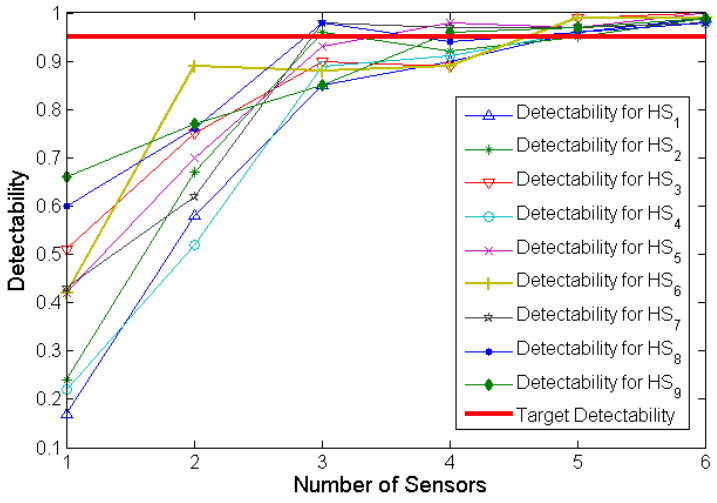

Figure 5-5: Detectability for HS_i ($i = 1 \sim 9$) at optimum designs

Table 5-7: Optimum SN design for the fixed-end plate case study

Sensor Index	1	2	3	4	5
Node Number	137	228	236	518	716
Frequency	1.3	0.2	1.3	0.3	1.4

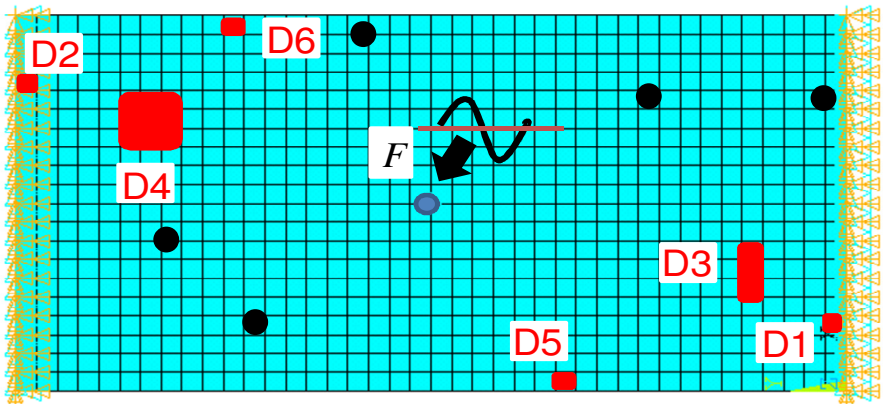

Figure 5-6: Sensor locations for the optimum SN design

5.4.2 Power Transformer Case Studies

The monitoring of power transformers enables the transition from the traditional time-based maintenance to the condition-based maintenance, resulting in significant reductions in maintenance costs [Leibfield 1998]. Due to the difficulties of direct measurement inside the transformer, the data that are actually most often used for both diagnosis and prognosis of transformers are obtained through indirect measurements [Rivera et al. 2000]. For example, measurements of temperature are firstly accomplished at accessible points and a modeling of the gradient can then be used to induce the maximum temperature in some areas; electric parameters and analysis of moisture content of the cooling oil are often performed for the diagnosis

and condition-based maintenance of transformers, with frequency response analysis of electric characteristics being common [Allan et al. 1992]; the vibrations of the magnetic core and of the windings could characterize transitory overloads and permanent failures before any irreparable damage occurs. This case study aims at designing an optimum SN on the front wall surface of a power transformer. The measurements of the transformer vibration responses induced by the magnetic field loading enables the detection of mechanical failures of winding support joints inside the transformer.

Description of the case study

In this study, the winding support joint loosening is considered as the failure mode, the detection of which will be realized by collecting the vibration signal, induced by the magnetic field loading with a fixed frequency on the power transformer core, using the optimally designed SN at the external surface of the transformer. The validated finite element (FE) model of a power transformer was created in ANSYS 10 as shown in previous chapters in Fig. 3-13 and Fig. 4-24. Figure 5-7 shows 12 simplified winding support joints with 4 for each winding. The transformer is fixed at the bottom surface and a vibration load with the frequency of 120 Hz is applied to the transformer core. The joint loosening was realized by reducing the stiffness of the joint itself. Different combinations of the loosening joints will be treated as different health states of the power transformer which will be detailed in the next subsection.

The uncertainties in this case study are modeled as random parameters with corresponding statistical distributions listed in Table 5-8, which includes the material

properties, such as Young's modulus's, densities, Poisson ratios, for support joints and windings, as well other parts in the power transformer system. Besides, the geometry parameters are also considered as random variables. These uncertainties will be propagated into the structural vibration responses and will be accounted for when designing an optimum SN.

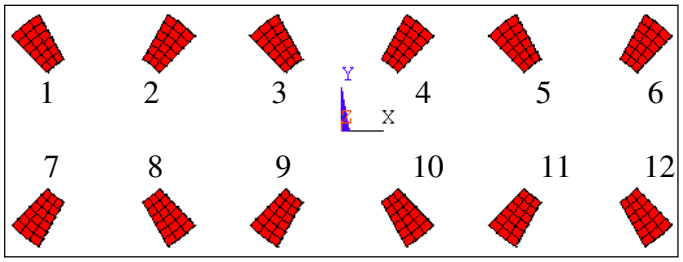

Figure 5-7: Winding support joints and their numberings

Table 5-8: Random property of the power transformer

Random Variable	Physical Meaning	Randomness (cm, g, degree)
X_1	Wall Thickness	N (3, 0.06^2)
X_2	Angular width of support joints	N(15, 0.3^2)
X_3	Height of support joints	N(6, 0.12^2)
X_4	Young's modulus of support joint	N(2e12, $4e10^2$)
X_5	Young's modulus of loosening joints	N(2e10, $4e8^2$)
X_6	Young's modulus of winding	N(1.28e12,$3e10^2$)
X_7	Poisson ratio of joints	N(0.27, 0.0054^2)
X_8	Poisson ratio of winding	N(0.34, 0.0068^2)
X_9	Density of joints	N(7.85, 0.157^2)
X_{10}	Density of windings	N(8.96, 0.179^2)

Health States and Simulations

For the purpose of demonstrating the proposed SN design methodology, 9 representative health states (see Table 5-9) were selected from all possible combinations of 12 winding support joint failures. Among these 9 selected health states, HS_1 denotes the healthy condition without any loosening joint, whereas HS_2 to HS_9 are health states with either one or two loosening joints. According to the statistical properties of random parameters in Table 5-8, 200 sets of random samples were generated and the simulations for each of 9 health states were carried out and the vibration response of the displacement amplitudes for all the finite element nodes on the outer wall surfaces were saved as the simulation results. The stress contour of the healthy state power transformer at the nominal values of the random parameters from the structural simulation is shown in Fig. 5-8, whereas the vibration response of the covering wall is shown in Fig.5-9. The first 100 sets of simulation results were used as the training data set and the others were used as testing data set. These simulation results were later used to evaluate the SN detectability. As mentioned in the previous section, this case study problem is formulated as designing an SN on the surface of the covering wall of the power transformer to minimize the cost of the SN while satisfying the detectability constraints for each health state, i.e., the detectability should be greater than a target detectability of 0.95.

Table 5-9: Definition of system health states

Health State	HS_1	2	3	4	5	6	7	8	9
Loosening Joints	-	1	2	3	1,2	1,3	1,5	1, 9	1, 11

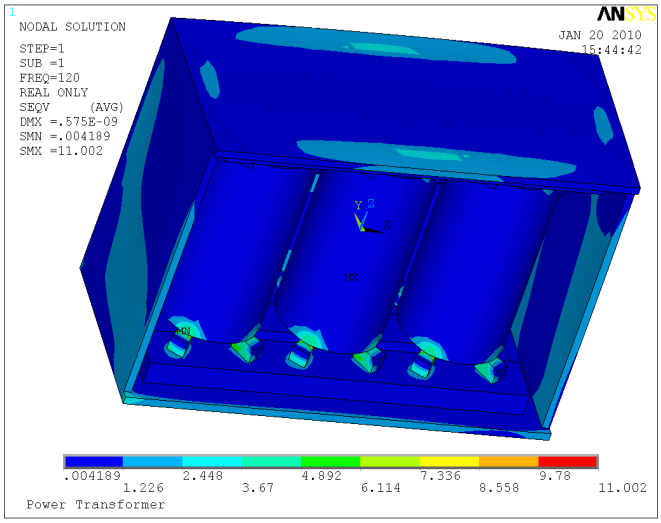

Figure 5-8: Stress contour of the winding support for the healthy state of power transformer

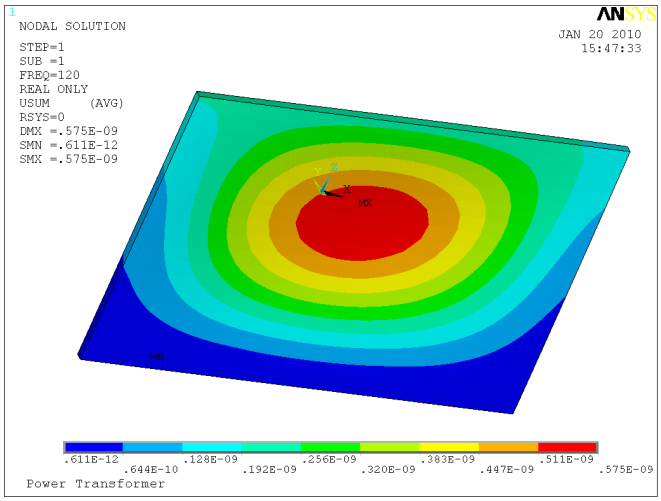

Figure 5-9: Vibration displacement contour of the power transformer covering wall for the healthy state of power transformer

As the vibration displacement amplitude of each node on the surface of the covering wall was used as the simulated sensor (accelerometer) output. Thus, the

design variables in this case study include: (1) total number of accelerometers, (2) location of each accelerometer, and (3) the direction (X or Z) of each accelerometer.

Results and Discussion

Following the flowchart shown in Fig. 5-2 and the detectability analysis procedure listed in Table 5-4, the SN design problem in this case study was solved using the genetic algorithm. To account for the stochastic feature of the GA, the SN design problem is repeatedly solved 1000 times, in which 615 runs can successfully converge to a feasible solution with 9 sensors and all constraints satisfied whereas 385 runs failed to find a feasible SN design. Further in the 615 successful runs, only 17 runs successfully converged to the global optimum design with a total number of 9 sensors and detectability values for all health states are over the target detectability value 0.95. Figure 5-10 shows the detectability for each of 9 health states at the optimum SN design versus different total numbers of sensors. With the target detectability being 0.95, we obtained the optimum SN design on the outer wall surface (140cm x 90cm) with totally 9 sensors, as shown in Table 5-10 and Fig. 5-11. The detectability for each health state at the optimum design is listed in Table 5-11.

The results of the power transformer case study demonstrate that the proposed SN design framework is capable to tackle the SN design problems for complicated engineered systems with multiple system health states and a variety of system input uncertainties. The authors also would like to address the following comments for the readers to better understand the problem. Firstly, in this case study, the GA was implemented for the design optimization and repeatedly executed for 1000 times. Although, for most of times as discussed above, the optimization converged to a

feasible design with the same minimum number of sensors, the convergence to local minima was also observed. Thus, it would be interesting to investigate other optimization algorithms (e.g., the particle swarm optimization [Valle et al. 2008]) to make the SN design process more robust; secondly, due the computational time, only 100 samples were simulated for each health state, resulting in 2 decimal digits of precision in the detectability estimates. To obtain more accurate results, more samples from the structural simulation are needed. Lastly, to make the SN design more reliable, the redundancy could be easily integrated to the proposed SN design framework by adding the redundancy as an additional set of design variables and the SN reliability as an additional constraint.

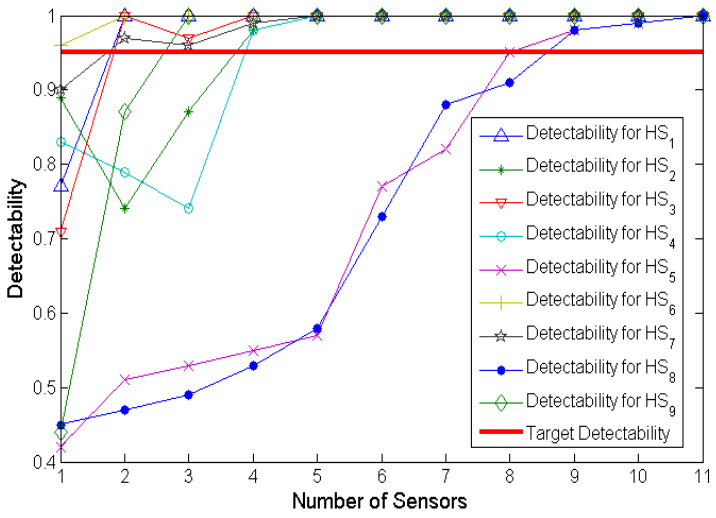

Figure 5-10: Detectability for HS_i (i = 1 ~ 9) at optimum designs

Table 5-10: Optimum SN design for the power transform case study

Sensor Index	Location (cm)		Direction
	x	z	
1	-56.4	0.0	Z
2	67.2	-34.4	X
3	-2.6	-30.0	Z
4	49.7	-34.4	X
5	-57.9	30.0	X
6	-30.6	15.3	X
7	27.5	30.0	X
8	39.3	35.2	X
9	59.1	0.0	X

Table 5-11: Detectability at optimum design for the power transform case study

HS_1	HS_2	HS_3	HS_4	HS_5	HS_6	HS_7	HS_8	HS_9
1	1	1	1	0.98	1	1	0.98	1

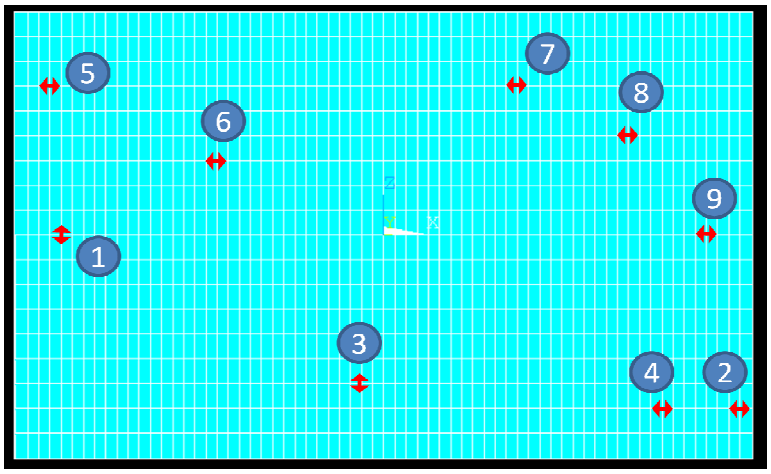

Figure 5-11: Optimal design of the distributed SN for power transformer case study

5.5 Summary

This chapter presented the generic design framework for SN design optimization using the detectability measure while accounting for uncertainties in material properties and geometric tolerances. The proposed work defined the detectability measure to quantify the performance of a designed SN in a probabilistic form. Then, detectability analysis was developed based on structural simulation and health state classification, where the Mahalanobis distance classifier was proposed for health state classification. Finally, the generic SN design framework was formulated as a mixed integer nonlinear programming (MINLP). The genetic algorithm was used as the optimizer to solve the SN design optimization problem. The power transformer case study demonstrated that the proposed generic SN design framework is feasible to handle multiple failure modes and uncertainties in material properties and geometric tolerances.

Chapter 6: A Generic Framework for Structural Health Prognostics

Structural heath prognostics utilize sensory signals to monitor the health condition of an engineered system in the operational stage and predict the remaining useful live (RUL). The predictive remaining useful life information enables the system to be proactively maintained against potential system failures. This chapter presents the research solution to the fourth challenging question, as identified in Chapter 1, which is how remaining useful lives can be predicted accurately and timely under highly uncertain operational conditions.

Structural health prognostics can be broadly applied to various engineered artifacts in an engineered system. However, techniques and methodologies for health prognostics become application-specific. Difficulties in developing an application-generic methodology mostly result from heterogeneity of sensory data, a wide range of data acquisition frequency and size, and different characteristics in uncertain manufacturing and operational conditions. This chapter thus aims at formulating a generic framework for structural health prognostics, which is composed of four core elements: (i) a generic health index system, (ii) a generic offline training scheme using the sparse Bayesian learning (SBL), (iii) a generic online prediction scheme using the similarity-based interpolation (SBI), and (iv) an uncertainty propagation map for prognostic uncertainty management. This generic structural health prognostics framework is generally applicable to different engineered systems. The rest of Chapter 6 is organized in the following way. Section 6.1 provides an overview of the proposed framework, whereas Sections 6.2 to 6.5 presents the above mentioned

four core elements of the prognostics framework respectively. Two cases studies are presented in Section 6.6 to demonstrate the effectiveness of the proposed generic structural health prognostics methodology.

6.1 Overview of the Framework

Figure 6-1 outlines the proposed generic framework for structural health prognostics. This framework is unique in that it offers the general approaches for defining structural health index, building background health knowledge, and predicting RULs.

The proposed generic health index system can model the health state of an engineered component or system using two health index measures: (i) Physics Health Index (PHI), and (ii) Virtual Health Index (VHI). The PHI uses a dominant physical signal as a direct health measure. With the growing complexity of engineered systems and embedded sensor networks, the mapping of a multitude of heterogeneous sensory signals to a dominant health measure is getting more and more difficult. In such cases, the VHI is proposed which uses a normalized health index as a function of multiple physical signals.

The proposed generic offline training process is of great importance to structural health prognostics because online prediction is made based on background health knowledge built in the offline training process. In the offline process, it is very important to build statistically rich background health knowledge, which can account for manufacturing variability and uncertain operational conditions. On the other hand, the statistically rich background health knowledge should be efficiently managed to enable real-time RUL prediction in the online predicting process, especially when

sensory data are massive and heterogeneous. The SBL scheme, such as the relevance vector machine (RVM), is a state-of-the-art technique for statistical regression that provides a regression result with not only a probabilistic form but also a great sparseness feature.

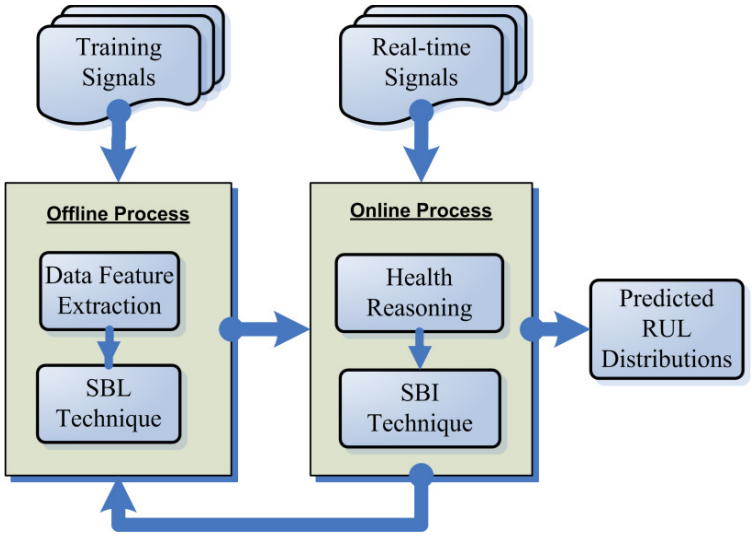

Figure 6-1: A generic framework for structural health prognostics

Table 6-1: Procedure of the generic structural health prognostics framework

STEP1	Defining the prognostics problem and determining sensor configurations;
STEP2	Acquiring training sensory signal sets from offline system unit;
STEP3	Performing the offline learning process using the SBL technique with the training sensory signals and building the background health knowledge;
STEP4	Acquiring testing sensory signals from online system units;
STEP5	Predicting the *RUL* distributions using the SBI technique through the online prediction process, which employs the background health knowledge obtained from STEP 3.

The online prediction process employs the background health information for the health prognostics using the SBI technique. This framework also enables the continuous update of the health information and prognostics results in real-time with new sensory signals. Table 6-1 details the proposed unified prognostics framework with the five steps. STEP 2 to STEP 5 can be repeated to update the RUL distributions as new training sensory signals are acquired.

6.2 Generic Health Index System

This task considers massive training/testing sensory signals from embedded sensor networks over a complex engineered system. In this section, a generic health index system is proposed, which is composed of two distinguished health indexes: Physics Health Index (PHI) and Virtual Health Index (VHI).

Physics Health Index (PHI): this health index requires ample understanding of physics-of-failures of engineered system units. The PHI is thus applicable if sensory signals are directly related to physics-of-failures. In general, the PHI uses a dominant physical signal as a direct health metric. In the literature, most engineering practices of health prognostics are based on various PHIs. For example, the vibration signal has been used to characterize the health condition of the roll bearing by [Gabreel et al. 2005]; the radio frequency impedance has been used for the prognostics of electronic solder joint degradation [Kwon et al. 2008]; the battery impedance value has been used to monitor the health condition of space application batteries [Saha et al. 2009]; and the capacitance of generator stator winding has been used for the wet bar detection and prognostics for water-cooled turbine generators [Inoue et al. 2003], and

so on. Just like the examples above, when sensory signals are directly related to physics-of-failures, it is straightforward and comprehensive to use the PHI for extracting health conditions of engineered system units. Otherwise, the application of the PHI is limited. It is expected that the mapping of a multitude of heterogeneous sensory signals to the dominant physical signal is getting more and more difficult with the growing complexity of engineered systems and embedded sensor networks.

Virtual Health Index (VHI): the VHI is proposed as a possible solution to overcome the difficulty of the PHI above. This health index is applicable when there is no dominant physical signal. One-dimensional VHI can be extracted from multi-dimensional sensory signals using advanced data processing techniques, such as weighted averaging methods [Xue et a;. 2008], Mahalanobis distance measure [Nie et al. 2007], flux-based methods [Baurle and Gaffney 2008].

This study employs a linear data transformation method to construct the VHI, and this transformation method is a special case of weighted averaging methods. Suppose there are two groups of multi-dimensional sensory dataset that represent the system faulty and healthy states, $\mathbf{Q}_0$ of $M_0 \times N$ matrix and $\mathbf{Q}_1$ of $M_1 \times N$ matrix, respectively, where M_0 and M_1 are the numbers of dataset for system faulty and healthy states and N is the dimension of each dataset. With these two data matrices, a transformation matrix $\mathbf{T}$ can be obtained to transform the multi-dimensional sensory signal into the one-dimensional VHI as

$$\mathbf{T} = \left(\mathbf{Q}^T\mathbf{Q}\right)^{-1}\mathbf{Q}^T\mathbf{S}_{off} \tag{6.1}$$

where $\mathbf{Q}=[\mathbf{Q}_0; \mathbf{Q}_1]^T$, $\mathbf{S}_{off} = [\mathbf{S}_0, \mathbf{S}_1]^T$, $\mathbf{S}_0$ is a $1\times M_0$ zero vector and $\mathbf{S}_1$ is a $1\times M_1$ unity vector. This transformation matrix $\mathbf{T}$ can transform any sensory signal from the

offline or online prediction process to the normalized VHI as $\mathbf{H} = \mathbf{T} \cdot \mathbf{Q}_{off}$ or $\mathbf{H} = \mathbf{T} \cdot \mathbf{Q}_{on}$ where $\mathbf{H}$ is a $1 \times N$ vector, $\mathbf{Q}_{off}$ and Q_{on} are offline and online sensory signals respectively. The VHI can also be denoted as $h(t_i)$ for $i = 1,\ldots, N$, varying between 0 and 1. Since this VHI contains health condition signatures extracted from multi-dimensional sensory signals, it can be used to construct background health knowledge (e.g., predictive health degradation curve) in the offline training process and to further conduct the online prediction process.

6.3 Generic Offline Training Scheme

The proposed offline training process aims at building background health knowledge using training sensory signals from offline system units. The SBL is employed to build the statistical form of background health knowledge, such as predictive health degradation curves for an engineered component of interest.

The SBL is a generalized linear model in a Bayesian form and it shares the same functional form of the support vector machine (SVM). The SVM is a pervasive machine learning technique using a linear combination of kernel functions centered at a subset of the training data, known as support vectors. Despite its widespread success, the SVM suffers from a critical limitation, being that it makes point predictions rather than statistical predictions. To overcome this problem, Tipping has formulated this generalized linear model in a Bayesian form, named the relevance vector machine (RVM) [Tipping 2001]. It achieves comparable machine learning accuracy to the SVM but provides a full predictive distribution with substantially fewer kernel functions. To improve the efficiency and convergence of the RVM, several advances have been made for the original RVM, for example, the variational

RVM [Bishop and Tipping 2000], adaptive kernel RVM [Nonero and Hansen 2002] and so on. This section briefly discusses a sparse linear regression model and the RVM with the sparse Bayesian learning for data regression and feature extraction.

Sparse Bayesian Learning

This dissertation proposes to use a sparse Bayesian learning scheme for the offline training process. During offline training, an unknown true health index function value $f(t)$ needs to be predicted at an arbitrary point t with a set of health index values, $h_1,\cdots,h_N$, measured at training points $t = \{t_1,\cdots, t_N\}$:

$$h(t) = f(t) + \varepsilon(t) \tag{6.2}$$

where $\varepsilon(t)$ is the measurement noise. Under a linear model assumption, the health index function $f(t)$ can be a linear combination of some known basis functions $\phi_i(t)$, i.e.,

$$f(t) = \sum_{i=1}^{M} \omega_i \phi_i(t) \tag{6.3}$$

where $\boldsymbol{\omega} = (\omega_1,\cdots,\omega_M)$ is a vector consisting of the linear kernel function weights. Equation (6.2) can then be written in a vector form as:

$$\mathbf{h} = \boldsymbol{\Phi} \cdot \boldsymbol{\omega} + \boldsymbol{\varepsilon} \tag{6.4}$$

where $\boldsymbol{\Phi}$ is an $N \times M$ kernel matrix, whose i^{th} column is formed with the values of a basis function $\phi_i(t)$ at all the training points, and $\boldsymbol{\varepsilon}=(\varepsilon_1, \cdots, \varepsilon_N)$ is the noise vector.

To develop linear regression models with the optimum weights .. different approaches have been developed, for example the least square estimate (LSE), maximum likelihood estimation (MLE), and support vector machines (SVM). In many applications, the LSE and MLE estimates suffer from over-fitting. Although the

SVM-based approach overcomes the over-fitting problem, it provides only point estimates for basis function weights rather than statistical distributions, which is a critical aspect especially for the decision-making under various types of uncertainties. Another desirable property is sparseness, in which the least number of basis functions is desired in the function representation, while all the other basis functions are pruned by setting their corresponding weight parameters to zero. Sparseness property is extremely useful for fast computation during the online real-time prognostics process. The sparse Bayesian learning methodology, known as the RVM, provides an elegant approach to the sparse linear models by treating the parameters as random variables. With this treatment, both the statistical outputs and the good sparseness can be obtained. The remainder of this subsection will briefly introduce the RVM technique with the sparse Bayesian learning for data regression and feature extraction.

The RVM is a special case of a sparse linear model, where the basis functions are formed by a kernel function centered at the training points $t = \{t_1, \cdots, t_N\}$:

$$h(t) = \sum_{i=1}^{N} \omega_i \phi(t, t_i) \tag{6.5}$$

The study in this dissertation uses a multi-kernel RVM, consisting of several different types of kernels as:

$$h(t) = \sum_{m=1}^{M} \sum_{i=1}^{N} \omega_{mi} \phi_m(x, x_i) \tag{6.6}$$

The sparseness property enables automatic selection of the proper kernel at each location by pruning all irrelevant kernels. A sparse weight prior distribution can be assigned, in such a way that a different variance parameter is assigned for each weight, as:

$$p(\boldsymbol{\omega} \mid \boldsymbol{\alpha}) = \prod_{i=1}^{M} N\left(\omega_i \mid 0, \alpha_i^{-1}\right) \tag{6.7}$$

where $\boldsymbol{\alpha} = (\alpha_1,\cdots,\alpha_M)$ is a vector consisting of M hyper parameters, which are treated as independent random variables. To specify this hierarchical Bayesian inference model, prior distributions for $\boldsymbol{\alpha}$ must be defined. For a scale hyper parameter (α_i), it is common to use a Gamma prior distribution as:

$$p(\alpha_i) = Gamma(a_i, b_i) \tag{6.8}$$

where a_i and b_i are the hyper-parameters and initially set to a flat Gamma distribution. The weight prior $p(\boldsymbol{\omega})$ can be obtained by integrating over the hyper-parameters as

$$p(\boldsymbol{\omega}) = \int p(\boldsymbol{\omega} \mid \boldsymbol{\alpha})\, p(\boldsymbol{\alpha})\, d\boldsymbol{\alpha} \tag{6.9}$$

Assuming independent, zero-mean, Gaussian noise with a variance vector $\boldsymbol{\beta}^{-1}$, i.e., $\boldsymbol{\varepsilon} \sim N(0, \boldsymbol{\beta}^{-1}\mathbf{I})$ where $\mathbf{I}$ is an identify matrix, we have the likelihood of the observed data as:

$$p(h \mid \boldsymbol{\omega}, \boldsymbol{\alpha}, \boldsymbol{\beta}) = N\left(h \mid \boldsymbol{\Phi}\boldsymbol{\omega}, \boldsymbol{\beta}^{-1}\mathbf{I}\right) \tag{6.10}$$

where $\boldsymbol{\Phi}$ is either an $N\times N$ or an $N\times(N\times M)$ kernel matrix for the single and multi-kernel cases, respectively. This matrix is formed by all the basis functions evaluated at all the training points, i.e., $\boldsymbol{\Phi} = [\phi(t_1),\cdots,\phi(t_N)]$ where $\phi(t_i) = [\phi(t_1-t_i),\cdots,\phi(t_{i-1}-t_i), \phi(t_{i+1}-t_i),\cdots, \phi(t_N-t_i)]$. In order to make predictions using the Bayesian model, the parameter posterior distribution $p(\boldsymbol{\omega}, \boldsymbol{\alpha}, \boldsymbol{\beta} \mid h)$ needs to be computed. However, this posterior distribution cannot be computed analytically owing to its complexity and thus approximations must be made through the decomposition of the posterior distribution and employing appropriate iterative optimization methods, such as marginal likelihood optimization [Tipping and Faul 2003], expectation maximization

(EM) algorithms [Hogg et al. 2005] or incremental optimization algorithms [Syros 2008].

This SBL scheme can be applied on the system training dataset to construct the background knowledge of system degradation with a set of predictive health degradation curves (h^p) where each of them is represented in a statistical form as shown in Eq. (6.3). By applying the SBL, only a few critical basis points of the kernel functions will be employed to build the background health knowledge without losing the representativeness and uncertainty information. This desirable sparseness will substantially speed up the online prediction process and make it feasible for real-time prognostics applications.

6.4 Generic Online Prediction Scheme

The proposed online prognostics process aims at predicting the *RUL*s for online system units by employing a set of predictive health degradation curves built in the offline learning process. This online prediction process involves two procedures: (i) determination of initial health condition and (ii) RUL prediction using the similarity-based interpolation (SBI).

Initial Health Condition

Component and system units tested in the online prediction process may have different initial health conditions, due to manufacturing variability or different service lives. So determination of initial health conditions for component units is of great importance to precise *RUL* prediction. In the first step, health index data can be generated from testing sensory signals of online system units, based on either the PHI or the VHI. Then, the predictive degradation curve (h^p) as the background knowledge

will be employed to determine a time-scale initial health state (T_0, or initial age) corresponding to the initial health condition where T_0 is a time state with the optimum fitting between online health data and predictive health degradation curve. The optimum fitting can be formulated as

$$\begin{aligned} &\text{To determine } T_0, \\ &\min_{T_0} \sum_{j=1}^{N} \left(h(t_j) - h^p(t_j) \right)^2, \text{ subject to } T_0 \in [0, L - \Delta t] \end{aligned} \tag{6.11}$$

where $h(t_j)$ and $h^p(t_j)$ are the online health data and predictive health degradation data at t_j; N the number of data; T_0 the time-scale initial health state (or initial age); Δt the time span (= $t_N - t_1$) of the online health index data; L the time span of a predictive health degradation curve, which is the total life of an offline system unit. This optimization process basically moves the online health index data $h(t_j)$ along the time axis to find the best time-scale initial health state (T_0) by minimizing the fitting error with the predictive health degradation curve $h^p(t_j)$. Once T_0 is determined, the projected remaining life of the online system unit on a given projected health degradation curve can be calculated as

$$RUL = L - \Delta t - T_0 \tag{6.12}$$

As the predictive health degradation curve in Eq. (6.5) is statistically obtained, the time-scale initial health state (T_0) and projected *RUL* will be statistically modeled instead of a point estimate. To construct the histogram of the projected *RUL*, we generate a random sample set from the statistical information of the kernel function weights ($\boldsymbol{\omega}$) for the RVM regression in Eq. (6.10). These samples will result in random realizations of the predictive health degradation curve in Eq. (6.5) and further random realizations of the projected *RUL*s in Eq. (6.12). Through this sampling

process, we can observe the propagation of the uncertainties in raw sensory signals to the probability distributions of the projected *RUL*s, which will be discussed at the end of this section.

It should be noted above that different predictive health degradation curves are generated for different offline units in the offline training process. Repeating this process will provide different projected *RUL*s (RUL_i for $i = 1,\cdots,K$) on different predictive health degradation curves (h^p) where K is the number of offline system units. The projected *RUL*s can then be used to model the predictive *RUL* of an online unit. The remainder of this section will introduce the definition of similarity weights and the *RUL* interpolation.

Similarity-Based Interpolation

This study proposes the Similarity-Based Interpolation (SBI) to predict the *RUL* of an online unit. The predictive *RUL* of an online unit is a linear interpolation function in terms of the projected *RUL*s (RUL_i for $i = 1,\cdots, K$) of the offline units. The predictive *RUL* of an online unit can be expressed as

$$RUL = \frac{1}{W}\sum_{i=1}^{K}\left(W_i \cdot RUL_i\right) \quad \text{where} \quad W = \sum_{i=1}^{K} W_i \tag{6.13}$$

where RUL_i is the projected *RUL* on the i^{th} predictive health degradation curve; W_i is the i^{th} similarity weight. Then the predictive *RUL* of an online unit will be primarily determined as a linear function of RUL_i having larger degrees of similarity. The similarity weights can be defined as the inverse of the square-sum error as

$$W_i = \left[\sum_{j=1}^{N}\left(h_i(t_j) - h_i^p(t_j)\right)^2\right]^{-1} \tag{6.14}$$

It is obvious that greater weight is given to the offline units with greater similarity to

the online unit. In other words, the offline units with greater weight have greater similarity to the online unit in manufacturing and service conditions. The similarity weights must be random due to the randomness in the predictive health degradation curve, $h_i^p(t_j)$, in Eq. (6.5). Using the random samples of $h_i^p(t_j)$, we can generate random sample sets of both similarity weights and projected *RUL*s (RUL_i for i = 1,⋯,K) and then construct the histogram of the predictive *RUL* of an online unit using Eq. (6.13).

6.5 Generic Prognostic Uncertainty Management

In summary, the uncertainty propagation from the raw sensory signals to the predictive *RUL* is shown in Figure 6-2. In the offline training process, uncertainties in the raw data are propagated to the health index. The SBL technique uses the uncertainties of the health index and builds the predictive health degradation curves in a stochastic fashion. Finally, in the online prediction process, the SBI predicts the predictive *RUL* of an online system unit in Eq. (6.13) using the predictive health degradation curves of all offline system units.

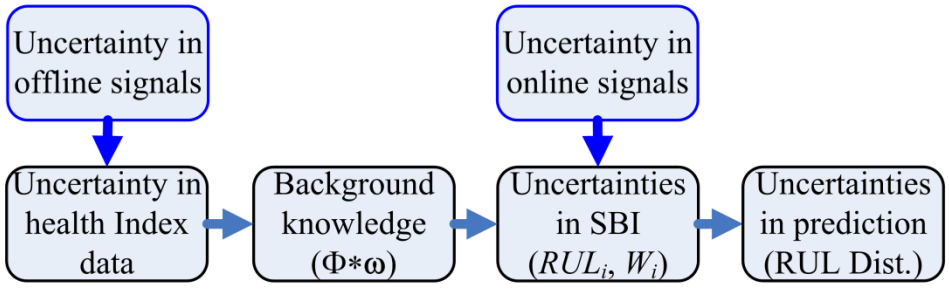

Figure 6-2: Uncertainty propagation map in the structural health prognostics framework

6.6 Case Studies

This section demonstrates the effectiveness of the proposed generic framework for structural health prognostics with two case studies: (i) IEEE Prognostics and Health Management (PHM) 08 Challenge Problem and (ii) electric cooling fan.

6.6.1 IEEE PHM 08 Challenge Problem

The dataset provided by the 2008 *IEEE* PHM Challenge problem consists of multivariate time series signals that are collected from an engine dynamic simulation process. Each time series signal represents a degradation instance of the engine system [Saxena and Goebel 2008]. The data for each cycle of each engine unit include the unit ID, cycle index, 3 values for an operational setting and 21 values for 21 sensor measurements. The sensory signals were contaminated with measurement noise and also each engine unit starts with a different initial health state. It is found that three operational settings have a substantial effect on engine degradation behaviors and result in six different operation regimes as shown in Table 6-2. The 21 sensory signals were obtained from six different operation regimes. The dataset was divided into training and testing subsets. The sensory signals were obtained from 218 offline engine units, so the number of training dataset is 4578 (=21×218) in total. The unit operated normally at the beginning of each time series and stopped until a fault condition was developed. The fault grows in magnitude until the system failure, at which time one or more limits for safe operation have been reached. There is no specific failure threshold defined. In the testing dataset, the time series signal ends some time prior to system failure. The objective of the problem is to predict the number of remaining operational cycles before failure in the testing dataset.

Table 6-2: Six different operation regimes

Regime ID	Operating parameter 1	Operating parameter 2	Operating parameter 3
1	0	0	100
2	20	0.25	20
3	20	0.7	0
4	25	0.62	80
5	35	0.84	60
6	42	0.84	40

The proposed prognostics framework takes the following steps: i) sensor data screening, ii) constructing the VHI, iii) SBL on the VHI to build the background health knowledge, iv) determination of initial health condition, and v) *RUL* predictions of online system units using the SBI. Steps i) to iii) corresponds to the offline training process involving the training dataset, whereas the online prediction process continues in steps iv) and v) that engages the testing dataset. These steps will be explained in detail in the following subsection.

Adjusting Cycle Index

To account for different initial degradation condition, an adjusted cycle index is proposed as: $C_{adj} = C - C_f$ where C is the operational cycle of the training data for an engine unit and C_f is the cycle-to-failure of an engine unit. The cycle index 0 indicates engine unit failure whereas negative cycle indices are realized prior to the failure. By setting the unit failure to a baseline, health degradation can be clearly displayed even with different initial degradation conditions and degradation paths.

Sensor Signal Screening

Among 21 sensory signals, some signals contain no or little degradation information of an engine unit whereas the others do. To improve the *RUL* prediction accuracy and efficiency, important sensory signals must be carefully selected to characterize degradation behavior for engine unit health prognostics. This study thus intended to screen sensory signals by observing the degradation behaviors of the 21 sensory signals. Seven sensory signals (2, 3, 4, 7, 11, 12 and 15) were selected in this study [Wang et al. 2008]

Building VHI

As discussed above, seven sensory signals were used for engine prognostics study. Based on the signals, we built the VHI to represent the engine health degradation process. Different transformation matrices $\mathbf{T}_k$ must be constructed using Eq. (6.1) for different operation regimes (k =1 to 6) because health degradation paths strongly depend on operation conditions. So, different $\mathbf{Q}_0$ and $\mathbf{Q}_1$ matrices can be built for different operation regimes. For a given operation regime, health index data to represent system failure and healthy states must be carefully identified to build $\mathbf{Q}_0$ and $\mathbf{Q}_1$. In this study $\mathbf{Q}_0$ was created with the health index data in a system failure condition, $-4 < \text{VHI} \leq 0$, in the adjusted cycle index, while $\mathbf{Q}_1$ with those in a healthy condition, $-300 < \text{VHI}$, in the adjusted cycle index. Different $\mathbf{Q}_0$ and $\mathbf{Q}_1$ can be created by repeating this process for all different operating regimes. As shown in Table 6-3, a 7×6 transformation matrix $\mathbf{T}_k$ can be constructed using Eq. (6.1), in which each column is a transformation vector for the corresponding operation regime. The dots in Figure 6-3 represent the VHI data obtained using $\mathbf{H} = \mathbf{T}_k \cdot \mathbf{Q}_{off}$ with the

training dataset of an offline engine unit.

Table 6-3: Transformation matrix (**T**) for the VHI

Regime 1	Regime 2	Regime 3	Regime 4	Regime 5	Regime 6
-0.03352	0.00420	0.01725	0.07551	0.04861	0.06308
-0.00358	-0.00571	-0.01046	-0.00551	-0.00720	-0.01003
-0.00760	-0.00741	-0.00624	-0.00695	-0.00891	-0.01105
0.03902	0.06381	0.05371	0.04381	0.05489	0.03470
-0.29961	-0.34434	-0.30928	-0.39681	-0.51199	-0.50965
0.07080	0.05048	0.07701	0.06448	0.08791	0.10163
-0.67360	-1.36813	-1.62036	-2.68974	-1.25800	-0.49316

Sparse Bayesian Learning on VHI

Figure 6-4 displays the randomly realized VHI data and the randomness is mainly due to the measurement noise from the signals. Thus, RVM regression can be used to model the VHI data in a stochastic manner. As discussed in Section 6.3, the RVM is Bayesian representation of a generalized sparse linear model, which shares the same functional form with the SVM. In this study, the linear spline kernel function was used as a basis function for the RVM. To build the predictive health degradation curves ($h_t^p(t)$, i=1, 2, ···, 218) for 218 offline engine units, the RVM regression model can be formed with statistical coefficient vector ($\boldsymbol{\omega}$) in the generalized sparse linear model of Eq. (6.5).

Figure 6-3 shows the health degradation curve with a desirable sparseness by only employing a small set of critical data points. Besides, the regression model gives both the mean and the variation of the predictive health degradation curve, as shown in

Figure 6-4. These predictive health degradation curves for the offline units altogether construct background health knowledge which characterizes the system degradation behavior. Later, this background knowledge can be used for modeling the predictive *RUL* distributions of online engine units. Some degradation curves for this challenge problem are exemplified in Fig. 6-5.

Determination of Initial Health Condition

The online prediction process employed testing dataset obtained from 218 online system units. The adjusted cycle index was used to determine an initial health condition. As explained in Section 6.4, the optimization problem in Eq. (6.11) was solved to determine a time-scale initial health degradation state (T_0) with the testing dataset for an online engine unit while minimizing the square-sum error between the online health data, $h(t_j)$, and predictive health degradation data, $h^p(t_j)$. Then, the predicted *RULs* and similarity weights of each online engine unit can be obtained using Eqs. (6.12) and (6.14) with L=224, Δt = 87. Figure 6-6 shows the process to determine the initial health degradation state (T_0) with the online testing data, $h(t_i)$, for the first engine unit and the predictive health degradation curve, $h^p(t)$, for the first unit. It should be noted that the offline learning process generates different predictive health degradation curves from K identical offline units. Repeating this process provided different projected *RUL*s (RUL_i for $i = 1,\cdots, K$) on different predictive health degradation curves. The projected *RUL*s can be used to predict the *RUL* of an online unit in next section.

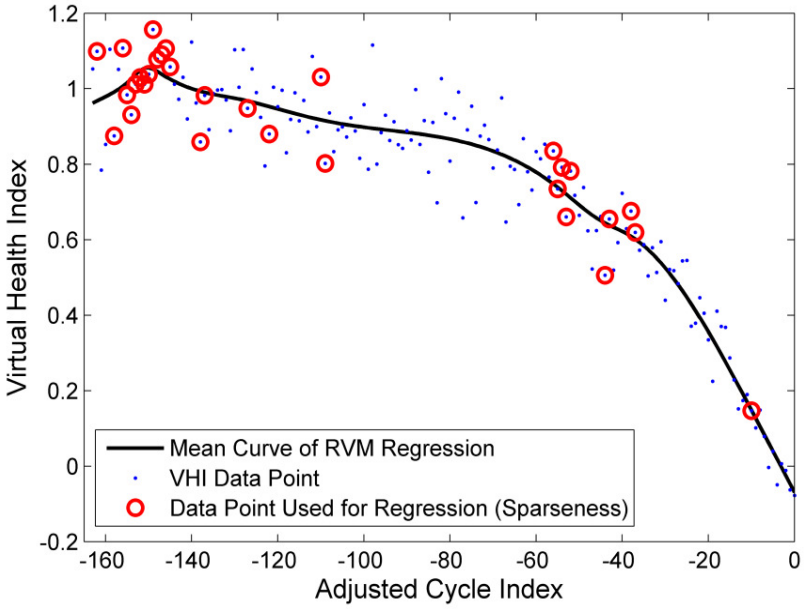

Figure 6-3: Sparseness of the RVM regression

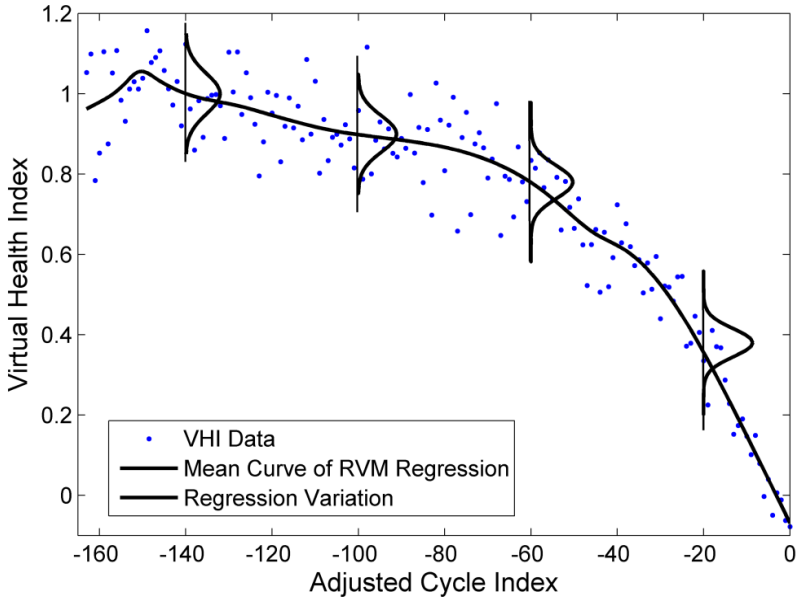

Figure 6-4: VHI and the RVM regression

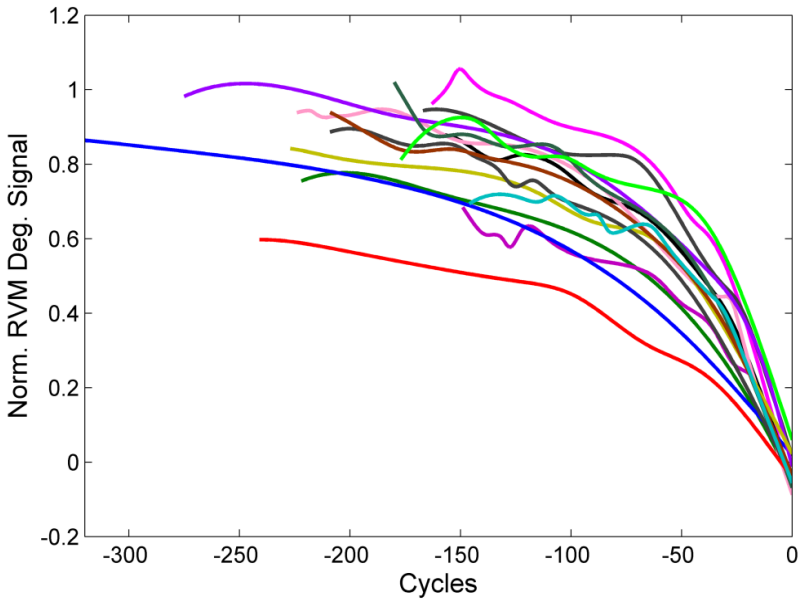

Figure 6-5: Background Degradation Knowledge from SBL

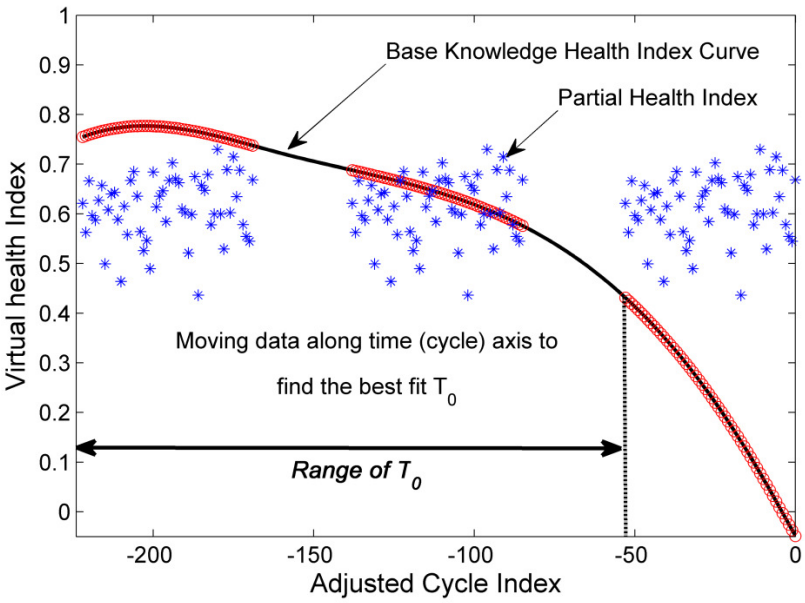

Figure 6-6: Determination of initial health index

Online RUL Prediction

From 218 offline engine units, the same number of the predictive health degradation curves and projected *RUL*s was obtained for each online engine unit. Likewise, the same number of similarity weights was sought for each online engine unit using Eq. (6.14). Equation (6.13) modeled the *RUL* prediction for each online engine unit as a function of the projected *RUL*s while considering the first 50 largest similarity weights. Note that $h_i(t_i)$ and $h_i^p(t_i)$ are random as mentioned in Section 6.3. Thus, the similarity weights were modeled in a statistical manner, so was the *RUL* of the online unit. Using the mean and covariance matrices of the relevance vector coefficients for the RVM regression in Eq.(6.6), the random samples of the coefficients result in the random samples of the similarity weights for the projected *RUL*s of the engine unit. The randomness of the similarity weights and projected *RUL*s is then propagated to the predictive *RUL* of the engine unit through Eq. (6.13). Figure 6-7 shows the *RUL* histogram and the true value with the testing dataset for the first four online engine units.

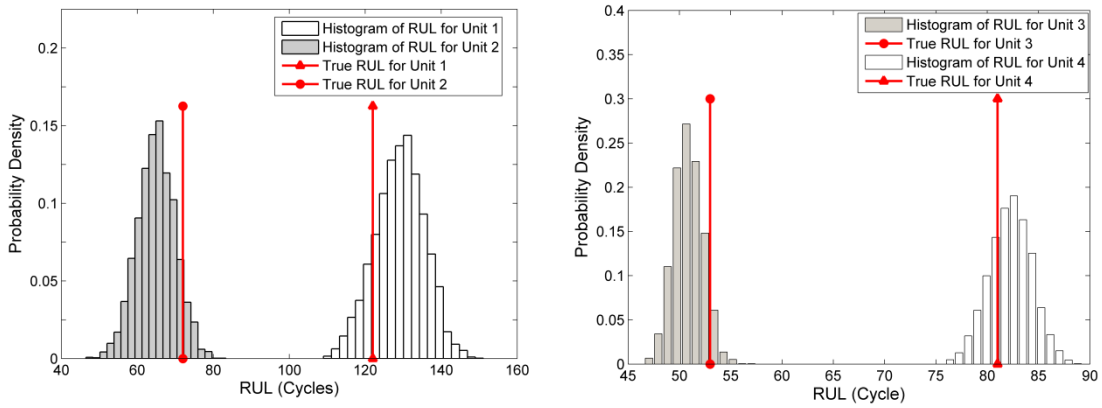

(a) (b)

Figure 6-7: Predicted *RUL* histograms with true RULs for

(a) units 1 and 2, and (b) units 3 and 4

Using the mean value of the predictive RUL with the testing dataset, the cumulative score loss was then calculated using Eq. (6.15), which was used in the IEEE PHM challenge problem competition. An average score loss of 5.224 is obtained for the testing dataset and the result is more accurate compared with the best average score loss of 12.956 in the competition.

$$
\begin{aligned}
d_k &= \text{Predicted } RUL_k - \text{True } RUL_k \\
S_k &= \begin{cases} e^{-d_k/13} - 1, & d_k \le 0 \\ e^{-d_k/10} - 1, & d_k \ge 0 \end{cases} \\
\text{Average Score Loss, } S &= \frac{1}{K}\sum_{k=1}^{K} S_k
\end{aligned}
\tag{6.15}
$$

6.6.2 Electric Cooling Fan

In this section, the generic prognostics framework is applied to the health prognostics of electronic cooling fan units. Cooling fans are one of the most critical parts in system thermal solution of most electronic products and have been a major failure contributor to many electronic systems [Tian 2006]. This study aims to demonstrate the proposed health prognostics methodology with 32 electronic cooling fans.

In the experimental study, thermocouples and accelerometers were used to measure temperature and vibration signals. To make time-to-failure testing affordable, the accelerated testing condition for the DC fan units was sought with inclusion of a small amount of tiny metal particles into ball bearings and an unbalanced weight on one of the fan units. The experiment block diagram of DC fan accelerated degradation test is shown in Figure 6-8. As shown in the diagram, the DC fan units were tested with 12V regulated power supply and three different signals

were measured and stored in a PC through a data acquisition system. Figure 6-9 (a) shows the test fixture with 4 screws at each corner for the DC fan units. As shown in Figure 6-9 (b), an unbalanced weight was used and mounted on one blade for each fan. Sensors were installed at different parts of the fan, as shown in Figure 6-10. In this study, three different signals were measured: the fan vibration signal from the accelerometer, the Printed Circuit Board (PCB) block voltage, and the temperature measured by the thermocouple. An accelerometer was mounted to the bottom of the fan with superglue, as shown in Figure 6-10 (a). Two wires were connected to the PCB block of the fan to measure the voltage between two fixed points, as shown in Figure 6-10 (b). As shown in Figure 6-10 (c), a thermocouple was attached to the bottom of the fan and measures the temperature signal of the fan. Vibration, voltage, and temperature signals were acquired by the data acquisition system and stored in PC. The data acquisition system from National Instruments Corp. (NI USB 6009) and the signal conditioner from PCB Group, Inc. (PCB 482A18) were used for the data acquisition system. In total, 32 DC fan units were tested at the same condition and all fan units run till failure.

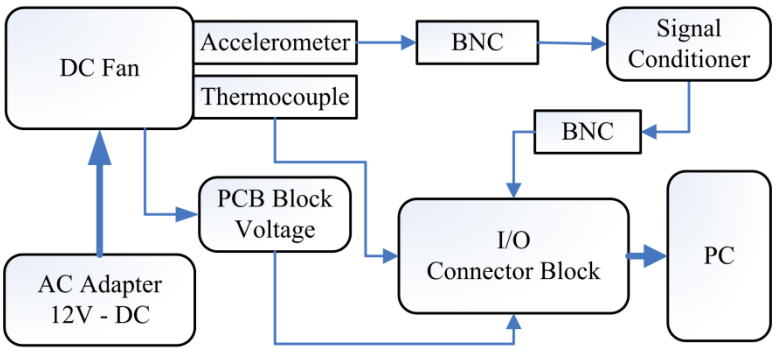

Figure 6-8: Electronic Fan Degradation Test Block Diagram

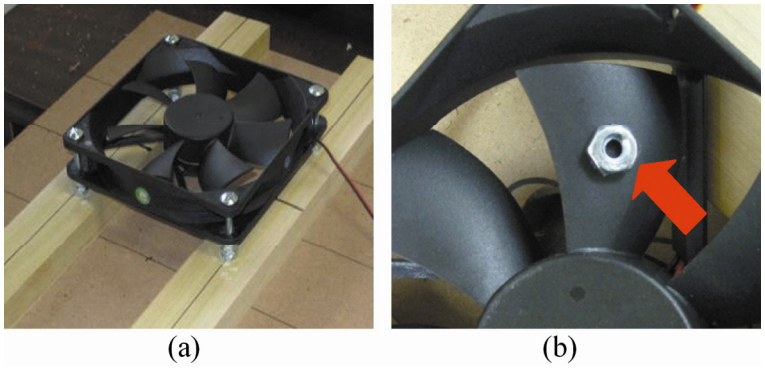

Figure 6-9: DC fan testing setup: (a) fixture and (b) the unbalance weight

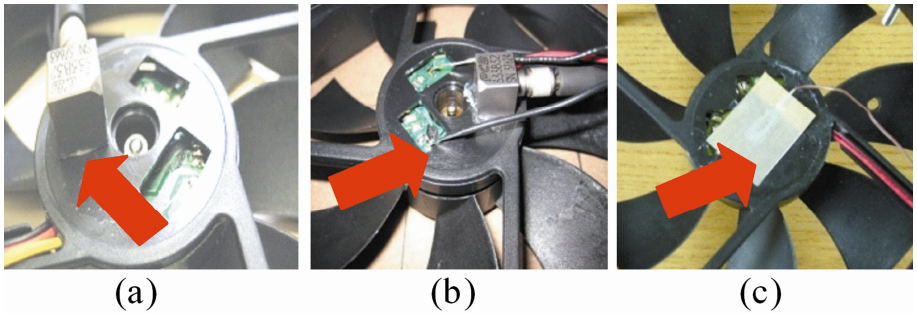

Figure 6-10: Sensor installations for DC fan test

(a) accelerometer, (b) voltage measurement, and (c) thermocouples

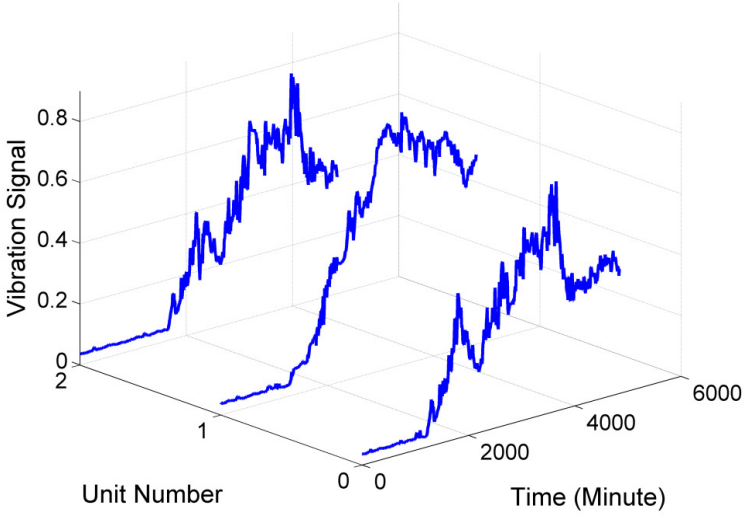

Figure 6-11: Sample degradation signals from DC fan testing

The sensory signal screening found that the fan PCB block voltage and the fan temperature did not show clear degradation trend, whereas the vibration signal showed health degradation behavior. This study involved the root mean squares (RMS) of the vibration spectral responses at the first five resonance frequencies and defined the RMS of the spectral responses as the PHI for the DC fan prognostics. Among 32 fan units, Figure 6-11 shows the RMS signals of three fan units to demonstrate the health degradation behavior. The RMS signal gradually increases as the bearing in the fan degrades over time. It was found that the PHI is highly random and non-monotonic because of metal particles, sensory signal noise, and input voltage noise. For the DC fan prognostics, the first 28 fan units were employed for the training dataset in the offline training process, while the rest were used to produce the testing dataset in the online prediction process. Following the same procedures of the previous case study, the prognostics work performed two distinguished processes: the offline training to obtain the predictive health degradation curves of the fan units using the RVM regression and the online prediction to predict and update the predictive *RUL*s of three online testing fan units using the SBI.

The *RUL* predictions for the three online testing fan units were conducted after 2000-, 3000-, and 4000-minute uses and the results are shown in Table 6-4. The prediction results of the online testing fan units are quite accurate with the maximum error of 314 minutes of the fourth fan after 2000–minute use. As more fan test data were used in the online prediction process, the prediction results become more accurate. The mean of the *RUL* prediction error after 4000–minute use are much smaller than those after 2000– and 3000-minute uses. As did in the previous case

study, the final *RUL* prediction was made in a statistic manner. Figure 6-12 shows the histogram of the predicted *RUL* for the first online testing fan after three different operation periods. Various statistical information of the predicted *RUL*, such as variation and confidence interval of prediction, can be provided to condition-based maintenance.

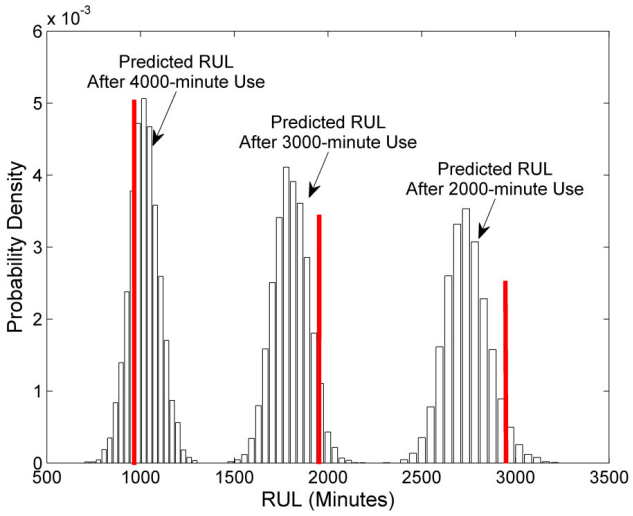

Figure 6-12: Predicted *RUL* histogram for a DC fan

Table 6-4: Prognostics results for DC fans

Predicted Mean of RUL (Minutes)				True Life
Operation time, *T*	2000	3000	4000	
Test Fan 1	2768	1802	1018	4957
Test Fan 2	3615	2563	1394	5468
Test Fan 3	3325	2298	1211	5124
Test Fan 4	4107	2588	1662	5793
Error, %	3.961	2.950	1.636	

6.7 Summary

This chapter presented the generic probabilistic framework for structural health prognostics and uncertainty management. The proposed two health indexes (PHI and VHI) provide the generic framework to define the degree of health condition regardless of system complexity, sensory data size, physical data types, and so on. The proposed prognostics framework is also generic in that it can predict the RULs of online units while considering various uncertainty sources, such as data acquisition, manufacturing, and operation processes. The framework is composed of two steps: the offline training (or learning) and online prediction processes. In the offline training process, the SBL scheme was employed to build predictive health degradation curves for offline training units in a statistical and sparse form. A set of curves become the background health knowledge while considering uncertainty in operational and manufacturing conditions. With this background knowledge, the SBI technique was then proposed for predicting and continuously updating the *RUL* in a statistical manner in the online prediction process. The proposed prognostic framework with an uncertainty propagation map enables the statistical prediction of RULs. Two engineering case studies (PHM challenge problem and the electric cooling fan prognostics problem) were used to demonstrate the effectiveness of the proposed generic structural health prognostics methodology. Due to the generic capability of the proposed prognostics framework, its wide application to other engineered systems is promising.

Chapter 7: Conclusion and Future Work

7.1 Conclusion of the Research Work

The work presented in this dissertation focused on advancing two essential and co-related research areas for the development of resilient engineered systems: system RBDO and system prognostics and health management (PHM). System RBDO will ensure high reliability of engineered systems in their early lifecycles, whereas capitalizing on PHM technology at the early design stage can transform passively reliable (or vulnerable) systems into adaptively reliable (or resilient) systems while considerably reducing their lifecycle cost.

To make an engineered system resilient, system reliability first needs to be ensured during the design and manufacturing stage. Thus, technical developments in Chapter 3 and Chapter 4 addressed the system RBDO area, focusing on addressing challenges for producing a reliable engineered system considering multiple system failure modes and input uncertainties. Two research questions regarding system RBDO were posed: how system failure modes and their interactions can be analyzed in a statistical sense, and how limited data for input manufacturing variability can be used for RBDO. As an engineered system enters its operational stage from the design and manufacturing stage, it could be vulnerable due to uncertain operational conditions as well as system performance degradation. Thus, Chapter 5 and Chapter 6 focused on addressing challenges in making an adaptive reliable engineered system that can be proactive to system failures during the operational stage. This can be accomplished through monitoring of the system performance degradation and

predicting the system remaining useful life. The third and fourth research questions in this dissertation work addressed system PHM: how sensor networks can be designed to effectively monitor system health degradation under highly uncertain operational conditions, and how accurate and timely remaining useful lives of systems can be predicted under highly uncertain operational conditions. Research solutions to these four research questions were presented in Chapter 3 to Chapter 6, accordingly.

Subsection 7.2 summarizes the principal contributions to the field and the significance of this research. Subsection 7.3 discusses limitations of the developed techniques and the recommended future work.

7.2 Principal Contributions and Significances

The proposed research solutions make significant contributions in various engineering applications as discussed below:

Contribution 1: A generalized framework for system reliability analysis

This dissertation has contributed significant advancement in our knowledge through the development of an innovative probability decomposition theory and a generic system reliability analysis framework regardless of the system structure and its size. The method developed here delivers a unique contribution by defining the CI-event. In aid of this definition, the probability of an *Nth*-order joint safety event can be decomposed into the probabilities of the first to *Nth*-order CI-events through the developed probability decomposition theorem. Subsequently, system reliability of any series system can be explicitly expressed in terms of the probability of the CI-events and can be evaluated using advanced

probability analysis methods. To facilitate the system reliability analysis for large-scale system applications, the CI-matrix and SS-matrix are innovatively defined to store the probabilities of CI-events and to represent any system structure in a compact and comprehensive matrix form, respectively. With the SS-matrix, the BDD technique automates the process to identify a system's mutually exclusive path sets, of which each path set is a series system. With these technical contributions, a generic system reliability analysis framework is formed that substantially enhances our capability to assess system reliability for complex systems and provides a solid foundation for engineering resilience analysis and design.

Contribution 2: Reliability analysis with evolving, insufficient and subjective data sets

The Bayesian reliability methodology developed in this dissertation presents a unique contribution by providing a new paradigm for system reliability prediction. This methodology enables the use of evolving, insufficient, and subjective data sets. Bayesian reliability analysis incorporates the reliability analysis with a Bayesian updating mechanism, and a generic definition of Bayesian reliability is introduced as a function of a predefined confidence level. Subsequently, Bayesian reliability is integrated to RBDO, referred to as the Bayesian reliability-based design optimization (Bayesian RBDO) methodology. The contribution of Bayesian RBDO is to provide a systematic design platform that enables engineering system design in the presence of evolving, insufficient and subjective data sets. The close-form relationship between Bayesian reliability,

user-desired confidence level, and the data sample size is developed, which provides designers with a guideline to set appropriate target Bayesian reliabilities when the data for uncertainty is insufficient. In order to develop more a stable Bayesian RBDO that is free of numerical singularities, an innovative approach for Bayesian reliability sensitivity analysis is developed through one-to-one mapping of Bayesian reliability with the mean value of the reliability distribution.

Contribution 3: Generic SN design for PHM

A generic probabilistic detectability measure is defined for evaluating the performance of any given SN, and a generic SN design framework is developed to build a cost-effective and reliable SN for health condition monitoring of an operating system. In the presented work, the detectability measure is defined as the probability of correct detection of each predefined health state. Subsequently, a generic detectability analysis is developed by integrating structural simulations with health-state classification tools. The generic SN design framework is formulated as a mixed-integer nonlinear programming problem using the detectability measure, and artificial intelligence algorithms such as the genetic algorithm (GA) are employed to solve the SN design optimization problem. The generic SN design tool provides a solid foundation for resilience-driven system design.

Contribution 4: Generic structural health prognostics

The proposed generic framework for structural health prognostics makes four technical contributions: (1) a generic health index system regardless of system complexity, sensory data size, physical data types, and so on; (2) an efficient

offline training process with the SBL scheme to build predictive background health knowledge in a statistical and sparse form; (3) a real-time online prediction process with the SBI technique in a statistical manner; and (4) a generic uncertainty propagation map to systematically manage uncertainties and errors in RUL prediction.

Contribution 5: A solid foundation for resilience-driven system design

This research advances two essential and co-related research areas for a resilient engineered system design: system RBDO and prognostics and health management (PHM). These will provide a solid foundation for resilience-driven system design because they are the pillar technologies for the resilience-driven system design process.

7.3 Recommended Future Research

Although the proposed research solutions and advanced methodologies developed in this dissertation have addressed critical challenges in both system RBDO and PHM, it is still a grand challenge to unify these technique advances and develop a resilience-driven system design methodology. Further research and technical developments are needed to make the resilience-driven system design methodology feasible and effective. The rest of this section presents a few open questions in the resilient engineered system design and provides possible approaches to address these questions.

- Allocation of system capacity into subsystems and components from the perspective of system resilience

The proposed system RBDO and PHM methods can design engineered systems with target reliability and detectability. However, little or no study has been done to allocate the system capacity into subsystems and components to meet the target system resilience. To answer this question, a resilience allocation problem has to be carefully defined in order to allocate target reliabilities of subsystems and components while minimizing the system lifecycle cost.

- Cost benefit analysis of resilience engineered system design

  As the resilience-driven system design framework involves development in both RBDO and PHM, a generic cost model must be developed as a function of the resilience—redundancy, reliability and PHM efficiency levels—while considering the PHM cost model and PHM benefit model.

- Sensor noise in the SN design

  In the current work, randomness of the sensor outputs is considered mainly due to the variability of structural systems, and the sensor noise from SN itself is not considered. Considering the sensor noise in SN design optimization will enhance the robustness of the SN and needs further investigation.

- Integration of RBDO and PHM

  Two core research topics—system RBDO and PHM—are separately developed to address their own challenges. However, their integration has not been studied in this research. To address this problem, a resilience-driven system design problem should be carefully defined with conceptual and mathematical definitions of engineering resilience and resilience analysis methods. To this end, the multidisciplinary system design optimization framework has to be employed.

- Designing a PHM system

  The existing PHM methodology enables the RUL prediction of structural components. However, there has been little effort to design PHM systems by enhancing sensing, detection, and prediction functions. In order to address this issue, a metric for sensing, detection, and prediction functions needs to be appropriately defined, and corresponding analysis methods need to be further developed.

Appendices

Appendix A: Derivation of the Probability Decomposition Theorem

Hailperin [3 *] divided the sample space of a system with N number of the component events into 2^N mutually exclusive and collectively exhaustive (MECE) events, each consisting of a distinct intersection of the component events E_i and their complements $\bar{E}_i$, i =1,...,N. They are called the basic events. For example, in the case of 3 (=N) component events, one finds the 2^3=8 basic events to be $E_1E_2E_3$, $\bar{E}_1E_2E_3$, $E_1\bar{E}_2E_3$, $E_1E_2\bar{E}_3$, $\bar{E}_1\bar{E}_2E_3$, $\bar{E}_1E_2\bar{E}_3$, $E_1\bar{E}_2\bar{E}_3$, and $\bar{E}_1\bar{E}_2\bar{E}_3$. For any system with N number of components, there are 2^N basic events and any event can be expressed as a linear combination of the basic events. The basic events can be classified into N+1 groups where the basic events in i^{th} group include i number of component failure events as

$$0^{\text{th}}\ \text{Group:} \quad \bigcap_{i=1}^{N} E_i$$

$$1^{\text{st}}\ \text{Group:} \quad \bar{E}_j \bigcap_{i=1, i\neq j}^{N} E_i,\ j = 1, 2, \cdots, N$$

$$\vdots \qquad\qquad \vdots$$

$$r^{\text{st}}\ \text{Group:} \quad \bigcap_{\substack{k_1=1 \\ k_2=k_1+1 \\ \vdots \\ k_r=k_1+r}}^{N} \bar{E}_{k_j} \bigcap_{\substack{i=1 \\ i\neq k_j}}^{N} E_j,\ j = 1, 2, \cdots, r$$

$$\vdots \qquad\qquad \vdots$$

$$N^{\text{th}}\ \text{Group:} \quad \bigcap_{i=1}^{N} \bar{E}_i$$

---

[*] Hailperin, T., 1965, "Best possible inequalities for the probability of a logical function of events." *Am. Math. Monthly,* 72(4), 343–359.

For example, the basic event in the 0th group, $E_1E_2\ldots E_N$ ($\equiv E_1 \cap E_2 \cap \ldots \cap E_N$), has no component failure event, whereas the basic events ($\bar{E}_1E_2E_3 \ldots E_N$ and $E_1\bar{E}_2E_3 \ldots E_N$) in the 1st group have one component failure event.

The probability of any order CI events can be expressed as a linear combination of the probabilities of the basic events in the N+1 group. For the system with 2 components, the coefficients of the linear combinations are shown in Tables A1. For example, the first column of Table A1 can be expressed as

$$\begin{aligned} P(E_1) &= 1\times P(E_1E_2) + 0\times P(\bar{E}_1E_2) + 1\times P(E_1\bar{E}_2) + 0\times P(\bar{E}_1\bar{E}_2) \\ &= \left[P(E_1E_2), P(\bar{E}_1E_2), P(E_1\bar{E}_2), P(\bar{E}_1\bar{E}_2\bar{E}_3) \right] \\ &\times \left[1 \quad 0 \quad 1 \quad 0\right]^T \end{aligned}$$

Grouping the basic events into N + 1 different groups can give us the compact expression of the linear combinations. Then it is possible to express the summation of the probabilities of the CI events as a linear combination of the probabilities of the basic events in a compact manner. For the system with 2 components, the coefficients of the linear combinations are shown in Tables A2. For example, the first column of Table A2 can be expressed as

$$\begin{aligned} &\sum_{i=1}^{2} P(E_i) \\ &= 2\times P(E_1E_2) \\ &+ 1\times\left[P(\bar{E}_1E_2) + P(E_1\bar{E}_2) \right] \\ &+ 0\times P(\bar{E}_1\bar{E}_2) \end{aligned} \tag{A1}$$

Using the tables A2, the probabilities of the second and third-order joint events can be decomposed into the CI events as

$$P(E_1E_2) = \frac{1}{2}\left[P(E_1) + P(E_2) - P(E_{12})\right] \quad \text{(A2)}$$

Table A1: Probability Decomposition of 2 components system

Basic Events \ CI Events	$P(E_1)$	$P(E_2)$	$P(E_{12})$
$P(E_1E_2)$	1	1	0
$P(\bar{E}_1E_2)$	0	1	1
$P(E_1\bar{E}_2)$	1	0	1
$P(\bar{E}_1\bar{E}_2)$	0	0	0

Table A2: Probability Decomposition of 2 components system with grouping

Events \ CI Events Basic	$P(E_1)+P(E_2)$	$P(E_{12})$
$P(E_1E_2)$	2	0
$P(\bar{E}_1E_2)+P(E_1\bar{E}_2)$	1	1
$P(\bar{E}_1\bar{E}_2)$	0	0

Considering a general system with N number of the components in total, Table A3 displays a linear combination of the CI events in the general system. For a given general system, the following equations can be developed for two different cases as:

Table A3: Probability Decomposition of N components system

	$P(E_i)$	$P(E_{ij})$	$P(E_{ijk})$	$P(E_{ijkl})$	$P(E_{ijklm})$	…	$P(E_{12\ldots N})$
$\bigcap_{i=1}^{N} E_i$	C_N^1	0	C_N^3	0	C_N^5	…	1, N is odd 0, N is even
$\sum_{j=1}^{N} P\left(\bigcap_{i=1, i\neq j}^{N} E_i \overline{E}_j\right)$	C_{N-1}^1	C_{N-1}^1	C_{N-1}^3	C_{N-1}^3	C_{N-1}^5	…	0, N is odd 1, N is even
$\sum_{\substack{j=1 \\ k=2 \\ j<k}}^{N} P\left(\bigcap_{\substack{i=1 \\ i\neq j,k \\ j<k}}^{N} E_i \overline{E}_j \overline{E}_k\right)$	C_{N-2}^1	$2 * C_{N-2}^1$	C_{N-2}^1 $+C_{N-2}^3$	$2 * C_{N-2}^3$	C_{N-2}^3 $+C_{N-2}^5$	…	1, N is odd 0, N is even
$\sum_{\substack{j=1 \\ k=2 \\ r=3 \\ j<k<r}}^{N} P\left(\bigcap_{\substack{i=1 \\ i\neq j,k,r}}^{N} E_i \overline{E}_j \overline{E}_k \overline{E}_r\right)$	C_{N-3}^1	$3 * C_{N-3}^1$	$3 * C_{N-3}^1$ $+C_{N-3}^3$	C_{N-3}^1 $+3 * C_{N-3}^3$	$3 * C_{N-3}^3$ $+C_{N-3}^5$	…	0, N is odd 1, N is even
⋮	⋮	⋮	⋮	⋮	⋮	…	⋮
$P\left(\bigcap_{i=1}^{N} \overline{E}_i\right)$	0	0	0	0	0	0	0

Case I: N is an odd number

$$\sum_{i=1}^{N} P(E_i) - \sum_{\substack{i=1;\\ j=2;\\ i<j}}^{N} P(E_{ij}) + \cdots + (-1)^{m-1} \sum_{\substack{i=1;\\ j=2;\\ \vdots\\ l=m\\ i<j<\cdots<l}}^{N} P\left(E_{\underbrace{ij\cdots l}_{m}}\right) + \cdots + (-1)^{N-1} P(E_{12\cdots N})$$

$$= \left(C_N^1 + C_N^3 + \cdots + C_N^N\right) \cdot P\left(\bigcap_{i=1}^{N} E_i\right)$$

$$+ \left(C_{N-1}^1 - C_{N-1}^1 + C_{N-1}^3 - C_{N-1}^3 + \cdots + C_{N-1}^{N-2} - C_{N-1}^{N-2}\right) \cdot \sum_{j=1}^{N} P\left(\overline{E}_j \bigcap_{i=1, i\neq j}^{N} E_i\right)$$

$$+ \left(C_{N-2}^1 - 2C_{N-2}^1 + C_{N-2}^1 + C_{N-2}^3 - 2\cdot C_{N-2}^3 + C_{N-2}^3 + C_{N-2}^5 + \cdots\right) \cdot \sum_{\substack{j=1\\ k=2\\ j<k}}^{N} P\left(\overline{E}_j \overline{E}_k \bigcap_{\substack{i=1\\ i\neq j,k}}^{N} E_i\right) +$$

$$\cdots + (0-0+0-0+\cdots) P\left(\bigcap_{i=1}^{N} \overline{E}_i\right)$$

$$= 2^{N-1} \cdot P\left(\bigcap_{i=1}^{N} E_i\right)$$

Case I: N is an odd number

$$\sum_{i=1}^{N} P(E_i) - \sum_{\substack{i=1;\\ j=2;\\ i<j}}^{N} P(E_{ij}) + \cdots + (-1)^{m-1} \sum_{\substack{i=1;\\ j=2;\\ \vdots\\ l=m\\ i<j<\cdots<l}}^{N} P\left(E_{\underbrace{ij\cdots l}_{m}}\right) + \cdots + (-1)^{N-1} P(E_{12\cdots N})$$

$$= \left(C_N^1 + C_N^3 + \cdots + C_N^{N-1}\right) \cdot P\left(\bigcap_{i=1}^{N} E_i\right)$$

$$+ \left(C_{N-1}^1 - C_{N-1}^1 + C_{N-1}^3 - C_{N-1}^3 + \cdots + C_{N-1}^{N-1} - C_{N-1}^{N-1}\right) \cdot \sum_{j=1}^{N} P\left(\overline{E}_j \bigcap_{i=1, i\neq j}^{N} E_i\right)$$

$$+ \left(C_{N-2}^1 - 2C_{N-2}^1 + C_{N-2}^1 + C_{N-2}^3 - 2\cdot C_{N-2}^3 + C_{N-2}^3 + C_{N-2}^5 + \cdots\right) \cdot \sum_{\substack{j=1\\ k=2\\ j<k}}^{N} P\left(\overline{E}_j \overline{E}_k \bigcap_{\substack{i=1\\ i\neq j,k}}^{N} E_i\right) +$$

$$\cdots + (0-0+0-0+\cdots) P\left(\bigcap_{i=1}^{N} \overline{E}_i\right)$$

$$= 2^{N-1} \cdot P\left(\bigcap_{i=1}^{N} E_i\right)$$

From the equations above, the general formula for decomposing the probability of the N^{th}-order joint event can be developed and expressed as

$$P\left(\bigcap_{i=1}^{N} E_i\right)$$

$$= \frac{1}{2^{N-1}}\left[\sum_{i=1}^{N} P\left(E_i\right) - \sum_{\substack{i=1;\\ j=2;\\ i<j}}^{N} P\left(E_{ij}\right) + \cdots + \left(-1\right)^{m-1} \sum_{\substack{i=1;\\ j=2;\\ \vdots\\ l=m\\ i<j<\cdots<l}}^{N} P\left(E_{\underbrace{ij\cdots l}_{m}}\right) + \cdots + \left(-1\right)^{N-1} P\left(E_{12\cdots N}\right)\right] \quad \text{(A3)}$$

Appendix B: Response Surface of Vehicle Side Impact Model

The response surface for ten constraints of vehicle side impact model is constructed as $\{G_i < g_i, i=1, 2, \ldots, 10\}$ where g_i are from vector g = [1, 32, 32, 32, 0.32, 0.32, 0.32, 4, 9.9,15.7] and G_i are as follows.

$$G_1 = 1.16 - 0.3717X_2X_4 - 0.00931X_2X_{10} - 0.484X_3X_9 + 0.01343X_6X_{10};$$

$$G_2 = 28.98 + 3.818X_3 - 4.2X_1X_2 + 0.0207X_5X_{10} + 6.63X_6X_9 - 7.7X_7X_8 + 0.32X_9X_{10};$$

$$G_3 = 33.86 + 2.95X_3 + 0.1792X_{10} - 5.057X_1X_2 - 11X_2X_8 - 0.0215X_5X_{10} - 9.98X_7X_8 + 22X_8X_9;$$

$$G_4 = 46.36 - 9.9X_2 - 12.9X_1X_8 + 0.1107X_3X_{10};$$

$$G_5 = 0.261 - 0.0159X_1X_2 - 0.188X_1X_8 - 0.019X_2X_7 + 0.0144X_3X_5 + 0.0008757X_5X_{10} + 0.08045X_6X_9 + 0.00139X_8X_{11} + 0.00001575X_{10}X_{11};$$

$$G_6 = 0.214 + 0.00817X_5 - 0.131X_1X_8 - 0.0704X_1X_9 + 0.03099X_2X_6 - 0.018X_2X_7 + 0.0208X_3X_8 + 0.121X_3X_9 - 0.00364X_5X_6 + 0.0007715X_5X_{10} - 0.0005354X_6X_{10} + 0.00121X_8X_{11} + 0.00184X_9X_{10} - 0.018X_2^2;$$

$$G_7 = 0.74 - 0.61x_2 - 0.163X_3X_8 + 0.001232X_3X_{10} - 0.166X_7X_9 + 0.227X_2^2;$$

$$G_8 = 4.72 - 0.5X_4 - 0.19X_2X_3 - 0.0122X_4X_{10} + 0.009325X_6X_{10} + 0.000191X_{11}^2;$$

$$G_9 = 10.58 - 0.674X_1X_2 - 1.95X_2X_8 + 0.02054X_3X_{10} - 0.0198X_4X_{10} + 0.028X_6X_{10};$$

$$G_{10} = 16.45 - 0.489X_3X_7 - 0.843X_5X_6 + 0.0432X_9X_{10} - 0.0556X_9X_{11} - 0.000786X_{11}^2;$$

Glossary

CDF:	Cumulative Distribution Function
CIM:	Complementary Intersection Method
DBDO:	Detectability Based Design Optimization
FOB:	First Order Bounds
FORM:	Second Order Bounds
LP:	Linear Programming
PDF:	Probability Density Function
PHI:	Physical Health Index
PoD:	Probability of Detection
PHM:	Prognostics and Health Management
RBDO:	Reliability Based Design Optimization
RUL:	Remaining Useful Life
RVM:	Relevance Vector Machine
SBI:	Similarity Based Interpolation
SBL:	Sparse Bayesian Learning
SN:	Sensor Network
SOB:	Second Order Bounds
SORM:	Second-Order Reliability Method
SVM:	Support Vector Machine
VHI:	Virtual Health Index

Bibliography

Adjiman, C.S., Androulakis, I.P., Floudas, C.A., 2000, "Global optimization of mixed-integer nonlinear problems," AIChE J. 46, 1769–1797.

Akers, B., 1978, "Binary decision diagrams," IEEE Trans. Comput, C-27(6):509–16.

Allan, D., Brundell, M., Boyd, K., and Hinde, D., 1992, "New techniques for monitoring the insulation quality of in-service HV apparatus," IEEE Trans. Elect. Insulation, vol. 27, pp. 578–585.

Allen, J.K. and Choi, H.J., 2009, "A Meta-modeling Approach for Uncertainty Analysis of Nondeterministic Systems," J. Mech. Des., Vol. 131(4). 041008(10).

Azarbayejani1,M.,, El-Osery, A.I., Choi, K.K., and Taha, M.M.R., "A probabilistic approach for optimal sensor allocation in structural health monitoring," Smart Mater. Struct. 17 (2008) 055019 (11)

Bae, Ha-Rok, et al., Uncertainty quantification of structural response using evidence theory, AIAA journal, 2003, vol. 41, no10, pp. 2062-2068.

Bagdonavicius, V., and Nikulin, M., 2000, "Estimation in Degradation Models with Explanatory Variables," Lifetime Data Analysis, 7, pp. 85–103.

Bai, X.G., Asgarpoor, S., "Fuzzy-Based Approaches to Substation Reliability Evaluation," Electric Power Systems Research, Vol. 69, Issue 2-3, pp197–204 May, 2004.

Beck, J.L., and Au, S.-K., "Bayesian Updating of Structural Models and Reliability Using Markov Chain Monte Carlo Simulation," Journal of Engineering Mechanics, pp. 380-391, April, 2002.

Bishop C. and Tipping M. E., Variational Relevance Vector Machines, In: Proceedings of Uncertainty in Artificial Intelligence, 2000.

Bjerager P, 1988, "Probability Integration by Directional Simulation," ASCE J Engng Mech 114, pp. 1285–302.

Bocca, M., Cosar, E.I., Salminen, J., and Eriksson, L.M., "A Reconfigurable Wireless Sensor Network for Structural Health Monitoring," 4th International Conference on Structural Health Monitoring of Intelligent Infrastructure (SHMII-4), 22-24, July, 2009, Zurich, Switzerland.

Boulanger, M. and Escobar, L. A., 1994, "Experimental design for a class of accelerated degradation tests," Technometrics, 36, pp. 260–272.

Brotherton, T., Jahns, J., Jacobs, J., and Wroblewski, D., 2000, "Prognosis of Faults in Gas Turbine Engines," Proceedings of the IEEE Aerospace Conference, IEEE, New York, Vol. 6, pp. 163 –171.

Bucher, C. G., 1988, "Adaptive Sampling – An Iterative Fast Monte Carlo Procedure," Structural Safety, Vol. 5, pp. 119-126.

Buczak, A.L, Wang, H., Darabi, H., and Jafari, M.A., "Genetic algorithm convergences study for sensor network optimization," Inform. Sci. 133 267–82, 2001

Byington, C.S., Kalgren, P.W., Johns, R., and Beers, R.J., 2003, Embedded diagnostic/prognostic reasoning and information continuity for improved avionics maintenance. Proceedings of AUTOTESTCON 2003: IEEE Systems Readiness Technology Conference, pp. 320-329.

Byington, C., Watson, M., and Edwards, D., 2004, "Data-Driven Neural Network Methodology to Remaining Life Predictions for Aircraft Actuator Components," In: Proceedings of the IEEE Aerospace Conference, New York.

Carey, M. B. and Koenig, R. H., 1991, "Reliability assessment based on accelerated degradation: A case study," IEEE Transactions on Reliability, 40, pp. 499–506.

Chakrabarty, K., and Chiu, P.K., "Grid coverage for surveillance and target location in distributed sensor networks," IEEE Trans. Comput. 51 1448–53, 2002

Chang, F-K and Markmiller, J F C, "A new look in design of intelligent structures with SHM," Proc. 3rd European Workshop: Structural Health Monitoring pp 5–20, 2006

Chen, X., Hasselman, T.K., and Neill, D. J., "Reliability-Based Structural Design Optimization for Practical Applications," 38th AIAA SDM Conference, AIAA-97-1403, 1997.

Chiao, C. H., and Hamada, M., 1996, "Using degradation data from an experimet to achive robust reliability for light emmitining diodes," Quality and Reliability Engineering International, 12, pp. 89–94.

Chinnam, R., 1999, "On-line reliability estimation of individual components using degradation signals," IEEE Transactions on Reliability, 48, 403–412.

Chinnam, R.B., and Baruah, P., A, 2004, "Neuro-fuzzy for estimating mean residual life in condition-based maintenance systems," In: International Journal of Materials and Product Technology, 20(1/23) 166-179.

Chung, T.H., Mohamed, Y., and AbouRizk, S., 2004, "Simulation Input Updating Using Bayesian Techniques," Proceedings of the 2004 Winter Simulation Conference, pp. 1238-1243.

Choi, K.K., Du, L., and Youn B. D., 2006, " An Inverse Possibility Analysis Method for Possibility-Based Design Optimization," AIAA Journal, Vol.44 No (11), pp 2682-2690.

Coolen, F. P. A. and Newby, M. J., 1994, "Bayesian reliability analysis with imprecise prior probabilities," Reliability Engineering and System Safety, Vol.43, No.1, pp75–85.

Der Kiureghian, A., and Song J., 2008, "Multi-scale reliability analysis and updating of complex systems by use of linear programming," Reliability Engineering & System Safety, Vol. 93, No.2, pp.288-297.

Ditlevsen, O., and Bjerager, P., 1984, "Narrow Reliability Bounds for Structural Systems." Journal of the Engineering Mechanics, ASCE, Vol. 110, No.5, pp. 671-693.

Doksum, K. A. and Hoyland, A., 1992, "Models for variable-stress accelerated life testing experiment based on Wiener processes and the inverse Gaussian Distribution," Technometrics, 34, pp. 74–82.

Dowling, N. E., 1993, Mechanical Behavior of Materials, Prentice Hall: Englewood Cliffs.

Du, L. and Choi, K. K., "An inverse analysis method for design optimization with both statistical and fuzzy uncertainties", Structural and Multidisciplinary Optimization, Vol. 37, No. 2, pp 1615-1488 December, 2008.

Du, L., Choi K.K., Youn, B.D., and Gorsich D., 2006, "Possibility-Based Design Optimization Method for Design Problems with Both Statistical and Fuzzy Input Data," J. Mech. Des., Vol. 128, Issue 4, 928(8)

Du, X., 2008a, "Unified Uncertainty Analysis by the First Order Reliability Method," ASME J. Mech. Des., 130(9), pp. 091401(10).

Du, X., 2008b, "Saddlepoint Approximation for Sequential Optimization and Reliability Analysis," Journal of Mechanical Design, 130(1), pp. 011011-011011.

Du, X., and Chen, W., 2004, “Sequential Optimization and Reliability Assessment Method for Efficient Probabilistic Design,” ASME J. Mech. Des., 126(2), pp. 225–233.

Du, X., Sudjianto, A., and Chen, W., 2004, "An Integrated Framework for Optimization under Uncertainty Using Inverse Reliability Strategy," ASME Journal of Mechanical Design, Vol.126, No.4, pp. 561-764.

Engelund S, and Rackwitz R., 1993, “A Benchmark Study on Importance Sampling Techniques in Structural Reliability,” Struct Safety, 12, pp. 255–276.

Fickas, E.T., Martz, H.F., and Waller, R.A., 1988, “Bayesian Reliability Analysis of Series Systems of Binomial Subsystems and Components,” Technometrics, Vol. 30, No. 2, pp. 143-154.

Field, R.V.J., and Grogoriu, M., 2006, “Optimal design of sensor networks for vehicle detection, classification and monitoring,” Probab. Eng. Mech. 21 305–16.

Flynn, E.B., and Todd, M.D., 2010, “A Bayesian approach to optimal sensor placement for structural health monitoring with application to active sensing,” Mechanical System and Signal Processing, Vol.24, No. 4, pp. 891-903

Gebraeel, N et. al., 2004, “Residual-life Prediction from Vibration Degradation Signals: A Neural Network Approach,” IEEE Trans.on Industrial Electronics, vol. 51, No.3, pp.694-700.

Gebraeel, N et. al., 2005, “Residual-life Distributions from Component Degradation Signals: A Bayesian Approach,” IIE Trans., vol. 37, pp. 543–557.

Gebraeel., N, and Hernandez L., 2009, “Advanced prognostics for aircraft electrical power systems,” SAE Int J Aerosp, Vol. 1, No. 1, pp.1059–1063.

Gavin, H. P., and Yau, S. C., 2008, "High-order limit state functions in the response surface method for structural reliability analysis," Structural Safety, Vol.30, No.2, pp. 162-179

Gunawan, S., and Papalambros, P. Y., 2006, "A Bayesian Approach to Reliability-Based Optimization with Incomplete Information," Journal of Mechanical Design, 128(4), pp. 909-918.

Guratzsch, R. F. and Mahadevan, S., 2006, "Sensor placement design for SHM under uncertainty," Proc. 3rd European Workshop: Structural Health Monitoring pp 1168–75

Haldar A., and Mahadevan S., 2000, Probability, Reliability, and Statistical Methods in Engineering Design, John Wiley & Sons, Inc., Ch8, pp.238-248.

Hamada, M., 1995, "Analysis of experiments for reliability improvement and robust reliability," in Recent Advances in Life-Testing and Reliability, CRC Press.

Harrell, F. E., Lee, K.L., Califf, R.M., Pryor, D.B., and Rosati, R.A.,2006, " Regression Modeling Strategies for Improved Prognostic Prediction," Statistics in Medicine, 32(2), pp.143-152.

Hasofer, A.M., and Lind, N.C., 1974, "Exact and Invariant Second-Moment Code Format," Journal of the Engineering Mechanics, ASCE, Vol. 100, pp. 111-121.

Hazelrigg, G.A., 1998, "A Framework for Decision-Based Engineering Design," ASME, Journal of Mechanical Design, Vol. 120, pp. 653-658, December.

Heimes, F. O., 2008, "Recurrent Neural Networks for Remaining Useful Life Estimation," In: IEEE International Conference on Prognostics and Health Management.

Helton, J. C., Johnson, J.D., Oberkampf, W.L., and Sallaberry, C.J., 2006, "Sensitivity analysis in conjunction with evidence theory representations of

epistemic uncertainty; Reliability engineering & systems safety," vol. 91, No. 10-11, pp. 1414-1434.

Helton, J. C., Johnson, J.D., Oberkampf, W.L., and Sallaberry, C.J., 2008, Representation of Analysis Results Involving Aleatory and Epistemic Uncertainty, Sandia Report, SAND2008-4379.

Heredia-Zavoni, E., and Esteva, E.L., 1998,"Optimal instrumentation of uncertain structural systems subject to earthquake motion," Earthq. Eng. Struct. Dyn., 27, 343–62.

Herrmann, J.W., 2009, "Design Optimization with Imprecise Random Variables," SAE International, 2009-01-0201.

Hogg, R., McKean, J., and Craig, A., 2005, Introduction to Mathematical Statistics, 359-364, Upper Saddle River, NJ, Pearson Prentice Hall.

Huang, H. and Zhang, X., 2009, "Design Optimization with Discrete and Continuous Variables of Aleatory and Epistemic Uncertainties" J. Mech. Des., Vol.131, Issue 3, 031006 (8).

Huang, H.Z., Zuo, M.J., Sun, Z.Q., , 2006, "Bayesian Reliability Analysis for Fuzzy Lifetime Data," Fuzzy Sets and Systems, Vol.157, Issue 12, pp1674–1686.

Huang, R., Xi, L., Li, X., Liu, R., Qiu, H., and Lee, J., 2007, "Residual Life Predictions for Ball Bearings Based on Self-organizing Map and Back Propagation Neural Network Methods," Mechanical Systems and Signal Processing, 21(1) 193-207.

Inoue Y., Hasegawa, H., Sotodate, M., Shimada, H., and Okamoto, T., 2003, "Technology for detecting wet bars in water-cooled stator winding of turbine generators," IEEE IEMDC, 1337-1343.

Isukapalli, S. S., Roy, A., and Georgopoulos, P. G., 1998, "Stochastic Response Surface Methods (SRSMs) for Uncertainty Propagation: Application to

Environmental and Biological Systems," Risk Analysis, Vol.18, No.3, pp. 351-363.

Johnson NL, Kotz S, and Balakrishnan N., 1995, Continuous univariate distributions. New York: Wiley.

Jung, D.H., and Lee, B.C., 2002, "Development of a Simple and Efficient Method for Robust Optimization," International Journal for Numerical Methods in Engineering, Vol. 53, pp. 2201-2215.

Karamchandani, A., 1987 "Structural System Reliability Analysis Methods." Report No. 83, John A. Blume Earthquake Engineering Center, Stanford University, Stanford, CA.

Keller K, Swearingen K, Sheahan J, Bailey M, Dunsdon J, Przytula KW et al., 2006, "Aircraft electrical power systems prognostics and health management," In: Proceedings of the 2006 IEEE aerospace conference.

Kim, C., and Choi, K. K., 2008, "Reliability-Based Design Optimization Using Response Surface Method With Prediction Interval Estimation," Journal of Mechanical Design, 130(12), pp. 121401-121412.

Kim, N. H., Wang, H., and Queipo, N. V., 2006, "Efficient shape optimization under uncertainty using polynomial chaos expansions and local sensitivities," AIAA Journal, Vol. 44, No. 5, pp. 1112-1115.

Kim Y-D, Shim J-M, Park W-Y, Kim, S-J, Hyun D-S, and Lee D-D, 2009, "Structure Vibration Analysis of a Power Transformer (154kV/60MVA/Single Phase)," International Journal of Electrical Power and Energy Systems Engineering, 2(4), pp.249-253.

Kirkgaard, P.H., and Brincker, R., 1999, "On the optimal location of sensors for parameter identification of linear structural systems," Mech. Syst. Signal Process. 8(6), 639–647.

Kleiber, M., and Hien T.D., 1992, The Stochastic Finite Element Method, New York, NY, Wiley.

Kloess, A., Mourelatos, Z.P., and Meernik, P.R., 2004, "Probabilistic analysis of an automotive body-door system", Int.J. of Vehicle Design, Vol.34, No.2, pp.101-125.

Kumar S, and Pecht, M., 2007, Health monitoring of electronic products using symbolic time series analysis. In: AAAI fall symposium on artificial intelligence for prognostics.

Kumar, S., 2009, Development of Diagnostic and Prognostic Methodologies for Electronic Systems based on Mahalanobis Distance, Doctoral Thesis, University of Maryland College Park.

Kwon, D., Azarian, M., and Pecht, M., 2008, "Detection of Solder Joint Degradation Using RF Impedance Analysis," In: IEEE Electronic Components and Technology Conference, Lake Buena Vista, FL, 606-610.

Lee, C.Y., 1959, "Representation of switching circuits by binary-decision programs," Bell Syst Tech J., 38:985–99.

Lee, S., and Chen, W., 2009, "A comparative study of uncertainty propagation methods for black-box-type problems," Structural and Multidisciplinary Optimization, 37(3), pp. 239-253.

Lee, I., Choi, K. K., and Gorsich, D., 2009, "Sensitivity analyses of FORM-based and DRM-based performance measure approach (PMA) for reliability-based design optimization (RBDO)," International Journal of Numerical Methods in Engineering, 82(1), pp. 26-46.

Lee, I., Choi, K. K., Du, L., and Gorsich, D., 2008, "Dimension reduction method for reliability-based robust design optimization," Computers & Structures, 86(13-14), pp. 1550-1562.

Lee, S.H., and Kwak, B.M., 2006, "Response Surface Augmented Moment Method for Efficient Reliability Analysis," Structural Safety, Vol. 28, pp. 261-272.

Leibfield, T., 1998, "Online monitors keep transformers in service," IEEE Computer Appl. Power, pp. 36–42.

Li, D. S., Li, H. N. and Fritzen, C. P., 2006, "On the physical significance of the norm based sensor placement method," Proc. 3rd European Workshop: Structural Health Monitoring, pp. 1135–43

Li, H.-N., Li, D.-S. and Song, G.-B., 2004," Recent applications of fiber optic sensors to health monitoring in civil engineering," Engineering Structures, 26(11): p. 1647-1657.

Liang, J., Mourelatos, Z. P., and Nikolaidis, E., 2007, "A Single-Loop Approach for System Reliability-Based Design Optimization," ASME J. Mech. Des., 129(12), pp. 1215–1224.

Lin, C. Y., Huang, W. H., Jeng, M. C., and Doong, J. L., 1997, "Study of An Assembly Tolerance Allocation Model Based on Monte Carlo Simulation," Journal of Materials Processing Technology, 70, pp. 9–16.

Ling, Q., Tian, Z., Yin, Y., and Li, Y., 2009, "Localized Structural Health Monitoring Using Energy-Efficient Wireless Sensor Networks," IEEE Sensors Journal, Vol. 9, No. 11, pp.1596 - 1604.

Liu, J., Wang, W., Golnaraghi, F., and Liu K., 2008, "Wavelet Spectrum Analysis for Bearing Fault Diagnostics," Meas. Sci. Technol. 19, 015105 (9).

Lopez, L., 2007, "Advanced electronic prognostics through system telemetry and pattern recognition methods," Microelectron Reliab, 47(12):1865–73.

Lu, C. J., 1995, "Degradation processes and related reliability models," Ph.D. thesis, McGill University, Montreal, Canada.

Lu, C. J. and Meeker, W. Q., 1993, "Using degradation measures to estimate a time-to-failure distribution," Technometrics, 35, pp. 161–174.

Mahadevan, S., and Raghothamachar, P., 2000, "Adaptive Simulation for System Reliability Analysis of Large Structures," Comput. Struct., 77, pp. 725–734.

Mahadevan, S., Zhang, R.X., and Smith, N., 2001 "Bayesian networks for system reliability reassessment," Structural Safety, Vol. 23, No. 3, pp. 231-251.

McDonald, M., and Mahadevan, S., 2008a, "Design Optimization with System-Level Reliability Constraints," ASME J. Mech. Des., 130(2), pp. 021403(10).

McDonald, M. and Mahadevan, S., 2008b, "Reliability-Based Optimization with Discrete and Continuous Decision and Random Variables," J. Mech. Des., Vol.130, Issue 6, 061401 (13).

Meeker, W.Q., and Escobar, L. A., 1998, Statistical Methods for Reliability Data, JohnWiley and Sons: New York.

Meeker, W. Q., Escobar, L.A., and Lu, C. J., 1998, "Accelerated degradation tests: Modeling and analysis," Technometrics, 40, pp. 89–99.

Melchers, R. E., 1989, "Importance Sampling in Structural Systems," Structural Safety, Vol. 6, pp. 6-10.

Merl, D., Escalante, A., and Prado, R., 2005, "Comparison of Bayesian, Maximum Likelihood and Parsimony Methods for Detecting Positive Selection," AMS2005-03 Report.

Mina, J. and Verde, C., 2005, "Fault Detection Using Dynamic Principal Component Analysis by Average Estimation," In: 2nd International Conference on Electrical and Electronics Engineering and XI Conference on Electrical Engineering, Mexico City, Mexico. September 7-9.

Mobley, R.K., 2002, An Introduction to Predictive Maintenance, Elsevier, 2nd Edition, Chapter 1.

Mourelatos, Z.P. and Zhou, J., 2006, "A Design Optimization Under Uncertainty Using Evidence Theory," J. Mech. Des., , Vol.128, Issue 4, 901(8).

Myers, R.H., and Montgomery, D.C., 1995, Response Surface Methodology: Process and Product in Optimization Using Designed Experiments, John Wiley & Sons, Inc. New York, NY, USA.

Niederreiter, H., and Spanier, J., 2000, Monte Carlo and quasi-Monte Carlo methods, Berlin: Springer.

Noh, Y., Choi, K., and Du, L., 2009, "Reliability-based design optimization of problems with correlated input variables using a Gaussian Copula," Structural and Multidisciplinary Optimization, 38(1), pp. 1-16.

Nonero J. Q. and Hansen L. K., 2002, Time Series Prediction Based on the Relevance Vector Machine with Adaptive Kernels, In: International Conference on Acoustics, Speech, and Signal Processing, 985 – 988.

Ntotsios, E., Christodoulou, K., and Papadimitriou, C., 2006, "Optimal sensor location methodology for structural identification and damage detection," Proc. 3rd European Workshop: Structural Health Monitoring, pp 1160–7.

Orchard, M., Kacprzynski, K., Goebel, K., Saha, B., and Vachtsevanos, G., 2008, "Advances in Uncertainty Representation and Management for Particle Filtering Applied to Prognostics," In: IEEE International Conference on Prognostics and Health Management.

Papadimitriou, C., Beck, J.L., and Au, S-K, 2000, "Entropy-based optimal sensor location for structural model updating," J. Vib. Control , (6) 781–800.

Pandit, S.M., and Wu, S.M., 1993, Time series and system analysis with applications, John Wiley, New York.

Pecht, M., 2008, Prognostics and health management of electronics. New York (NY): Wiley-Interscience.

Pecht, M., and Jaai, R., 2010, "A prognostics and health management roadmap for information and electronics-rich systems," Microelectronics Reliability, Volume 50, Issue 3, Pages 317-323.

Qiu, H., Eklund, N., Iyer, N., and Hu X., 2008, "Evaluating of Filtering Techniques for Aircraft Engine Condition Monitoring and Diagnostics," In: IEEE International Conference on Prognostics and Health Management.

Quigley, J., and Walls, L., 1999, "Measuring The Effectiveness of Reliability Growth Testing," Quality and Reliability Engineering International, Vol. 15, pp. 87-93.

Rahman, S., and Rao, B.N., 2001, "A Perturbation Method for Stochastic Meshless Analysis in Elastostatics," Int. J. Numer. Meth. Engng., Vol. 50, pp. 1961-1991.

Rahman, S. and Xu, H., 2004, "A Univariate Dimension-Reduction Method for Multi-Dimensional Integration in Stochastic Mechanics," Probabilistic Engineering Mechanics, Vol. 19, pp. 393-408.

Rajagopal, R., 2004, "Bayesian Methods for Robustness in Process Optimization," Ph.D. Thesis, Industrial Engineering and Operations Research, Penn. State University.

Ramachandran, K., 2004, "System reliability bounds: a new look with improvements," Taylor & Francis, pp. 265 - 278.

Rao, S. S., 1992, Reliability-Based Design, McGraw-Hill, Inc., Ch. 4.

Rasmussen, C. E. and Williams, C. K. I., 2006, Gaussian Processes for Machine Learning, the MIT Press.

Rivera, H. L., Garcia-Souto, J.A., and Sanz, J., 2000, "Measurement of Mechanical Vibrations at Magnetic Cores of Power Transformers with Fiber-Optic

Interferometric Intrinsic Sensor," IEEE Journal on Selected Topics in Quantum Electronics, Vol.6, No. 5, September/October.

Royset, J., Der Kiureghian, A., and Polak, E., 2001, "Reliability-Based Optimal Design of Series Structural Systems," J. Eng. Mech., 127(6), pp. 607–614.

Saha, B., Goebel K., Poll S. and Christophersen J.., 2009a, "Prognostics Methods for Battery Health Monitoring Using a Bayesian Framework," IEEE Transaction on Instrumentation and Measurement, 58(2) 291-296.

Saha, B, Celaya J, Wysocki P, Goebel K. 2009b, "Towards prognostics for electronics components," In: Proceedings of the 2009 IEEE aerospace conference, March, pp. 1–7.

Saha, B., Goebel, K., Poll, S., and Christopherson, J., 2007, "An ntegrated Approach to Battery Health Monitoring using Bayesian Regression, Classification and State Estimation," In: Proceedings of IEEE Autotestcon, New York.

Saxena, A., and Goebel, K., 2008, "Damage Propagation Modeling for Aircraft Engine Run-to-Failure Simulation," In: IEEE International Conference on Prognostics and Health Management.

Schulz, V. and Schillings, C., 2009, "Problem Formulations and Treatment of Uncertainties in Aerodynamic Design", AIAA Journal, vol. 47 no. 3, pp647-654.

Sentz, K. and Ferson, S., 2002, Combination of Evidence in Dempster-Shafer Theory. Technical Report SAND2002-0835, Sandia National Laboratories.

Seo, H.S., and Kwak, B.M., 2003, "An Improved Reliability Analysis Using Design of Experiments and an Application to Tolerance Design," The 5th World Congress of Structural and Multidisciplinary Optimization, Lodo do Jesolo, Italy, May 19-23.

Shao, Y., and Nezu, K., 2000, "Prognosis Of Remaining Bearing Life Using Neural Networks," In: Proceedings of the Institute of Mechanical Engineer, Part I, Journal of Systems and Control Engineering, 214(3), pp.217-230.

Sharmin, R., Shah S., and Sundararaj U., 2008, "A PCA Based Fault Detection Scheme for Industrial High Pressure Polyethylene Reactor," Macromolecular Reaction Engineering, 2(1) 12-30.

Sobol, I.M., 1998, "On quasi-Monte Carlo Integrations," Math. Computers. Simul., 47, pp. 103–12.

Song, J., and Der Kiureghian, A., 2003, "Bounds on System Reliability by Linear Programming," J. Eng. Mech. 129(6), pp. 627–636.

Sotiris, V. and Pecht, M., 2007, "Support Vector Prognostics Analysis of Electronic Products and Systems," In: AAAI Fall Symposium on Artificial Intelligence for Prognostics, Arlington, VA, 120-127.

Spetzler, C. S., Von Holstein, S., and Carl-Axel, S., 1975, "Probability Encoding in Decision Analysis," Manage. Sci., 22(3), pp. 340-358.

Srivastava, A. N., and DAS, S., 2009, "Detection and Prognostics on Low-Dimensional Systems," IEEE Trans. on System, Man, and Cybernetics. Part C, Applications and Reviews, 39(1), 44-54.

Syros G., 2008, "Incremental Relevance Vector Machine with Kernel Learning," In: Proceedings of the 5th Hellenic conference on Artificial Intelligence: Theories, Models and Applications, 301-312.

Tanner, Neal A., Wait, Jeannette R., Farrar, Charles R., Sohn, Hoon, 2003, "Structural Health Monitoring Using Modular Wireless Sensors," Journal of Intelligent Material Systems and Structures, 14: 43-56

Tian, X., Cooling Fan Reliability, 2006, "Failure Criteria, Accelerated Life Testing, Modeling, and Quantification," In: IEEE Annual Reliability and Maintainability Symposium.

Tipping, M. E., 2001, "Sparse Bayesian Learning and the Relevance Vector Machine," Journal of Machine Learning Research, 1, 211-244.

Tipping, M. E., and Faul A., Fast Marginal Likelihood Maximization for Sparse Bayesian Models, In: Proceedings of the Ninth International Workshop on Artificial Intelligence and Statistics, 2003.

Thoft-Christensen, P., and Murotsu, Y. Application of Structural Reliability Theory. Springer Verlag, Berlin, 1986.

Tseng, S., Hamada, M. and Chiao, C., 1995, "Using degradation data to improve fluorescent lamp reliability," Journal of Quality Technology,27, 363–369.

Udwadia, F.E., "Methodology for optimal sensor locations for parameter identification in dynamic systems," ASCE J. Eng. Mech. 120 368–90, 1994.

Urmanov, A., 2007, "Electronic prognostics for computer servers," In: Proceedings of the 53rd annual reliability & maintainability symposium (RAMS), pp. 65–70.

Utkin, L.V., Gurov, S.V.: A General Formal Approach for Fuzzy Reliability Analysis in the Possibility Context. Fuzzy Sets Syst. 83, 203–213 (1996).

Valle, Y.D., Venayagamoorthy, G.K., Mohagheghi, S., Hernandez, J-C, and Harley, R.G., "Particle Swarm Optimization: basic concepts, variants and applications in power systems," IEEE Transaction on Evolutionary Computation, Vol.12, No.2, April, 2008.

Varghese, P., Braswell, R.N., Wang, B., and Zhang, C., 1996, "Statistical Tolerance Analysis Using FRPDF and Numerical Convolution," Computer-Aided Design, Vol. 28, No. 9, pp. 723-732.

Wallsten, T. S., and Budescu, D. V., 1983, "Encoding Subjective Probabilities: A Psychological and Psychometric Review," Manage. Sci, 29(2), pp. 151-173.

Wang, L, Kodiyalam, S., "An Efficient Method for Probabilistic and Robust Design with Non-normal Distributions," 43rd AIAA SDM Conference, Denver, Colorado, April 2002.

Wang, P., & Vachtsevanos, G., 2001, "Fault prognostics using dynamic wavelet neural networks." Artificial Intelligence for Engineering Design and Manufacturing, 15, pp. 349-365.

Wang, P., Youn, B.D., Xi, Z., and Kloess, A., 2009, "Bayesian Reliability Analysis With Evolving, Insufficient, and Subjective Data Sets," J. Mech. Des., Vol. 131, Issue 11, 111008(11).

Wang, T., Yu, J., Siegel, D., and Lee, J., 2008, "A Similarity-Based Prognostics Approach for Remaining Useful Life Estimation of Engineered Systems," In: IEEE International Conference on Prognostics and Health Management.

Weber, P., and Jouffe, L., 2006, "Complex System Reliability Modelling with Dynamic Object Oriented Bayesian Networks (DOOBN)," Reliability Engineering and System Safety, Vol. 91, pp. 149-162.

Wei, D. L., Cui, Z. S., and Chen, J., 2008, "Uncertainty quantification using polynomial chaos expansion with points of monomial cubature rules," Computers & Structures, Vol. 86, No.23, pp. 2102-2108.

Wei, J., Realff, J., 2004, "Sample average approximation methods for stochastic MINLPs," Comp. Chem. Eng., 28, 333–346.

Whitmore, G. A., Crowder, M. I., and Lawless, J. F., 1998, "Failure inference from a marker process based on bivariate model," Lifetime Data Analysis, 4, pp. 229–251.

Winkler, R. L., 1967, "The assessment of Prior Distributions in Bayesian Analysis," J. Am. Statist. Assoc. 62, pp. 776-800.

Wu, Y. T., 1994, "Computational Methods for Efficient Structural Reliability and Reliability Sensitivity Analysis," AIAA Journal, Vol. 32, No. 8.

Wu, Y. T., Millwater, H. R., and Cruse, T. A., 1990, "Advanced Probabilistic Structural Analysis Method for Implicit Performance Functions," AIAA Journal, 28(9), pp. 1663–1669.

Wu, Y-T., Shin, Y., Sues, R. H., and Cesare, M. A., 2001, "Safety-Factor Based Approach for Probability-Based Design Optimization," AIAA-2001-1522, 42nd AIAA/ASME/ASC /AHS/ASC SDM Conference & Exhibit, Seattle, Washington.

Xiao, Q., and Mahadevan, S., 1998, "Second –Order Upper Bounds on Probability of Intersection of Failure Events." Journal of Engineering Mechanics, ASCE, Vol. 120, No.3, pp.49-57.

Xu, H., and Rahman, S., 2004, "A Generalized Dimension-Reduction Method for Multidimensional Integration in Stochastic Mechanics," International Journal for Numerical Method in Engineering, Vol. 61, pp. 1992-2019.

Yamazaki, F., and Shinozuka, M., 1988, "Neumann Expansion for Stochastic Finite Element Analysis," Journal of Engineering Mechanics, ASCE, Vol. 114, pp. 1335-1354.

Yan, J., and Lee, J., 2005, "Degradation Assessment and Fault Modes Classification Using Logistic Regression," J. Manuf. Sci. Eng., 127(4) 912(3).

Youn, B.D., and Choi, K.K., 2004 "A New Response Surface Methodology for Reliability-Based Design Optimization," Computers and Structures, Vol. 82, pp. 241-256.

Youn, B.D., Choi, K.K., and Du, Liu, 2004, “Adaptive Probability Analysis Using An Enhanced Hybrid Mean Value (HMV+) Method,” Journal of Structural and Multidisciplinary Optimization, Vol. 28, No. 4, pp. 319-333.

Youn, B.D., Choi, K. K., and Du, L., 2005a, “Adaptive Probability Analysis Using An Enhanced Hybrid Mean Value (HMV+) Method,” Journal of Structural and Multidisciplinary Optimization, Vol. 29, No. 2, pp.134-148.

Youn, B.D., Choi, K. K., and Du, L., 2005b, “Enriched Performance Measure Approach (PMA+) for Reliability-Based Design Optimization,” AIAA Journal, Vol. 43, No. 4, pp. 874-884.

Youn, B.D., Choi, K. K., and Gorsich D., 2008a, “Integration of Possibility-Based Optimization to Robust Design for Epistemic Uncertainty,” J. Mech. Des., Vol. 129, Issue 8, 876(7).

Youn, B.D., Choi, K.K., and K. Yi, 2005c, "Performance Moment Integration for Quality Assessment in Reliability-Based Robust Design Optimization," Mechanics Based Design of Structures and Machines, Vol. 33, pp. 185-213.

Youn, B. D., Wells, L. J., and Lee, H. K., 2007, “Probabilistic Fatigue Analysis Using the Eigenvector Dimension Reduction _EDR_ Method,” WCSMO, Seoul, Korea, Paper No. A0181.

Youn, B., and Xi, Z., 2009, "Reliability-based robust design optimization using the eigenvector dimension reduction (EDR) method," Structural and Multidisciplinary Optimization, 37(5), pp. 475-492.

Youn, B.D., Xi, Z., and Wang, P., 2008b, "Eigenvector dimension reduction (EDR) method for sensitivity-free probability analysis," Structural and Multidisciplinary Optimization, 37(1), pp. 13-28.

Youn, B.D. and Wang, P., 2008a, "Bayesian Reliability-Based Design Optimization Using Eigenvector Dimension Reduction Method," Struct. Multidisc. Optim., Vol. 36, No.2, pp107-123.

Youn, B.D., and Wang, P., 2009, "Complementary Intersection Method for System Reliability Analysis," J. Mech. Des., Vol. 131, Issue 4, 041004(15).

Youn, B.D. and Wang, P., 2008b, "A Generic Bayesian Approach to Real-Time Structural Health Prognostics," In: 12th AIAA/ISSMO Multidisciplinary Analysis and Optimization Conference, AIAA 2008-6503, Victoria, British Columbia Canada, September, 10 - 12.

Yu, D.C., Nguyen, T.C., and Haddawy, P., 1999, "Bayesian Network Model for Reliability Assessment of Power Systems," IEEE Transactions on Power Systems, Vol. 14, No. 2, pp. 426-432, May.

Zhao, X., Gao, H., Zhang, G., Ayhan, B., Yan, F. and Kwan, C., 2007, "Active health monitoring of an aircraft wing with embedded piezoelectric sensor/actuator network: I. Defect detection, localization and growth monitoring, " Smart Materials and Structures, 16(4): p. 1208-1217.

Zhao, Y. G. and Ono, T., 2001, "Moment methods for structural reliability," Structural Safety, Vol. 23, pp. 47-75.

Zhang R., Mahadevan S., 2000, "Model uncertainty and Bayesian updating in reliability–based inspection". Structural Safety, 22(2), 145-160.

Zhou J., and Mourelatos Z.P., 2008 "A Sequential Algorithm for Possibility-Based Design Optimization," J. Mech. Des., Vol. 130, Issue 1, 011001(10).

Zhou, L., Penmetsa, R. C., and Grandhi, R. V., 2000, "Structural System Reliability Prediction Using Multi-Point Approximations for Design," Eighth ASCE Specialty Conference on Probabilistic Mechanics and Structural Reliability, Paper No. PMC2000-082.

Zou, T., and Mahadevan, S., 2006a, "A Direct Decoupling Approach for Efficient Reliability Based Design Optimization," Struct. Multidiscip. Optim., 31(3), pp. 190–200.

Zou, T., and Mahadevan, S., 2006b, "Versatile Formulation for Multi-Objective Reliability-Based Design Optimization," ASME J. Mech. Des., 128, pp.1217–1226.